ElmECO

Book of Abstracts

11th International Conference

September 12-15, 2024

Electromagnetic Devices and Processes in Environment Protection

Lublin, Poland

Organization Committee:

1. **Dr. Eng. Oleksandr Boiko - Chair**
2. Prof. Paweł Surdacki - Vice Chair
3. Prof. Henryka Danuta Stryczewska
4. Prof. Grzegorz Komarzyniec
5. Prof. Michał Majka
6. Prof. Ryszard Goleman
7. Prof. Sławomir Kozak
8. Dr. Eng. Michał Łanczont
9. Dr. Eng. Tomasz Giżewski
10. Dr. Eng. Joanna Kozieł
11. M.Sc. Eng. Radosław Gad
12. M.Sc. Eng. Włodzimierz Janowski
13. M.Sc. Karolina Pasicka
14. Dr. Eng. Michał Aftyka
15. Dr. Eng. Joanna Michałowska
16. Dr. Eng. Michał Lech
17. Michał Pierzchała
18. M.Sc. Eng. Damian Kostyła
19. M.Sc. Eng. Alicja Zielonka

Scientific Committee:

1. **Henryka Danuta Stryczewska (Lublin, Poland)**
2. Shin-ichi Aoqui (Kumamoto, Japan)
3. Antoni Cieśla (Cracow, Poland)
4. Marian Ciszek (Wroclaw, Poland)
5. Marek Kocik (Gdansk, Poland)
6. Sławomir Kozak (Lublin, Poland)
7. Monika Lewandowska (Szczecin, Poland)
8. Michał Majka (Lublin, Poland)
9. Ryszard Pałka (Szczecin, Poland)
10. Grzegorz Raniszewski (Lodz, Poland)
11. Mariusz Stępień (Gliwice, Poland)
12. Paweł Surdacki (Lublin, Poland)
13. Agnieszka Szypłowska (Lublin, Poland)
14. Andrzej Wac-Włodarczyk (Lublin, Poland)
15. Andrzej Wilczek (Lublin, Poland)
16. Andrzej Zaleski (Wroclaw, Poland)
17. Marian Łukaniszyn (Opole, Poland)
18. Andrzej Sikorski (Bialystok, Poland)
19. Łukasz Szymański (Lodz, Poland)
20. Agnieszka Łękawa-Raus (Warsaw, Poland)
21. Leszek Kacprzyk (Poznan, Poland)
22. Grzegorz Komarzyniec (Lublin, Poland)
23. Janusz Kozak (Lublin, Poland)- Lublin University of Technology, Poland
24. Ryszard Goleman (Lublin, Poland)
25. Paweł Węgierek (Lublin, Poland)
26. Oleksandr Boiko (Lublin, Poland)
27. Joanna Michałowska (Lublin, Poland)
28. Tomasz Giżewski (Lublin, Poland)
29. Fumiaki Mitsugi (Kumamoto, Japan)
30. Makiko Kobayashi (Kumamoto, Japan)

Patronage:

PAN POLISH ACADEMY OF SCIENCES Committee of Electrical Engineering of the Polish Academy of Sciences

PTETS

Lubelskie Towarzystwo Naukowe

PAN POLISH ACADEMY OF SCIENCES

Ministry of Science and Higher Education Republic of Poland

Doskonała Nauka

ASSOCIATION OF POLISH ELECTRICIANS Lublin Branch

The Conference is co-financed by the Polish National budget, allocated by the Ministery of Science and Higher Education under the Excellent Science II Program „**Co-financing of Scientific Conferences**", grant no. KONF/SP/0473/2023/01.

Decentralised Energy Infrastructure Integrated with Superconductivity, Hydrogen and Natural Gas

Bartlomiej A. Glowacki[1),2)]
[1)]Department of Materials Science and Metallurgy, University of Cambridge, 27 Charles Babbage Road, CB3 0FS, England
[2)]Institute of Power Engineering – National Research Institute, ul. Mory 8, 01-330 Warsaw, Poland

The world is facing a relentless depletion of fossil fuel resources alongside an acceleration of climate change, largely attributed to greenhouse gas emissions. Energy demand is projected to surge by 56% between 2010 and 2040, and could increase fivefold by 2100, driven by population growth and rapid global industrialization. As energy needs in transportation and electricity supply continue to rise, the pressure on energy generation, storage, and consumption will intensify, necessitating transformative changes. In this context, liquid hydrogen and superconductivity emerge as promising solutions for the future.

The global energy supply is currently undergoing a significant transition, spurred in part by the imperative for a low-carbon future. With the anticipated growth in the integration of intermittent renewable energy sources, such as wind and solar, into the electrical grid, the demand for reliable energy storage systems is becoming increasingly critical. Research and development in this area are focused on mitigating the emerging energy challenges by creating efficient storage solutions. Integrating these systems—particularly hydrogen-based storage—with renewable energy will enable the capture and storage of surplus energy that would otherwise go to waste.

Despite the potential of these technologies, the high capital costs associated with energy storage systems remain a significant barrier to their widespread adoption. However, with strategic energy management, the profitability of these systems can be maximized by releasing stored energy during periods of high demand and prices. The advancement of the hydrogen economy, in tandem with superconducting technologies, is poised to drive substantial changes in the natural gas industry, paving the way for a more sustainable and resilient energy future.

Recent development of HTS large scale applications for energy transition

Mariusz Stępień
Silesian University of Technology, Gliwice, Poland

Introduction

High Temperature Superconductivity (HTS) is a technology having big potential for applications in energy sector. Features of superconductivity fits very well in expectations of modern electrical devices. They are very high energy density and high efficiency. Such properties enable to construct devices expected in modern energy transition. Unfortunately, superconductivity is a technology not enough reliable for wide market applications. It needs further development and laboratory investigation to ensure proper operation of electrical devices in real industrial conditions.

Superconducting technology can be exploited in devices at every stages (chains) of energy processing: during generation, transmission, storage and use of energy. The most common devices with HTS technology used for energy processing are generators and motors, transformers, transmission lines, coils and magnets and fault current limiters. Additionally the technology can be used (bulk superconductors) in magnetic levitation, suspension and magnetic cloaking. Because of complexity of superconducting technology and high cost of experimentation the research focused on this matter is usually carried out in a form of interinstitutional (very often international) collaboration. Presented in the paper examples of research on HTS superconductivity are related to activities undertaken within COST (Cooperation in Science and Technology) CA19108 initiative entitled: "High-Temperature SuperConductivity for AcceLerating the Energy Transition" [1].

HTS wires, tapes and bulks

The first step to construct highly efficient superconducting device is to use proper HTS material. Superconductor are used in a form of wires, tapes and as a bulk materials. Recent development of superconducting materials, apart technological processes, is focused on reduction of AC losses and increasing of critical current in self-magnetic field.

Very important part of development of HTS materials is proper numerical modelling, reflecting exact parameters of given superconductor. New approaches and new numerical tools are proposed to accelerate the effectiveness of modelling. Another important aspect is characterization of HTS materials in different operational environments.

A bit different area of investigation is related to bulk superconductors. They are achieving correct crystal structure (including expected pinning properties) and achieving the highest possible magnetization field. Pulse magnetic flux pumping is one of the most intensive developed processes.

Mentioned above efforts in development of HTS materials with enhanced features are directly related to development of large scale devices described in the next section.

Large scale HTS devices

Energy transition is a step in a direction of more sustainable and more efficient energy distribution and consumption. In every step of energy processing large scale superconducting devices are able to ensure better properties of the process [2].

Superconducting generators, as a first energy chain (production/generation) made usually as synchronous machines. They are very promising players in renewable energy market, e.g. in wind farms because of reduced mass and volume. Similar advantages are important for generation of energy in transportation (ferries, airplanes).

The second energy chain is distribution. HTS technology is entering fast to commercial market of energy cables and transmission lines, mostly in DC and AC high current cables.

The second group of HTS devices in energy distribution are transformers and fault current limiters (SFCL). The most important directions of development are increasing of energy density (increasing of the critical current) and integration of transformer and SFCL (transformer with SFCL functionality).

Important aspect of energy transition is possibility of energy storage. Superconducting technology offers possibility to store energy in magnetic field. There are numerous prototypes of SMES (Superconducting Magnetic Energy Storage) developed in recent two decades. Recent years researchers are trying to construct SMES based on MgB2. Some efforts are directed also to develop flywheels suspended at superconducting bearings and motor.

The last and the biggest group of superconducting applications are devoted to use of energy. In this range the most important development is carried out in area of electrical machines (motors) devoted for different application. Large group is transportation [3]. In this area also different superconducting devices are applied in propulsion systems, suspension, supplying, etc. It shows potential of application of superconducting devices also in transportation transition.

Summary and final paper

Presented in the abstract recent developments of HTS technology and devices is only a brief presentation of this important topic. The final paper will include detailed analysis of benefits and challenges related to this technology.

References

[1] COST, *Hi-Scale Technical Annex*, Proposal, 2020.., .
[2] M. Yazdani-Asrami et al, *Artificial intelligence methods for applied superconductivity...*, Supercond. Sci. Technol. 35 123001, 2022.
[3] R. Dorget et al, *3-D Semi-Analytical Model of a Superconducting ... Machine*, IEEE Trans. Magn., v. 57, no. 11, 2021.

Overview of the high power continuous-wave Ion Cyclotron Range of Frequencies system of the ITER tokamak

Walid Helou[1)], Walid Helou[1)], Francois Calarco[1)], Charlotte Barbier[1)], Alvaro Bustos[1)], Nicolas Ferrigno[1)], Margaret Graham[1)], David Guillermain[1)], Fabienne Kazarian[1)], Aparajita Mukherjee[1)], Amit Patel[1)], Kenji Saito[1)], and authors of [1)]
[1)]ITER Organization, Route de Vinon-sur-Verdon, CS 90 046, 13067 St. Paul Lez Durance Cedex, France
Corresponding author email: walid.helou@iter.org

Introduction

In a steady-state nuclear fusion reactor of the tokamak type, high-power Continuous-Wave (CW) Radio Frequency (RF) systems are needed, among other systems, to heat the plasma up to the required temperatures of 10-20 keV as well as to drive a non-inductive plasma-current which is required for the plasma confinement. The high power RF systems are also used for conditioning the vessel wall. This contribution overviews the Ion Cyclotron Range of Frequencies (ICRF, 40-55 MHz) system of the International Thermonuclear Experimental Reactor (ITER).

The ITER ICRF system

The ITER ICRF system, is a high power CW RF system operating at 40 to 55 MHz. In the framework of the ITER re-baselining [1, 2], the ITER ICRF system will feature one antenna and a source power of 10 MW for the first operation phase of ITER. Based on the outcome of the first operation phase of ITER, the system can be upgraded to 20 MW for the nuclear Deuterium-Tritium phases of ITER while keeping one antenna. The ITER ICRF system in its 10 MW configuration is sketched in FIG 1.

The ITER ICRF antenna, which is illustrated in FIG 2, is a phased array of 6×4 electrically-short radiating loops grouped in 8 triplets. The radiating elements are oriented, spaced and phased such as to couple waves to the plasma with the proper polarization and the proper radiating plane wave spectrum while reducing parasitic interactions at the plasma edge. The triplets of an antenna are fed through a specific internal circuit with embedded, compact and robust service-stubs providing cooling to the internal conductors of the coaxes and broad-banding the antenna's response. The stubs also provide the necessary mechanical support for the antenna's internal components and allow positioning vacuum RF feedthroughs at a location that is favourable from mechanical and neutronic points of view. The ITER ICRF array antenna is powered by 8 coaxial lines and a specific impedance matching network providing load-resilience (i.e. inherent immunity against fast loading variations). The ITER ICRF system in its 10 MW configuration is driven by 4 RF sources. The power is upgradable to 20 MW by connecting additional RF sources and high voltage power supplies.

The contribution overviews the ITER ICRF system, the RF design of the ITER ICRF antenna and the strategy that has been adopted to optimize the antenna's power coupling within the operation frequency range while ensuring compliance with the requirements on the maximum voltages (45 kV peak), and maximum electric fields (2-3 kV/mm). The contribution also overviews the ongoing R&D and prototyping works (such as RF feedthroughs and their dedicated testbed, the 3D-printed radiating elements, etc.) and discusses the various foreseen protection systems (such as the foreseen arc detection systems).

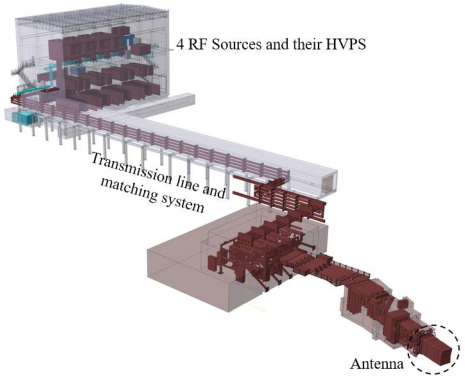

Fig. 1. The ITER ICRF system in its 10 MW configuration

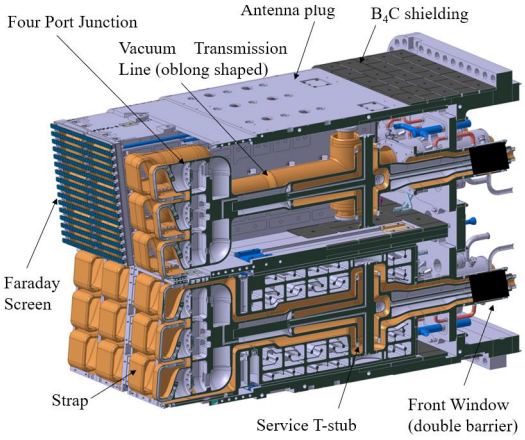

Fig. 2. The ITER ICRF antenna, 3.5m × 1.6m × 2.1m, ∼ 46t

References

[1] W. Helou, et al., *The ITER ICRF system: latest technological developments, coupling studies and compatibility with high Z wall*, 29th IAEA Fusion Energy Conference (FEC 2023), 16-21 October 2023, London, United Kingdom.

[2] P. Barabaschi, et al., *ITER Progress on ITER manufacturing, construction, commissioning and plans*, 29th IAEA Fusion Energy Conference (FEC 2023), 16-21 October 2023, London, United Kingdom.

Energy internet – The next generation smart grids

Divyanshu Bansal [1)], Umanand Loganathan[1)]
[1)]DESE, Indian Institute of Science, Bangalore

Abstract

The grid and micro-grids must cater to several distributed loads across a wide geography. In the context of the EV charging scenario, there can be millions of vehicles getting connected to the grid at specified periods of time when the grid can get overloaded. This will make the grid unstable. This is an important challenge to address. Currently, the grid and micro-grids are connected to several distributed devices that behave as both sources and sinks. During some periods, these devices pump power into the grid thereby behaving a sources and during some other periods, these same devices will act as sinks. A typical example is the EV battery charging wherein the batteries can both source and sink power. These devices are distributed throughout the micro-grid over a wide geography. In order to control the power flow from or to these devices, the power parameters need to be monitored and the data transmitted for interpretation and actuation. This implies that a strong communication layer that is tightly integrated to the power layer is needed. This is also a very important challenge that needs to be addressed. Traditionally, the loads presented to the grid are AC loads or loads made compatible for the AC grid. However today, there are several different types of loads with various requirements. Some of the loads are AC loads compatible with the traditional AC grid. There are several loads that do not require sinusoidal wave shape. There are many loads like lighting, laptops etc. that demand DC. As a consequence many DC micro-grids have come to co-exist alongside the AC micro-grids. In the three phase grid and micro-grids, phase imbalance is a serious issue. Due to unequal loading on the three phases of the grid, the grid utilisation is poor. The AC micro-grids and the DC-microgrids should be interfaced in a manner such that there is power sharing and also buffering to handle the load imbalances. The issue of load imbalance and power transaction between the AC and DC micro-grids and across the various AC and DC devices connected to these micro-grids is a significant challenge to be addressed. The challenges viz. grid instability, tight integration of communication layer along with power layer, load imbalance and interaction between AC and DC micro-grids are highly inter-linked and a coupled problem. An interesting application of the EV batteries connected to the grid is for stabilising the grid. The EV batteries are interfaced to the grid through power converters. The bi-directional DC-to-DC or DC-to-AC power converters are part of any EV charging station. The power flow and other power parameters are sensed at the points of every EV battery interface and the data communicated to central processing unit. The central unit will interpret the data from these charging interface units and provide supervisor reference control such that few of the batteries connected to the grid will act as buffers and the rest will act as sinks. The nature of the role for the EV batteries connect to the grid will be allocated by the central processing unit in a dynamic manner such that grid stability is always achieved. Such vehicle to grid interconnections need both power as well as information to flow together. A enabling technology for this would be the copper-with-optic fibre cable. These need to be used at every power level from transmission to distribution upto to the LV side, as the default cable interconnect. One of the most significant enabler would be the HVDC substations. The transmission and distribution should happen more and more through HVDC. Even downstream at the distribution level and low voltage levels, the bidirectional power converter topologies similar to that used in HVDC substations should be used. This should be mandatorily coupled with the use of copper-with-opticfibre links wherein power flow and information flow are tightly coupled. These two together will form the basis for "packet based energy transmission and distribution". A group of HVDC substations based on geography will be categorised together to form a "virtual energy router (VER)". Each port of the VER will be a HVDC substation along with a joule counter to keep track of the energy packets in and out of the port. All HVDC substations within a VER will share a common DC-link which will be the primary buffer for that VER. The VER port outputs can be either DC or AC depending on the nature of the loads downstream that the HVDC substation is catering to. There will be several VERs within a country at the transmission level. Further downstream, at the distribution levels too, there will be VERs at medium voltage levels and also at the low voltage levels to distribute power to the last mile loads. At medium voltage levels, the distribution substations will form the ports of VERs. Each VER must have a shared buffer. At the low voltage levels, bi-directional power converters will act as the ports of the VER. Here too, each VER must have a shared DC-link with probably batteries acting as buffers. In all cases, and throughout all hierarchical levels upto the last mile load, the copper-with-opticfibre cables are to be used to provide tight integration of both power flow and information flow. Every VER port must have joule counters. The power parameters and joule counter data has to be transmitted to the central processing unit of that VER. Once the existing power grid infrastructure is modified as above, packet based energy transmission and distribution is possible based on protocols similar to TCP/IP with appropriate modifications to handle power layer too.

The high voltage RF resonator test facility for the new vacuum feedthrough of the ASDEX Upgrade ICRF antennas

Oleksii Girka[1)], Walid Helou[2)], Helmut Faugel[1)], Helmut Fünfgelder[1)] and Volodymyr Bobkov
[1)]Max-Planck-Institut für Plasmaphysik, Boltzmannstraße 2, D-85748 Garching, Germany,
[2)]ITER Organization, Route de Vinon-sur-Verdon, CS 90 046, 13067 St. Paul Lez Durance Cedex, France

Introduction

The goal of the fusion research is to harness energy from the fusion of atomic nuclei. Under controlled laboratory conditions, the nuclear fusion of the two hydrogen isotopes - deuterium and tritium - results in the neutron release, production of a helium nucleus, and significant amount of energy. Just one gram of the fuel could produce the equivalent to the heat from burning around 11 tonnes of coal [1]. A steady-state magnetic nuclear fusion tokamak reactor requires auxiliary heating and current drive systems. There are three main ways to heat magnetic confinement plasmas: ohmic heating, high-frequency heating (Electron Cyclotron Resonance Heating and Ion Cyclotron Resonance Heating) and neutral beam injection. Vacuum feedthroughs are essential components in high-power RF systems interfacing with vacuum. Careful design, qualification, and testing are essential before installation to the vacuum chamber and connecting the antenna. This report presents the design of a new high voltage RF resonator test facility for the new vacuum feedthroughs of ASDEX Upgrade tokamak ICRF antennas.

ASDEX Upgrade ICRF vacuum feedthrough test facility

Heating plasmas with electromagnetic waves in the Ion Cyclotron Range of Frequencies (ICRF) is an established technique in magnetic confinement fusion research. The ion cyclotron frequency is about 15MHz/T for hydrogen. ICRF heating (ICRH) is usually realized with phased antenna arrays of radiating loops installed in the outer wall of the magnetic confinement fusion device vacuum vessel.

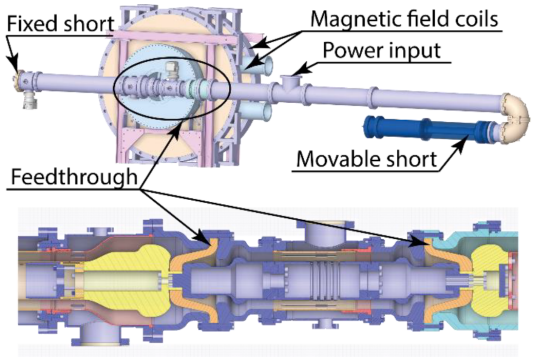

Fig. 3. Schematic of high voltage RF resonator

New vacuum feedthrough has been recently designed for the AUG ICRF system [2, 3]. The new feedthroughs have to be tested in laboratory environment before their installation in the tokamak vacuum vessel. A new high voltage RF resonator test facility design is reviewed in this report. The test facility is an extension of ISHTAR (Ion-cyclotron System Hardware Test Arrangement) [4] (including $\Phi 2m$ magnetic field coils) and is designed in two configurations: one with two new 9-inch windows featuring improved surrounding structures (corona rings or arc traps), and another with a 6-inch window combined with existing surrounding structures and new 9-inch window. High-power tests ($\sim$400 kW, $\leq$ 10 s) using an AUG ICRF generator are planned to reach the same voltage standoff as during ICRF system operation on AUG.

Acknowledgements

This work has been carried out within the framework of the EUROfusion Consortium, funded by the European Union via the Euratom Research and Training Programme (Grant Agreement No 101052200 — EUROfusion). Views and opinions expressed are however those of the author(s) only and do not necessarily reflect those of the European Union or the European Commission. Neither the European Union nor the European Commission can be held responsible for them. The views and opinions expressed herein do not necessarily reflect those of the ITER Organization. The authors acknowledge and specially thank Mr. Gerhard Siegl and Mr. Boris Mendelevitch for the generous support and fruitful discussions.

References

[1] R. Toschi, *Fusion Engineering and Design*, 36 1–8 (1997).

[2] O. Girka, W. Helou, H. Faugel, W. Tierens, V. Bobkov, *Fusion Engineering and Design*, 193 113646 (2023).

[3] H. Wedler, F. Wesner, W. Becker, R. Fritsch, *Fusion Eng. Design*, 24, 75-81 (1994).

[4] K. Crombé, S. Devaux, R. D'Inca, et al., AIP Conf. Proc. 1689, 030006 (2015).

Functional electronic materials based on wood, carbon nanotubes, and graphene

Agnieszka Lekawa-Raus[1)], Damian Łukawski[2)],
[1)] Centre for Advanced Materials and Technologies, CEZAMAT, Warsaw University of Technology, Poleczki 19 St., 02-922, Warsaw, Poland
[2)] Faculty of Materials Engineering and Technical Physics, Poznan University of Technology, Piotrowo 3 St., 60-965, Poznan, Poland

Abstract

The recent search for sustainable and low-carbon footprint materials has increased the interest in wood. Wood is a robust, porous, lightweight, and easily processable material. Simultaneously, it is natural, widely available, renewable, and biodegradable. It can be used as a raw material or turned into a wide range of composites and derivatives of varying properties. Enriching this carbon-based material and its composites and derivatives with carbon nanotubes (CNTs) and graphene can lead to the development of many novel applications and significantly change the functionality and performance. This includes a large range of electronic applications within the area of the Internet of Things.

Using natural materials in emerging electronic applications has sparked a significant shift towards more sustainable practices [1, 2]. The growing focus on sustainable and eco-friendly materials has heightened the interest of researchers in wood. This material is strong yet porous, light, and easy to manipulate. Additionally, it is a natural resource that is abundant, renewable, and capable of biodegradation. Wood can serve as a basic material or be transformed into diverse composites and derivatives with different characteristics. By integrating this carbon-based material, its composites and derivatives with carbon nanotubes (CNTs) and graphene, numerous innovative applications could emerge, profoundly altering its functionality and effectiveness. Being one of the first scientists to combine wood with carbon nanomaterials, we have shown that wood can be coated with CNTs and graphene using standard printing and coating techniques. Interestingly, we observed that CNTs and graphene can also be deposited on wood without the use of binders [3, 4]. Depending on the chosen technique of deposition and coating material, we turned wood superhydrophobic and antistatic. Moreover, we have shown a range of electronic applications such as wood-based flood sensors, motion sensors, temperature sensors, integrated floor heaters or wood dryers.

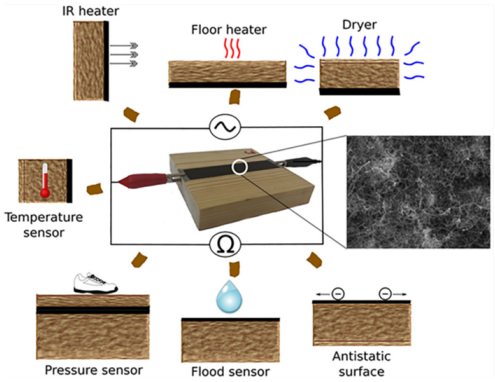

Fig. 4. Functional wood – carbon nanomaterials composites for IoT applications [3]

Further studies have shown that carbon nanomaterials can be easily integrated into wood binders and produce electroactive particleboards, keeping the international standards for reference composites [5, 6]. The most recent study considers the use of CNT-enriched wood sponges as medical electrodes [7]. However, the combination of wood, CNTs and graphene can provide many more interesting solutions. Our recent reviews analyse current progress in this area and indicate directions for future development [8, 9].

References

[1] Z. Hui, L. Zhang, G. Ren, G. Sun, H. Yu, W. Huang, *Green Flexible Electronics: Natural Materials, Fabrication, and Applications*, Adv. Mater. 35, 2211202, (2023).

[2] B. Ozlu, M. Ahmed, R. Muthoka, Z. Wen, Y. Bea, J. Youk, Y. Lee, M. Yoon, B. Shim, *Naturally derived electrically active materials for eco-friendly electronics*, Mater. Tod. Adv. 21 (2024) 100470

[3] D. Łukawski, A. Lekawa-Raus, F. Lisiecki, K. Koziol, A. Dudkowiak, *Towards the development of superhydrophobic carbon nanomaterial coatings on wood*, Prog. Org. Coat. 125, 23 (2018)

[4] D. Łukawski, A. Dudkowiak, D. Janczak, A. Lekawa-Raus, *Preparation and applications of electrically conductive wood layered composites*, Compos. Part A, 127, 105656 (2019)

[5] D. Łukawski et al. Int. J. Adhes. Adhes.132, (2024), 103678

[6] D. Łukawski et al. *Drewno* 62, 203 (2019).

[7] L. Kołodziej, O. Iwasińska-Kowalska, G. Wróblewski, M. Jakubowska, A. Lekawa-Raus, *Utilizing Cellulose Scaffolds as Electrodes for Electrophysiological Signal Monitoring*, under revision in Cellulose

[8] D. Łukawski, P. Hochmańska-Kaniewska, D. Janiszewska-Latterini, A. Lekawa-Raus, *Functional materials based on wood, carbon nanotubes, and graphene: manufacturing, applications, and green perspectives*, Wood. Sci. Tech 57, 989 (2023)

[9] D. Łukawski, P. Hochmańska-Kaniewska, D. Janiszewska, G. Wróblewski, J. Patmore, A. Lekawa-Raus, *Enriching WPCs and NFPCs with Carbon Nanotubes and Graphene*, Polymers 14, 745 (2022)

Via bottom-up synthesis of nanoobjects and nanocomposites towards brain-inspired electronics

Alexander Vahl[1),2),3)]
Department for Materials Science – Chair for Multicomponent Materials, Kiel, Germany[1)]
Kiel Nano, Surface and Interface Science KiNSIS, Kiel University, Kiel, Germany[2)]
Leibniz Institute for Plasma Science and Technology, Greifswald, Germany[3)]

Introduction

Recent developments in artificial intelligence are widely enabled by artificial neural networks, which exhibit a growing complexity and rely on increasingly large sets of training data and a rising expenditure in terms of computational resources and power consumption. The majority of contemporary artificial neural networks utilizes tailored integrated circuits, which are based on (mostly) conventional silicon technology and CMOS compatible processes. On the contrary, biological neuron assemblies form via bottom-up network development in soft matter and continued stimulus-dependent optimization via dynamic reconfigurations of network paths. Recently, these processes have become of crucial interest to implement comparable energy efficiency and robustness in technical systems. To fully harness the capabilities of neural networks in brain-inspired electronics, it appears mandatory to explore deposition approaches beyond conventional CMOS, including bottom-up processes, organic matrices and flexible substrates.

Abstract

Nanoobjects such nanoparticles or nanowires are interesting building units for bio-inspired electronics based on the self-ordered arrangement. In this talk, examples for applications in resistive switching and neuromorphic engineering are showcased at the example of brain-like dynamics and resistive switching in nanogranular structures. A particular focus lies on plasma-based gas phase synthesis of nanoparticles from supersaturated metal vapours as a promising pathway to create nanoparticles with tailored composition and morphology. For nanocomposites and individual nanoparticles alike, diffusive memristive switching with distinct, well-separable resistance states is found. By directly coating the nanocomposite layer on conductive atomic force microscopy tips, memristive switching was localised to the tip. As such, the reservoir of mobile Ag species for reversible filament formation was strongly confined, which resulted in a transition to a highly volatile switching regime [1]. Composite networks of AgAu nanoparticles and CNTs show diffusive memristive switching in lateral networks on the µm scale and exhibit excitation-dependent filament decomposition behaviour[1]. Surface coverage of the nanoparticles is of great importance for the switching dynamics of the system: in self-ordered, highly interconnected networks of metallic nanoparticles that are on the threshold of electrical percolation, dynamic transitions between multiple resistance states are observed, indicating avalanches of successive switching, criticality and scale invariance, similar to switching activity in neuron assemblies[3, 4]. The excellent compatibility of nanoparticle beam deposition methods with a wide range of (unconventional) substrates enables the incorporation of Ag nanoparticles into vacuum-compatible liquid-phase polymers to produce nanogranular metal-polymer nanocomposites. In these nanofluids, electrophoretic field-driven migration of particles and particle agglomerates can be used to reconfigure wide-ranging conductive bridges [5].

Acknowledgements

Funded by the Deutsche Forschungsgemeinschaft (DFG, German Research Foundation) –Project-ID 434434223 – SFB 1461.

References

[1] N. Carstens, A. Vahl, O. Gronenberg, T. Strunskus, L. Kienle, F. Faupel and A. Hassanien, *Enhancing Reliability of Studies on Single Filament Memristive Switching via an Unconventional cAFM Approach*, Nanomaterials 11, 265 (2021).

[2] M.-I. Terasa, P. Holtz, N. Carstens, S. Kaps, F. Faupel, A. Vahl and R. Adelung, *Sparse CNT Networks with Implanted AgAu Nanoparticles: A Novel Memristor with Short-Term Memory Bordering Between Diffusive and Bipolar Switching*, PLOS One 17, 3: e0264846 (2022).

[3] N. Carstens, B. Adejube, T. Strunskus, F. Faupel, S. Brown and A. Vahl, *Brain-like critical dynamics and long-range temporal correlations in percolating networks of silver nanoparticles and functionality preservation after integration of insulating matrix*, Nanoscale Advances 4, 3149-3160 (2022).

[4] M.-I. Terasa, M. Noll, B. Adejube, R. Madurawala, T. Birkoben, N. Carstens, T. Strunskus, S. Kaps, F. Faupel, A. Vahl, H. Kohlstedt and R. Adelung, *Brain-like critical dynamics and long-range temporal correlations in percolating networks of silver nanoparticles and functionality preservation after integration of insulating matrix*, Materials Today 69, 41-53 (2023).

[5] D. Nikitin, K. Biliak, P. Pleskunov, S. Ali-Ogly, V. Červenková, N. Carstens, B. Adejube, T. Strunskus, Z. Černochová, P. Štěpánek, L. Bajtošová, M. Cieslar, M. Protsak, M. Tosca, J. Lemke, F. Faupel, H. Biederman, A. Vahl and A. Choukourov, *Resistive switching effect in Ag-poly(ethylene glycol) nanofluids: Novel avenue toward neuromorphic materials*, Advanced Functional Materials (2024).

Gas-aggregated nanoparticles and where to apply them: from optics to neuromorphic science

Daniil Nikitin, Pavel Pleskunov, Kateryna Biliak, Mariia Protsak, Marco Tosca, Veronika Červenková, Andrei Choukourov,
Charles University, Faculty of Mathematics and Physics, V Holešovičkách 2, 18000 Prague, Czech Republic

Introduction

Nanoparticles (NPs) of metals, semiconductors, or polymers represent objects of the typical size 1 – 100 nm with properties that significantly deviate from the properties of bulk material. Due to this, NPs have been found prospective in many applications, including catalysis, sensing, optical coatings, electronics, and biomedicine. Various physical and chemical methods have been proposed to fabricate NPs. Among them, magnetron sputtering-based gas aggregation sources (GAS) occupy a special place due to several benefits, e.g., high grade of chemical purity, simple tuning of NPs size, chemical composition and crystallinity, and an opportunity to deposit NPs onto different substrates. In this presentation, an introduction to the physics of gas-aggregated NPs will be combined with several applications to demonstrate the feasibility of this method.

Gas-phase synthesis of NPs

GAS is an instrument routinely used to fabricate gas-aggregated NPs in vacuum. The construction of sputter-based GAS was invented by Haberland in 1991, and since then, it has not significantly changed. GAS consists of a magnetron installed in the water-cooled aggregation chamber ending with a small orifice. Sputtering is performed in the atmosphere of inert gas, most often argon, at pressure of tens Pa to create conditions of supersaturation required for spontaneous nucleation and growth of metal NPs. The type of metal is limited only by the choice of commercially available sputtering targets. NPs can be deposited onto any vacuum-compatible substrate, such as silicon, polymer foils, textiles, and even liquids. Not only single-metal NPs but also more complex alloy or core-shell NPs can be produced by GAS. Several strategies have been proposed, including co-sputtering from the composite target or independent magnetrons, or in-flight modification. Furthermore, an admixture of reactive gases (O2 or N2) to argon leads to the formation of oxide and nitride NPs. In Charles University, we firstly used R.F. magnetron sputtering of polymeric targets inside the GAS to produce NPs of plasma polymers.

Applications of gas-aggregated NPs

Due to the purely physical and vacuum-based strategy of NPs fabrication, they are free of impurities, which makes them attractive for various applications. Single metal plasmonic NPs (Ag or Au) are used for Surface Enhanced Raman spectroscopy (SERS) detection of organic dyes in water or laser desorption/ionization mass spectrometry (nanoPALDI) of biomolecules. Instead of expensive noble metals, cheaper transition metals can be feasible alternative. Nb NPs were used for nanoPALDI, and V2O5 NPs demonstrated their efficiency for SERS. Recently, we produced the refractory plasmonic NPs of transition metal nitrides (TiN, ZrN, and HfN) by reactive-sputter GAS. These NPs demonstrate better stability at elevated temperatures vs. noble metals, which can be helpful for green energy applications, such as solar light absorbers.

Antibacterial Ag or Cu NPs demonstrate high efficiency against various pathogens, including those with antibiotic resistance. In combination with organic matrix, they form nanocomposite coatings protecting against the growth of bacterial biofilms.

Nowadays, catalysis for energy production is one of the hot topics worldwide. Gas-aggregated Pt NPs demonstrated better electrochemical results than conventional magnetron-sputtered nanostructured films. Furthermore, the NPs of tantalum oxynitride were found to be applicable for photoelectrochemical solar water splitting.

The novel and fascinating application of gas-aggregated NPs was found in neuromorphic science. In this field, researchers worldwide try to mimic the processes in biological neural networks using artificial devices based on the resistive switching effect. Interestingly, the solid percolating networks of gas-aggregated metal NPs stochastically change their resistance between insulative and conductive states with dynamics similar to the signal transmission in synapses. Inspired by this discovery, we deposited Ag NPs into the liquid dielectric matrix to form the neuromorphic nanofluidic system. In the electric field, NPs move toward biased electrode self-organizing in the 3D-conductive filaments. As a result, the resistivity of the medium between the electrodes changes. When the filament forms, it passes the electric current in a spiking regime similar to the percolating NPs networks. The lifetimes of individual states of the system were analyzed to understand the physics of the observed effect and to study the influence of additional factors, such as the viscosity of the liquid matrix and the temperature of the system.

Acknowledgment

The work was supported via the grant GACR 23-06925S from the Czech Science Foundation and via the Czech-German Mobility grant number 8J23DE016 from the Ministry of Education, Youth and Sports.

How to destroy cancer cells with nanotechnology?

Zbigniew Kołaciński

Abstract

Iron is one of the best elements for magnetization with electromagnetic radiation. It can be used as a tool for medical diagnosis and treatment. Electromagnetic heating of iron nanoparticles and ferro-fluids can be successfully used for non-invasive thermal ablation of cancer cells. Different types of electromagnetic waves have been used so far. For thermal ablation of cancer cells the used radio frequency should fall within the industrial, scientific and medical scope as well as the interaction with human body should be limited to minimum. Generally, the application of radio frequency energy fields for medical treatment is justified by deep tissue penetration.

The highly Fe doped CNTs (Fe-CNTs) as the carriers creating magnetic fluid will be presented. An excessive catalyst injection method using electrical furnace and microwave plasma reactor will be proposed. This way is possible to grow the Fe filled CNTs on a moving surface in continuous synthesis process. This allows producing uniform carpet of the Fe-CNTs carriers. Then the targeted therapies which can be effective if the carriers are able to distinguish the difference between cancerous and healthy cell's physiology are considered.

Ozone nano-mist generation by dielectric barrier discharges and automatic remote insect pest disinfection system in agriculture

Kenji Ebihara[1),2)], Fumiaki Mitsugi[2)], Shin-ichi Aoqui[3)], Oleksandr Boiko[4)], Henryka D. Stryczewska[4)]
[1)]Environment and Energy Laboratory, Japan
[2)]Faculty of Advanced Science and Technology, Kumamoto University, Japan
[3)]Faculty of Computer and Information Sciences, Sojo University, Japan
[4)]Department of Electrical Engineering and Electrotechnologies, Lublin University of Technology, Poland

Abstract
An automatic ozone nano-mist spraying system is developed to disinfect harmful insect pests in agricultural fields. High dense ozone of a maximum concentration of 110 g-O3/m3 is generated by dielectric barrier discharges. The water nano-mist consisting of nano-particles (200-1200nm size) is provided by an ultrasonic humidifier. In order to spray remotely on insect pests (seven species), the YOLO object detection architecture based on the deep learning is adopted to identify insect pests and the resulting disinfection conditions control remotely a microcomputer Raspberry Pi which is connected to the spraying system. The testing process of the object target pests took 7-9 seconds. The ozone nano-mist was exposed on the target pests. As a result, moths and whiteflies were disinfected within 30 seconds and aphids and beetles needed longer treatment time over 60 seconds.

Introduction
Ozone has been proved to kill a wide range of species including bacteria, fungus, viruses, insect pests and is an effective alternative to chemical pesticides in agricultural managements. Water mist in the form of droplets and particles is ozonized to produce reactive hydroxyl radical (*OH) with an oxidation potential of 2.86V. Recently, the form of ozone mists has been interested widely and applied to the disinfection of medical fields, food industries, and agricultural fields[1,2]. We develop an ozone nano-mist disinfection system in which the nano-mist consisting of water particles in the size of 100nm-1000nm reacts immediately with gaseous ozone to form the ozone nano-mist. This system is operated to spray the ozone nano-mist on target insect pests. YOLO-based pest detection architecture is adopted to perform processes such as detection and classification of insect pests in the agricultural field. This spraying system controlled by Raspberry Pi is employed for realistic application in the greenhouse. We implement disinfection experiments on selected seven insect pests.

Materials and Methods
The ozone nano-mist splaying system is mostly composed of an ozone nano-mist generator system, an image acquisition and detection system and an automatic remote spray. Fig.1 shows the ozone nano-mist generation system controlled by Raspberry Pi. The high frequency power (3.8-4.2 kV at 6 kHz) was applied between the electrodes. The water nano-mist was generated by the piezoelectric method that the transducer vibrating at an ultrasonic frequency of 1.7MHz was placed in the atomizer storing water. The ozonated nano-mist is prepared by injecting high dense ozone into the nano-mist atmosphere. The dielectric barrier discharge in oxygen provides gaseous ozone with high concentration of 110 g-O3/m3. The YOLOv5 detection architecture correctly detected and identified insect pests. The YOLO was implemented in Google Colaboratory providing access to the main computer.

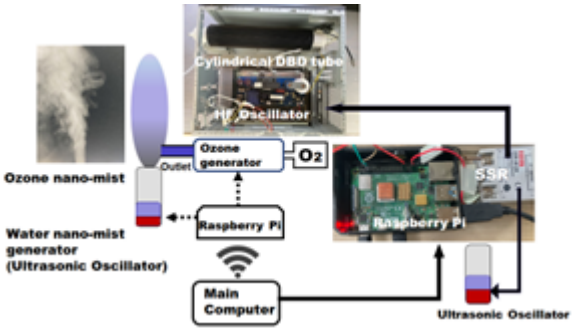

Fig. 5. Ozone nano-mist generation system

Results and Discussion
Seven typical harmful insect pests including aphids, moths, whiteflies, thrips, caterpillars, beetles and ants were selected to investigate disinfection effect. The initial process of the YOLO detection including train and validation consumed 8-9 minutes. The YOLO testing times was 7-9 sec depending on the conditions (figure, size, numbers) of the selected picture image. Winged insects such as moths, whiteflies and small larva of aphids were mostly killed with the high disinfection rate near 100

Conclusion
The ozone nano-mist using 110 g-O3/m3 has sufficient disinfectant performance to kill winged insect pests. The YOLO model is capable of correctly identifying the seven species of insect pests with high counting accuracy. The overall processes of the proposed disinfection spraying system were completely accomplished.

References
[1] K. Ebihara, et al., *Proc. 2022 Int. Conf. Electromagn. Devices Process. Environ. Prot. (ELMECO -10)*, May 2022, Session 1.
[2] K. Ebihara, et al., *Proc. 2017 Int. Conf. Electromagn. Devices Process. Environ. Prot. with Semin. Appl. Supercond. (ELMECO-9 & AoS)*, Dec. 2017.

Development of Methods for Modeling Low-Frequency Electromagnetic Field

Andrzej Demenko[1)]
[1)]Poznan University of Technology

Introduction

The presentation consists of four main parts. The first part presents three forms of description of electromagnetic field equations and briefly describes the history of the development of methods for modeling systems with electromagnetic fields. Part 2 focuses on describing the progress of numerical methods and discussing the latest approaches to the Finite Element Method (FEM). In the third part, attention was paid to the equivalence of the finite difference, finite element, and finite integral methods, as well as the method of electric and magnetic networks. The presentation features a new FEM approach in which the finite element is considered as a nodal, edge and facet. Such an approach leads to two types of models: (a) an edge model with unknown scalar potentials of the nodes and (b) a facet model with unknown edge values of vector potentials. Part 4 presents examples of the application of the new FEM approach. The methods for simulating the motion in a network models and for calculating electromagnetic forces and torques are discussed. The conclusion points out the analogy between the methods of solving circuit equations and the presented methods of solving field equations

Outline of electromagnetic modeling history

Modeling systems with electromagnetic fields has a long and interesting history. First, rheoelectric models were applied, e.g. Kirchhoff, in 1845, when the field equations were not yet known, used copper plate to determine the distribution of the electrostatic field in a capacitor. Thirty years later, in the Proceeding of the Royal Society, an article on the use of an electrolytic tank for field modeling was published. The article was written by William Grylls Adams.

Then, the application of models with conductive layers has become widespread resulting from the development of conductive paper production technology. Conductive paper systems were used in up to the 1960s. An example of a system with conductive paper is the EGDA analyzer built at the Institute of Mathematics of the Ukrainian Academy of Sciences. Conductive paper analyzer was applied by famous French mathematician Lucien Malavard.

In 1918, Karl Otto Heinrich Liebmann, a professor at the Technical University of Munich, presented a differential diagram, describing the value of a scalar field quantity at a given point based on the value of this quantity at neighboring points. He can be considered the father of the finite difference method (FDM). The FDM for physical fields was described in detail by Richard Courant in 1924 in the monograph "Methoden der mathematischen Physik" [1]. R. Courant is also considered the originator of the finite element method [1]. When discussing the FDM for solving physical field equations, we cannot forget the achievements of Richard Vynne Southwell and Lothar Collatz. The development of the FDM went hand in hand with the development of electrical analog systems for solving the equations of this method. The idea of such a system was presented in Russia by Semyon A. Gershgorin. In 1929, he published in Russian the work "On electric networks for the approximate solution of the differential equation of Laplace", in which he presented the idea of using an electric network to solve differential field equations. The first electric network models, later called network field analyzers, were built by Clemens Louis Beuken in the Netherlands in 1935, and Lev Israilevich Gutenmacher in Russia in 1940.

In the mid-1970s, attempts were made to design systems with a microprocessor network. However, these attempts were abandoned due to the dynamic development of single-processor digital computers and methods involving these computers. The ideas of microprocessor networks found application in digital parallel computing systems.

Numerical methods in electromagnetism

It is difficult to determine who initiated the use of numerical methods and digital techniques to solve electromagnetic field equations. Undoubtedly, one of the first was E. A. Erdelyi, who in 1965, together with S.V. Ahmed and R.D. Burtness published a paper on the use of the FDM for numerical calculations of the magnetic field in a DC machine at no-load [2]. Research in the following years resulted in the rapid development of the finite element method (FEM). The promoter of this method in electromagnetic calculations was P. P. Silvester, who in 1970, together with M. V. K. Chari, published a paper on the use of FEM for magnetic field problems. P. Silvester is the co-author of several books: (a) "Finite Elements in Electrical and Magnetic Field Problems" (with M.V.K. Chari, 1980), (b) "Finite Elements for Electrical Engineers" (with Ronald L. Ferrari, 3 editions in 1983, 1990 and 1996), (c) "Computer-Aided Design in Magnetics" (with David A. Lowther), (d) "Finite Elements for Wave Electromagnetics" (with Giuseppe Pelosi, 1994), (e) "Finite Element Software for Microwave Engineering" (with Tatsuo Itoh and Giuseppe Pelosi, 1996). Each of the mentioned coauthors has significant contributions to the development and implementation of the FEM for solving systems with an electromagnetic field.

The end of the 1970s begun a period of dynamic development of research on numerical methods for solving electromagnetic field differences began. The first conference on electromagnetic calculations, later known as COMPUMAG conference, was held in Oxford, in April 1976. The co-organizer of the conference was Bill Trowbridge, author of many articles on numerical methods in

electromagnetism, including two books [4, 5].

At the same time, Thomas Weiland developed and began propagating computational systems using the finite integral method (FIT) [6].

During the COMPUMAG conference in 1981, Alain Bossavit presented for the first time a communication on the edge element method [7]. He used the principles of Hassler Whitney integral geometry; see Geometric Integration Theory, Princeton Univ. Press, 1957. Bossavit's research disseminated a new approach to the FEM. In this approach, there are 4 Witney forms of the element: nodal, edge, facet and volume form. It should be noted that research on software that uses Whitney elements (Whitney forms) is still ongoing.

Over the last 30 years, a number of new ideas for using computers to calculate the electromagnetic field have been introduced, i.e. the cell method, methods of reluctance or permeance network. Approaches that allow combining various methods are being sought. These searches are related to the author's works on analogies between the most common methods of modeling the electromagnetic field [8, 9].

Dual models of element using Whitney forms

Based on the results of recent research, it is possible to generalize the applied schemes and numerical methods for analysing of systems with an electromagnetic field.

Despite the development of Whitney's approach, which considers four forms of the element, the classical approach, which comes from research on systems with a 2D field, is still widely used. The author of this article decided to present new, little-known approaches, which involve the interpolation functions of nodal, edge and facet elements. He used the languages of magnetic and electric circuit theory to describe elements and concentrated on the formulations using scalar and vector potentials for magnetic and electric fields. In these formulations there are 2 models of the element for magnetic and 2 for electric fields. Due to the location of the branches, these models were named by the author as edge and facet, respectively. The branches of edge models are associated with the element's edges. However the branches of the facet models are assigned to facets and pass through the facets of the elements. The nodes of these branches are the centers of two elements with a common facet.

The branch of the edge network contains the capacitance and conductance for electric field models and permeance for magnetic field models. Interpolation functions of the edge element are used to calculate the values of these quantities. The sources in the branches of the magnetic edge model are the currents in the loops around the edges. However, in the electrical edge model, the sources are the time derivatives of the loop fluxes. When forming FEM equations for a network composed of edge models of elements, it is taken into account that the integral of the scalar potential gradient along the edge is equal to the potential difference of the network nodes. As a result, a system of equations describing the scalar potentials of element nodes is obtained.

The branch of the facet electric model contains resistance and elastance. However, the branch of the facet magnetic network contains reluctance. To calculate the resistance, elestance and reluctance of the facet model, the interpolation functions of the facet element are applied. The branch sources in facet models are loop currents or derivatives of mesh loop fluxes in the loops assigned to the facets. FEM equations for facet models are obtained using the edge values of vector potentials. These values are the currents or fluxes in the loops around the edges. It is taken into account that the integral of the current or flux density on the surface of a given facet is the sum of the loop currents or fluxes around all edges of this facet. The obtained equations for a network with facet models of elements take the form of mesh/loop equations for a system with nodes located in the centers of the elements. The unknowns are the edge values of vector potentials, which represent mesh/loop currents or fluxes.

The edge and facet models discussed above are very similar to the models obtained using the FDM and FIT [9]. Therefore it can be concluded that: a) for the formulation using scalar potentials and nodal elements, FEM, FIT and FDM equations represent nodal equations of edge networks with branches associated with element edges, b) for the formulation using vector potentials and edge elements, FEM equations and equations of the equivalent FDM, and FIT represent the loop (mesh) equations of the facet network with nodes in element centers.

The presented circuit representation of network models of systems with electric and magnetic fields has many advantages. It facilitates the homogenization of systems with laminated cores and permanent magnets and allows for the modeling of virtual displacements when determining forces and torques, as well as limiting disturbances during simulating motion in finite element models. The discussed approach allows coupling the FEM with the method using circuit models [10].

It seems that the presented circuit representation of the FEM is also useful in teaching numerical methods in electrical engineering.

References

[1] R. Courant, D. Hilbert, *Methods of mathematical physics, vol. I*, New York, NY: Interscience Publishers, 1953.

[2] E.A. Erdelyi, S.V. Ahamed, R.D. Burtness, *Flux distribution in saturated dc machines at no-load*, IEEE Trans. Power App. Syst., PAS-84, 1965.

[3] P. P. Silvester, M.V.K. Chari, *Finite Element Solution of Saturable Magnetic Field Problems*, IEEE Trans. Power App. Syst., PAS-89, 1970.

[4] B. Trowbridge, *An Introduction to Computer Aided Electromagnetic Analysis*, Oxford, UK: Vector Fields Ltd, 1990.

[5] B. Trowbridge, P.J. Lawrenson, K. Binns, *Numerical Modeling of Electromagnetic Fields*, John Wiley & Sons, 1992.

[6] T. Weiland, *A Discretization Method for the Solution of Maxwell's Equations for Six-Component*

Fields, Electronics and Communications, AEU, Vol. 31, 1977.

[7] A. Bossavit, *Computational Electromagnetism: Variational Formulations, Complementarity, Edge Elements*, Academic Press, 2011.

[8] A. Demenko, J. Sykulski, *Network equivalents of nodal and edge elements in electromagnetics*, IEEE Trans. Mag., 2002.

[9] A. Demenko, J. Sykulski, *Analogies Between Finite-Difference and Finite-Element Methods for Scalar and Vector Potential Formulations in Magnetic Field Calculations*, IEEE Trans. Mag., 2016.

[10] A.S. Nunes, O. Chadebec, P. Kuo-Peng, P. Dular, G. Meunier, *A Coupling Between the Facet Finite Element and Reluctance Network Methods in 3-D*, IEEE Trans. Mag., 2017.

Multi-agent simulation of switched reluctance motors

Mykhaylo Zagirnyak[1)],
[1)]Kremenchuk Mykhailo Ostrohradskyi National University

Introduction

According to [1, 2, 3], the share of electricity consumed by electric motors worldwide is about 65

Purpose

The purpose of the work is to increase the information content in the simulation research of electromechanical processes of a switched reluctance motor by developing a mathematical model based on a multi-agent approach.

To achieve this goal, the following tasks need to be solved: develop the structure of the MS SRM model using multi-agent subsystems; standardize each agent to simplify its application and integration into the overall system; implement functions in the model for considering load, modifying switching laws, and determining electrical and mechanical characteristics.

Development of agents for the mathematical model of switched reluctance motor

The mathematical model of a switched reluctance motor (SRM) built on the basis of a multi-agent approach is shown in Fig. 1. The developed model consists of the following agents.

A1 is an agent for forming the dependencies of phase inductances on the rotor rotation angle, based on a linear approximation of the inductance. This agent also calculates the key points of the operating cycle of the SRM phase.

A2 is an agent for generating conditional motor phase switching functions, which allows considering the phase power supply delay, premature phase disconnection, and the application of reverse voltage to accelerate the current decay in the phase.

A3 is an agent for calculating the electromagnetic energy conversion in the phases of SRM, which is characterized by the use of basic universal functions that allow the implementation for various variations in the number of stator and rotor teeth. This agent also allows us to consider the asymmetry of the induction machine windings.

A4 is an agent for calculating the conversion of electromagnetic energy into mechanical energy (solving the equation of motion).

A5 is an agent for motor load forming that allows implementing three approaches to load formation: through a universal mathematical description; through a set of specialized load models; through vectors of the dependence of the resistance moment on time.

A6 is an agent for calculating the motor shaft rotation angle and cyclic rotation angle, which is used in agent A3 to generate phase voltages and inductances as a function of time.

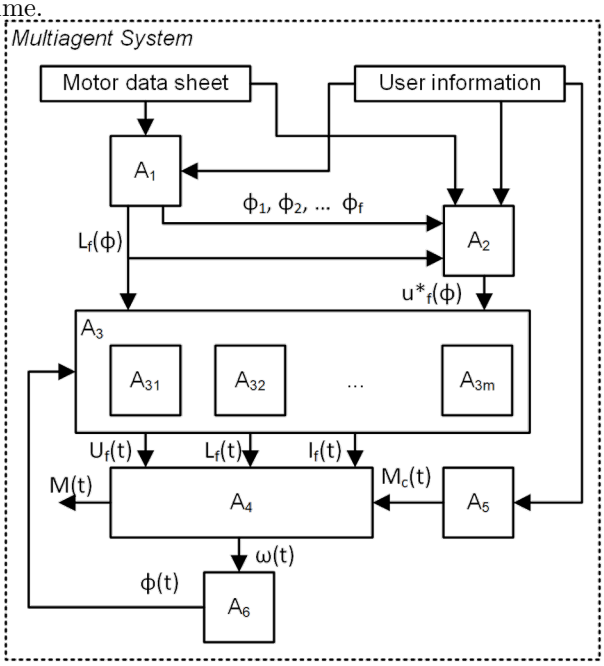

Fig. 6. Schematic diagram of the SRM mathematical model

Conclusion

The model for calculating energy conversion in complexes consisting of a power converter, SRM, and technological object has been enhanced. This improvement includes the use of a multi-agent subsystem, considers the resistance torque of the technological mechanism, and considers the design features of the motor.

References

[1] N. Istomina, "Optimization of switched-reluctance motor operation using a multiagent model," *Transactions of Kremenchuk Mykhailo Ostrohradskyi National University*, 2020.

[2] N. Istomina, M. Bačko, "Determination of inductance levels of switched reluctance motor," *SCYR*, 2013.

Eliminating the current pulsations at the terminals of electrochemical energy storage during the asymmetrical operation of a 4-wire converter

Dariusz Zieliński

Low-voltage distribution networks saturated with RE sources and large single-phase loads, i.e. EV chargers and heat pumps, are characterised by asymmetry and exceeding of phase voltage limits. Known consequences of this are outages of photovoltaic inverters, accelerated degradation of electronic equipment, but also increased losses in LV distribution transformers. These losses are mainly due to the high angular and amplitudinal asymmetry of voltage phasors on the transformer's low-voltage side. A panacea for solving the above problems is application of a 4-wire AC/DC converter with an active neutral branch, along with electrochemical energy storage. Converters of this type can operate with any current asymmetry and can be treated as three independent single-phase AC/DC converters working for a common energy storage unit. The ability to operate with any asymmetry of currents allows efficient and immediate symmetrisation of distribution network voltages, while it transfers the problem of power pulsation from the AC distribution network to the DC terminals of the energy storage, which is detrimental to it and shortens its life significantly.

To prevent these phenomena, a 4-wire power electronic converter was developed that allows independent control of each phase of a low-voltage line, along with an auxiliary DC/DC converter and a supercapacitor to compensate for electrochemical storage pulsations. The device uses control of the possibility of bidirectional regulation of active and reactive power, thus achieving actively controlled symmetrisation of the line phase loads resulting in the restoration of a symmetrical three-phase voltage system.

The presentation shows the effect of symmetrisation of line voltages with a 4-wire converter on power pulsations on electrochemical storage, and the effectiveness of compensation of these pulsations using an auxiliary DC/DC converter and a supercapacitor. The results shown were obtained following simulation model calculations and the power and voltage balance on the test bench.

Improving the efficiency of a three-phase transformer with a 4-wire DC/AC converter for voltage symmetrisation in asymmetrical networks with PV sources

Wojciech Jarzyna

Three-phase low-voltage networks with a neutral conductor, especially those with high saturation of photovoltaic systems, are characterised by asymmetry and voltage overshoot. A well known consequence of this are outages of photovoltaic generators, but also an increase in losses in LV distribution transformers. These losses are mainly due to the high asymmetry of voltage phasors on the low-voltage side. For example, a symmetrical three-phase system with phasor directions $\left[1, e^{j2\pi/3}, e^{j4\pi/3}\right]$, when the power flow of one of the phases is reversed due to PV sources, can take the directions $\left[1, e^{j\pi/3}, e^{j2\pi/3}\right]$. Such a condition results in the generation of harmful counter- and zero-order components. In addition to the dangerous effects associated with the operation of three-phase loads in such networks, these components contribute to increased active losses and losses in the transformer core. To prevent these phenomena, a 4-wire power electronic converter was developed that allows independent control of each phase of a low-voltage line. This control is expressed in the possibility of bidirectional regulation of active and reactive power, so that actively controlled symmetrisation of the phase loads of the line can be achieved resulting in the restoration of a symmetrical three-phase voltage system.

The presentation shows the effect of asymmetrical distribution of grid voltage phases on transformer losses, and estimates how this phenomenon affects the efficiency of transformers. In order to improve the symmetry of voltages and loads, a 4-wire DC/AC converter cooperating with energy storage was developed. This converter allows for independent bidirectional control of active and reactive power. In this way, it can actively influence the voltage system by symmetrising the low-voltage line loads. In this way, it also affects the reduction of symmetrical components of the voltages improving the efficiency of the transformer and other three-phase receivers.

The results shown were obtained following simulation model calculations and the bench power balance.

Sol-Gel Composite Material Development for Energy Harvesting

Makiko Kobayashi[1)],
[1)]Kumamoto University

Introduction

In recent years, the demand for sustainable energy solutions has significantly increased due to the growing emphasis on reducing carbon footprints and mitigating climate change. Among the various technologies being explored, energy harvesting through piezoelectric materials has emerged as a promising approach for wireless systems, especially those involving integrated sensors in hard-to-reach or remote locations and self-sustaining wearable devices.

Piezoelectric sol-gel composite films could be one of the good candidates due to robustness and flexibility [1]. In the past study, a 60µm thick piezoelectric lead-zirconate-titanate (PZT) /PZT composite film with a 20mm diameter silver paste top electrode was vibrated at a deflection displacement of 5 mm, generating 13.6Vp-p at 10Hz [2]. The development of sol-gel composites with piezoelectric charge constant (d33) is crucial for energy harvesting application. In this investigation, PZT/PZT samples with different d33 constant powder phase material were fabricated to evaluate piezoelectric ultrasonic performance.

Materials and Methods

Two types of PZT powders, namely HIZIRCO A(A) and HIZIRCO L(L) were purchased from Hayashi Chemical Industry Co., Ltd. The supplier provided PZT powders with 0.6 μm particle size specification. Table 1 shows the material properties of each powder. The piezoelectric charge constant (d_{33}) values of A and L are high and low, respectively, whereas there is no significant difference in the electromechanical coupling coefficient k_{33}. The piezoelectric voltage constant (g_{33}) values of L are higher than that of A.

The two PZT powders were mixed in a laboratory-made PZT sol-gel solution. After ball milling, the mixture was sprayed onto titanium substrates with a thickness of 3mm, a length of 30mm, and a width of 30mm. Subsequently, thermal treatments, drying process, and firing process, were conducted at 150 degC using a hot plate and at 650degC using an electrical furnace. The spray coating and thermal treatments were repeated until the film reached the desired thickness. 50μm was the target thickness in this time because of fabrication facility including piezoelectric film fabrication and poling process. Au top electrodes were fabricated by sputtering.

Table 1: Material properties of PZT raw powders

Parametr	HIZIRCO A	HIZIRCO L
ε_r	5500	1800
T_C (°C)	160	320
k_{33} (%)	70	70
d_{33} (pC/N)	660	400
g_{33} ($\times 10^{-4}$ V·m/N)	136	251

Results

Tables 2 and 3 show the measured film properties. By room temperature poling, d_{33} of the L/PZT film were the higher than A/PZT, even though the d_{33} of A is higher than that of L as shown in Table 1. By 200degC poling, d_{33} of the A/PZT film became slightly higher than A/PZT though it was much lower value than expectation from raw material.

Table 2: Material properties of A/PZT poled at RT and 200degC

Parametr	RT	200°C
ε_r	910	990
d_{33} (pC/N)	32.5	46.8
g_{33} ($\times 10^{-4}$ V·m/N)	40.3	53.4

Table 3: Material properties of L/PZT poled at RT and 200degC

Parametr	RT	200°C
ε_r	560	600
d_{33} (pC/N)	41.7	42.0
g_{33} ($\times 10^{-4}$ V·m/N)	84.1	79.0

Conclusions

Relative dielectric constants of PZT/PZT films were successfully controlled by PZT powder phase property. However, d_{33} control of the PZT/PZT film by PZT powder property was difficult. It was suspected that electrical field was not sufficiently applied to A powder phase during the poling because relative dielectric constant of A was much higher than that of sol-gel phase.

References

[1] M. Kobayashi, C.-K. Jen, and D. Lévesque, "Flexible ultrasonic transducers," *IEEE Transactions on Ultrasonics, Ferroelectrics and Frequency Control*, 2006.

[2] J.-L. Shih, M. Kobayashi, J.-F. Moison, and C.-K. Jen, "Energy harvesting using piezoelectric thick films fabricated by a sol-gel process," *Proc. CanSmart Meeting: International Workshop on Smart Materials and Structures*, 2008.

Antibacterial properties of iodine-doped amorphous carbon films

Masaaki Yamazato
University of the Ryukyus, Okinawa, Japan

Introduction

Amorphous carbon thin films have unique properties such as high hardness, transparency, chemical inertness, and biocompatibility. These unique properties are suitable for a hard coating film on mechanical tools, a wear-resistant film on hard disks, transparency coating film on optical components and medical instruments and devices.

In the medical field, infections are particularly likely to occur due to the presence of sick patients and those with weakened immune systems. Therefore, it is necessary to minimize infections caused by medical devices, known as device-related infections. Furthermore, after the Covid-19 pandemic, the development of antibacterial materials has become increasingly important, not only in the medical field but also in everyday use. It has been reported fluorinated amorphous carbon film, Ag-doped amorphous carbon film and Cu-doped amorphous carbon exhibit antibacterial properties [1-4]. Iodine is known as having a strong bactericidal efficacy. Iodine has a broad antibacterial spectrum and is effective against Gram-positive and Gram-negative bacteria, mycobacterium tuberculosis, spores, moulds, and viruses. Additionally, iodine shows bactericidal effects by reacting with proteins on the bacterial surface and inactivating bacteria due to its strong oxidising power and is thought to be different from ordinary drugs in that it does not form resistance. In this work, we investigated the antibacterial properties of iodine-doped amorphous carbon nitride (a-CNx:H) films.

Experimental

Films were deposited by RF plasma CVD with CH4 and N2 gasses. After film deposition, iodine doping was carried out in the vessel with Ar flow. The sample was placed in the petri dish with the iodine solid, then this dish was heated at 100°C. The antibacterial properties of sample against S. cerevisiae were estimated by the disk diffusion test and the survival test. In the disk diffusion test, sample is placed on the surface of the inoculated agar medium, and the bacteria are incubated. If the sample is antimicrobial, a growth inhibition area (halo) is formed around it. The antibacterial activity is assessed by measuring the diameter of the halo, which corresponds to the area where bacteria are unable to grow. The survival test, the same method as reported by H. Wang et al. was used [4]. Samples were placed in wells of a plate, and 0.2 ml of bacterial suspension was added to each well. The samples were immersed in the suspensions for 2 hours at 37°C. Following this, the samples were taken out and rinsed with 0.8 ml of phosphate-buffered saline (PBS) to remove the bacteria attached to them. The resulting mixture of bacterial suspension and rinsed PBS was spread onto an agar medium and then incubated at 37 °C for 48 hours [4]. The bactericidal activity was estimated by counting the number of bacterial colonies on each agar medium.

Results

The results of disk diffusion test for the non-dope a-CNx:H film (control sample) and iodine-doped a-CNx:H film with a composition ratio of carbon and iodine (I/C) of 0.25 were shown in Fig. 1(a) and (b), respectively. Iodine-doped film has a growth inhibition area around the sample, while the control sample has no halo area; therefore, these results show that iodine-doped films have antibacterial capability. Fig. 2 shows the relationship between diameter of the inhibition area and the composition ratio of iodine to carbon. This result suggests that the antibacterial efficiency may be determined by the iodine content in the films.

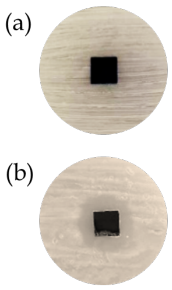

Figure 1. Disk diffusion test. (a) Control, (b) Iodine-doped sample.

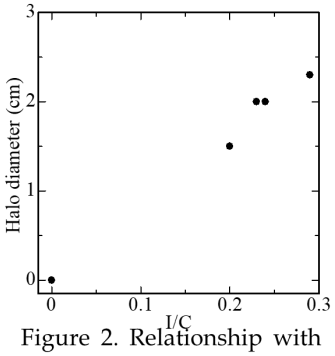

Figure 2. Relationship with iodine composition and halo diameter.

In the results of survival test, there was around 200 fungus colonies with control sample, while that was less than 3 with iodine-doped sample (I/C=0.25), these results showed the iodine-doped a-CNx:H films is one candidate for antibacterial coating material.

References

[1] F.R. Marciano, D.A. Lima-Oliveir, N.S. Da-Silva, E.J. Corat, V.J. Trava-Airoldi, *Antibacterial activity of fluorinated diamond-like carbon films produced by PECVD*, Surf. Coat. Technol. Vol. 204, 2986, 2010.

[2] A. Mazare, A. Anghel, C. Surdu-Bob, G. Totea, I. Demetrescu, D. Ionita, *Silver doped diamond-like carbon antibacterial and corrosion resistance coatings on titanium*, Thin Solid Films Vol. 357, 16, 2018.

[3] Y. Chan, C. Huang, K. Ou, P. Peng, *Mechanical properties and antibacterial activity of copper doped diamond-like carbon films*, Surf. Coat. Technol. Vol. 206, 1037, 2011.

[4] H. Wang, L. Wang, X. Wang, *Structure characterization and antibacterial properties of Ag-DLC films fabricated by dual-targets Hi-PIMS*, Surf. Coat. Technol. Vol. 410, 126967, 2021.

Observation of Seed Condition Change by Atmospheric Pressure Plasma Irradiation

Shin-ichi Aoqui[1)], Masaaki Yamazato[2)], Kouji Yamauchi[1)], Noriko Horibe[1)], Eiji Sakai[1)], Oleksandr Boiko[3)], Henryka D. Stryczewska[3)]
[1)]Dept. of Computer and Information Sciences, Sojo Univ., Japan
[2)]Faculty of Eng., Univ. of the Ryukyus, Japan
[3)]Dept. of Electrical Eng. and Electrotechnology, Lublin Univ. of Tech., Poland

Introduction

The use of plasma technology in agriculture has been focus of much research in recent years. These studies constitute a new research field called "plasma agriculture". Plasma can easily produce energetic and active particle species, which can have effects quite different from those of ordinary chemical reactions. In the case of agricultural applications, cost awareness is important, but generally the unit cost of atmospheric pressure plasma equipment is not very high and, in the case of seed irradiation, the treatment time is very short in comparison to the cultivation time. Plasma sources have often been studied using dielectric barrier discharges (DBD). However, DBD is expensive for large-scale treatments and it is not easy to obtain large power consumption. On the other hand, gliding arc discharge (GAD) is attractive for agricultural applications because GAD allow large power input and a low thermal stress at room temperature. Low initial and running costs and ease of maintenance are important factors in agricultural applications. Non-thermal equilibrium and non-steady-state properties are not a problem in seed treatment. We have previously investigated changes in seed surface conditions induced by GAD plasma irradiation, such as changes in water repellency and changes in seed water absorption properties. In the present study, seeds of pumpkin, radish (Raphanus sativus var. sativus), kidney bean and komatsuna (Japanese mustard spinach) were treated with single-phase GAD with several gas species, and the surface and cross-sectional conditions of the seeds were observed using a scanning electron microscope (SEM) (HITACHI Miniscope TM4000), and elemental composition was analysed using EDS.

Experiment

Fig. 1 shows gliding arc discharge system used in this study. Although the figure shows argon gas as the introduced gas, 4 different gases were used in this study: argon (Ar), argon (Ar) + oxygen (O2), carbon dioxide (CO2), and nitrogen (N2). The seeds were placed on a rotating sample holder to ensure uniformity of plasma irradiation. Iron was used for the electrodes.

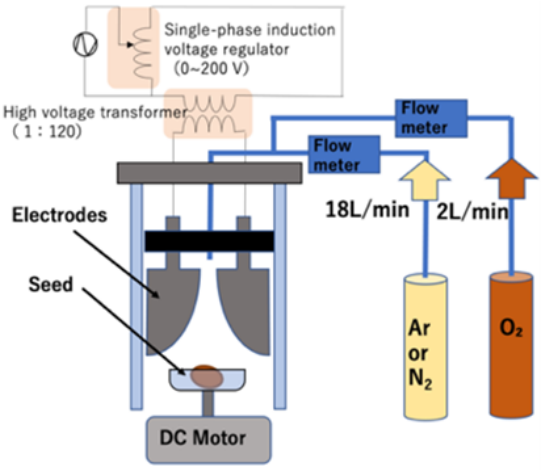

Fig. 7. Experimental setup for plasma irradiation

Total gas flow rates were maintained at 20 l/min for all gases. The mixing ratio of Ar to O_2 was 5:1. Three different positions of the discharge electrode and sample holder were used, and irradiation durations from 30 to 180 seconds were used. High-voltage probes and current probes were used to monitor the discharge to ensure its stability. Thermocouple thermometers were installed in the seed holders to measure the temperature rise during discharge.

Fig. 2 shows a cross-sectional SEM image of a pumpkin seed treated at a position directly exposed to argon (20 l/min) plasma. The right side was the plasma-exposed surface. 150 μm depth from the seed surface was analyzed for composition by EDS. Plasma irradiation caused changes in the structure of the tissue. Water droplet contact angles were measured, and it was confirmed that the wettability of the irradiated surface was improved. Plasma treatment reduced the contact angle of water droplets from 10% to 15It was confirmed that the seeds became hydrophilic.

References

[1] S. Aoqui, et al., *ELMECO and AoS*, 2017.
[2] S. Aoqui, et al., *IIAI-AAI*, 2015.
[3] S. Aoqui, et al., *Physics Procedia*, 2016.
[4] S. Aoqui, et al., *IEEE Transactions on Plasma Science*, 2016.

Pro-ecological aspects of soft magnetic material applications

Mariusz Najgebauer
Częstochowa University of Technology, Faculty of Electrical Engineering

Introduction

Magnetic cores made of soft magnetic materials are an integral part of transformers, electric machines and power electronic devices. Soft magnetic material properties, such as maximum induction, coercivity, permeability and specific loss, determine the final properties of devices, including their efficiency. The article presents the production method and properties of modern, commercially used soft magnetic materials, mainly in the context of their pro-ecological advantages, as well as the environmental benefits resulting from their use as magnetic core materials of electrical devices.

The basic magnetic materials used in electric machines are non-oriented and grain-oriented electrical steels. Non-oriented steels, due to the isotropy of their properties, are mainly used in rotating machines (generators, motors). Grain-oriented steels are characterized by the strong anisotropy of magnetic properties, resulting from the grains arrangement in the rolling direction (the Goss texture). The electrical steels have very good magnetic properties, but also some disadvantages (e.g. relatively high specific loss) that limit their use in high-frequency applications or in power electronic devices. For many years, intensive material research has been conducted to improve the properties of conventional magnetic materials and to develop materials with unique magnetic and mechanical properties. The results of this research are new types of soft magnetic materials, such as amorphous and nanocrystalline alloys, high-silicon electrical steels and soft magnetic composites.

Amorphous alloys

Amorphous alloys are magnetic materials that do not have a crystalline structure but are characterized by a lack of atoms order. This structure resembles glass, which is why these materials are also called as metallic glasses. The amorphous structure is obtained by rapid cooling the liquid material. This process takes place at a speed of 104-106 K/s, which allows the material to pass from the liquid phase to the solid phase, omitting the crystallization process.

Amorphous ribbons are characterized by lower values of saturation induction and higher magnetostriction coefficient, compared to grain-oriented electrical steels. On the other hand, the undoubted advantage of amorphous ribbons is their 3-4 times lower level of specific losses in relation to grain-oriented steel, which results from the high resistivity and small thickness of amorphous ribbons. Magnetic properties of amorphous ribbons and GO steel are compared in Fig. 1 [1-4].

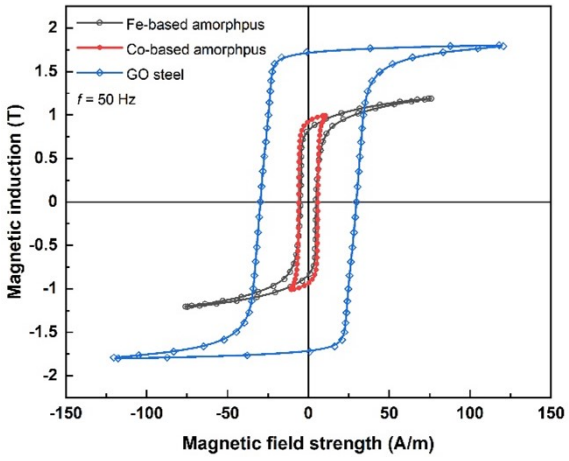

Fig. 8. Hysteresis loops for amorphous ribbons and GO steel [4]

Core losses of amorphous transformers are about 70-80% lower than those of conventional units with GO steel cores. taking into account the average lifetime of a transformer (30-35 years) and the continuous nature of its operation, even a small improvement in its efficiency (as a result of reducing core losses) can result in significant electricity savings. It is estimated that in the 6 most economically developed countries or regions of the world there are over 83 million distribution transformers in operation, of which nearly 3.6 million units are located in the European Union (EU-25). Losses arising in the cores of these transformers correspond to 33% of the total energy losses in the power system, which is about 2% of the generated electricity [5-7]. The operation of amorphous core transformers can be also considered as a way to reduce the greenhouse effect and related climate changes. The use of energy-saving amorphous transformers can contribute directly to the reduction of greenhouse gas emissions, as presented in Table I.

Table 4: Annual potential reduction of greenhouse gas emissions by application of AMDTs [4, 5-8]

Country /region	**CO_2 million tons**	**NO_x thous. tons**	**SO_2 thous. tons**
USA	60[1] / 35[2]	110	260
EU-25 / Europe	15[1] / 20[2]	70	160
Japan	17[1] / 10[2]	30	75
China	13[1] / 12[2]	90	210
India	3[1] / 3[2]	22	52
Australia	3[1]	—	—
Total	111[1] / 80[2]	322	757

[1] Leonardo ENERGY (European Copper Institute)
[2] US Environmental Protection Agency

Nanocrystalline alloys

Magnetic materials with a nanocrystalline structure are obtained in the controlled crystallization process of amorphous ribbons. Amorphous ribbons are annealed at a temperature higher than their primary crystallization temperature, usually 500-570°C. As a result of this process, two-

phase materials are obtained in which α-Fe(Si) grains are placed in the residual amorphous matrix. The crystalline phase covers about 70-80% of the total volume material. The optimal size of the α-Fe(Si) grains, which determines the best magnetic properties, is in the range from 10 nm to 15 nm. Nanocrystalline alloys have favourable magnetic properties, including: coercivity H_C lower than 1 A/m, "near-zero" magnetostriction $\lambda_S \approx 1 \cdot 10^{-7}$ and a very high initial permeability $\mu_i = 100 \cdot 10^3$. Saturation induction in nanocrystalline alloys ranges from relatively low values $B_S = 1.2$ T (Finemet) to high values $B_S = 1.5 - 1.8$ T (Nanoperm) and $1.6 - 2.1$ T (Hitperm). Nanocrystalline ribbons have very low energy losses in a wide frequency range, which is related to their very small thickness and high resistivity, as well as "near-zero" magnetostriction. Magnetic properties of amorphous and nanocrystalline ribbons are compared in Fig. 2 [2, 4, 8-10].

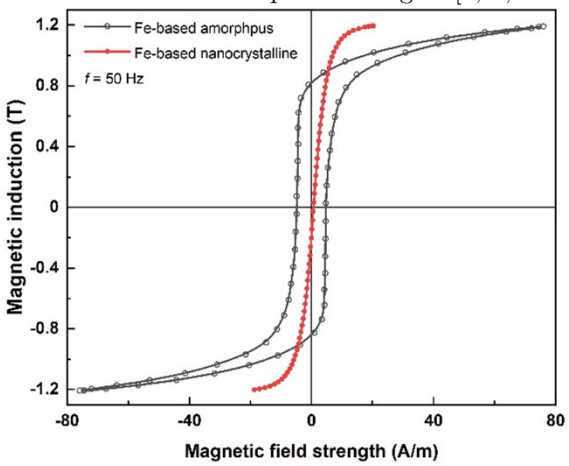

Fig. 9. Hysteresis loops for nanocrystalline and amorphous ribbons [4]

Nanocrystalline cores are often used in power transformers operating in Switched Mode Power Supplies (SMPS). The properties of nanocrystalline alloys, in particular low loss and high saturation induction, allow for a significant reduction in the size and weight of the transformer, and thus the entire SMPS system. It is estimated that transformers with Vitroperm cores may be even 50% smaller than transformers with ferrite cores, as depicted in Fig. 3.

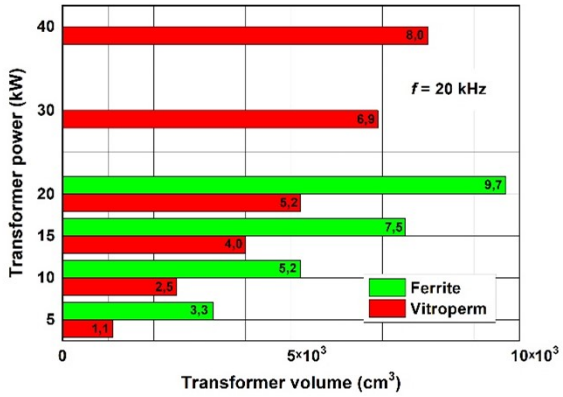

Fig. 10. Ferrite and nanocrystalline cores for SMPS systems [4]

High-silicon steels

The further reduction of magnetic losses in electrical steels by increasing the silicon content has become possible thanks to the Chemical Vapor Deposition process, developed in Japan by the JFE Steel Corporation. This process enables the production of electrical steel with a silicon content of approx. 6.5% on an industrial scale. In the CVD process, non-oriented 3% Si steel is annealed in SiCl4 atmosphere, which creates a high-silicon content layer of Fe3Si on steel surface areas. Next the material is reannealed in a pure hydrogen atmosphere, which causes the diffusion of silicon atoms inside the material. As a result, high-silicon steels with a microcrystalline structure with grains of 0.1-10 μm are obtained. High-silicon steels, due to the increased silicon content and microcrystalline structure, have "near-zero" magnetostriction, saturation induction of 1.84 T and low energy losses. Thus, these steels combine the advantages of conventional electrical steels (high saturation induction) and amorphous ribbons (low losses). Magnetic properties of high-silicon and NO steels are compared in Fig. 4 [4, 11-13].

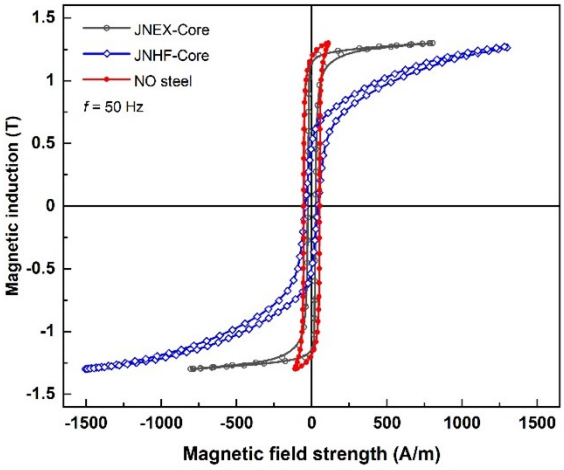

Fig. 11. Hysteresis loops of high-silicon and conventional steels [4]

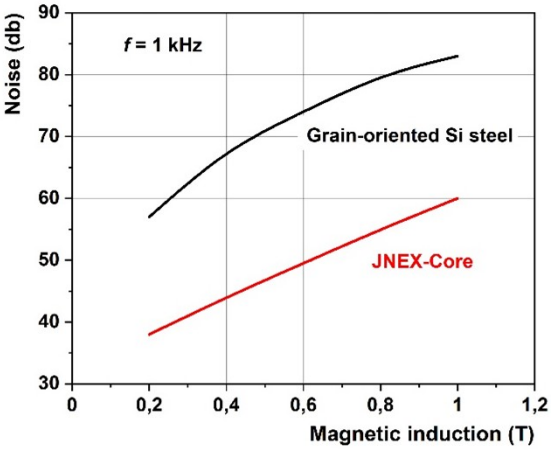

Fig. 12. Noise level generated by a transformer cores [4]

Due to the specific properties, high-silicon steels are mainly used for the production of packed cores for devices operating at increased frequencies (power electronics) and in devices with a reduced level of emitted noise. In the case of transformer cores operating at increased frequency, the use of high-silicon steels reduces the noise level by about

10-25 dB, as depicted in Fig. 5.

Soft magnetic composites

Soft magnetic composites are materials that combine favourable magnetic and mechanical properties, and thus enabling miniaturization and tailoring of magnetic circuits in electric machines. The main component of these materials is magnetic powder, obtained by grinding magnetic material in high-energy mills or by atomizing materials from the liquid phase. The magnetic powder is doped with dielectric binders (resins or polymers) and then formed into a final magnetic circuit. Dielectric binders create an insulating layer on powder grain surfaces. This layer isolates grains from each other, which affects the material physical properties. In addition, dielectric layers increase the resistivity of magnetic composites, which limits the eddy current flows and reduces magnetic losses, especially at higher frequencies. However, an increase in the dielectric content of magnetic composites deteriorates their magnetic properties (as depicted in Fig. 6), but at the same time improves their mechanical properties [4, 14-17].

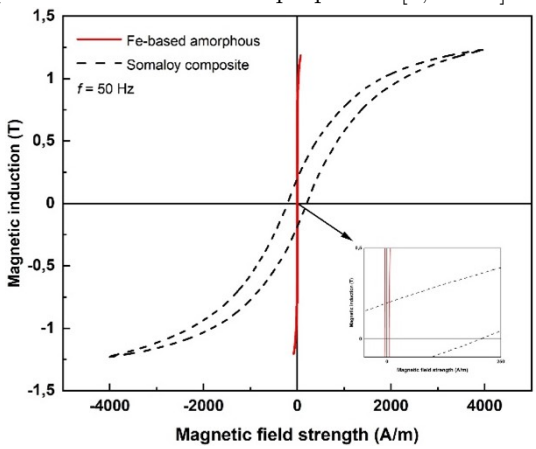

Fig. 13. Hysteresis loops of amorphous-based composite materials [4]

The use of soft composites in electrical devices combined with the appropriate design of their magnetic circuits allows to significantly reduce the number of used parts, reduce the size and weight of the device, as well as reduce manufacturing costs. The construction of a linear motor stator made of electrical steels and magnetic composites is depicted in Fig. 7. The stator made of electrical steels consists of several hundred elements grouped into blocks, while in the case of a magnetic composite the stator is made of two identical elements [18].

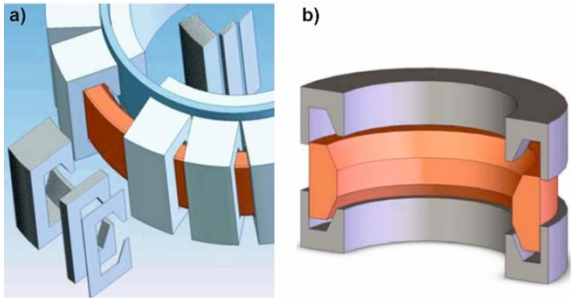

Fig. 14. Construction of the linear motor: a) stator made of Fe-Si steels, b) stator made of magnetic composite [4, 19]

The use of magnetic composites in electrical devices is also important for ecological reasons. The production of magnetic composite cores is an almost waste-free technology. In the case of composite materials, the cores are subjected to mechanical grinding, which ensures simple segregation and recycling of construction materials, while in the case of Fe-Si steel cores, this process is complicated and expensive [19].

Conclusions

New types of soft magnetic materials have favourable magnetic properties (such as high saturation induction, low magnetic losses and "near-zero" magnetostriction) or a unique combination of magnetic and mechanical properties. Their use in electrical machines and power electronic systems allows for improving the efficiency of devices, reducing their dimensions and total weight, as well as reducing the emitted noise. The benefits of using modern soft magnetic materials also include ecological benefits (reduction of greenhouse gas emissions, noise reduction, easier recycling of materials).

References

[1] F. Fiorillo, G. Bertotti, C. Appino, M. Pasquale, *Soft magnetic materials, in Wiley Encyclopedia of Electrical and Electronics Engineering*, John Wiley & Sons Inc., New Jersey, USA, vol. 19, pp. 425–445, 1999.

[2] M.E. McHenry, M.A. Williard, D.E. Laughlin, *Amorphous and nanocrystalline materials for applications as soft magnets*, Prog. Mater. Sci., vol. 44, no. 4, pp. 291–433, 1999.

[3] R. Hasegawa, *Present status of amorphous soft magnetic alloys*, J. Magn. Magn. Mater., vol. 215-216, pp. 240–245, 2000.

[4] M. Najgebauer, *Advances in contemporary soft magnetic materials – a review*, 10th International Conference on Electrical, Electronic and Computing Engineering (IcETRAN), East Sarajevo, Bosnia and Herzegovina, 2023, pp. 1-10, IEEE Xplore.

[5] N. DeCristofaro, *Amorphous metal in electric power distribution applications*, MRS Bulletin, vol. 23, pp. 50–66, 1998.

[6] R. Targosz (edit.), *The potential for global energy savings from high efficiency distribution transformers*, European Copper Institute, Belgium, 2005.

[7] M. Najgebauer, K. Chwastek, J. Szczygłowski, *Energy efficient distribution transformers*, Prz. Elektrotechniczn., vol. 87, no. 2, pp. 111–114, 2011.

[8] G. Herzer, *Soft magnetic nanocrystalline materials*, Scripta Matellurgica et Materialia, vol. 33, pp. 1741–1756, 1995.

[9] Y. Yoshizawa, *Magnetic properties and applications of nanostructured soft magnetic materials*, Scripta Mater., vol. 44, pp. 1321–1325, 2001.

[10] R.B. Schwarz, T.D. Shen, U. Harms, T. Lillo, *Soft ferromagnetism in amorphous and nanocrystalline alloys*, J. Magn. Magn. Mater., vol. 283, pp. 223–230, 2004.

[11] H. Haiji, K. Okada, T. Hiratani, M. Abe, M. Ninomiya, *Magnetic properties and workability of 6.5% Si steel sheet*, J. Magn. Magn. Mater., vol. 160, pp. 109–114, 1996.

[12] S. Crottier-Combe, et al., *The Magnetic Properties of Fe-Si 6.5 wt% alloys obtained by a $SiCl_4$-based CVD process*, J. Magn. Magn. Mater., vol. 160, pp. 151–153, 1996.

[13] M. Najgebauer, K. Chwastek, J. Szczygłowski, *Electrical steel sheets with high silicon content – properties and ap-*

plications (in Polish), Prz. Elektrotechniczn., vol. 80, no. 12, pp. 1225–1227, 2004.

[14] L.O. Hultman, Y. Zhou, *Soft magnetic composites – properties and applications*, Proc. World Congress on Powder Metallurgy and Particulate Materials, 13p., Orlando, USA, 2002.

[15] H. Shokrollahi, K. Janghorban, *Different annealing treatments for improvement of magnetic and electrical properties of soft magnetic composites*, J. Magn. Magn. Mater., vol. 317, pp. 61–67, 2007.

[16] L.A. Dobrzański, B. Ziębowicz, M. Drak, *Mechanical properties and the structure of magnetic composite materials*, J. Achiev. Mater. Manuf. Eng., vol. 18, pp. 79–82, 2006.

[17] M. Najgebauer, J. Szczygłowski, B. Ślusarek, M. Przybylski, A. Kapłon, J. Rolek, *Magnetic composites in electric motors in Lecture Notes in Electrical Engineering*, vol. 452, Springer, Cham, Switzerland, ch. 2, pp. 15–28, 2018.

[18] L.-O. Pennander, G. Nord, K. Maezawa, M. Saito, D. Berchowitz, *Design of soft magnetic composite components for tubular linear motors*, Proc. Motor and Drive System Conference, 9p., Miami, Florida, USA, 2006.

[19] L.O. Hultman, O. Andersson, *Advances in SMC technology – materials and applications*, Proc. International Congress & Exhibition, 6p., Copenhagen, Denmark, 2009.

Henryka Danuta Stryczewska1, Grzegorz Karol Komarzyniec1, Kenji Ebihara2, Shin-ichi Aoqui3, Masaaki Yamazato4, Mykhaylo Zagirnyak5

Key factors enhancing the electrical properties of nanofluids. A mini-review of the applications in the energy-related sectors

Oleksandr Boiko[1)], Henryka Danuta Stryczewska[1)], Grzegorz Karol Komarzyniec[1)], Kenji Ebihara[2)], Shin-ichi Aoqui[3)], Masaaki Yamazato[4)], Mykhaylo Zagirnyak[4)]
[1)]Department of Electrical Engineering and Superconductivity Technologies, Lublin University of Technolology, Lublin, Poland
[2)]Environment and Energy Laboratory, Kumamoto, Japan
[3)]Faculty of Computer and Information Sciences, Sojo University, Kumamoto, Japan
[4)]Department of Electrical and Electronics Engineering, University of the Ryukyus, Okinawa, Japan
[5)]Department of Systems of Automatic Control and Electric Drive, Kremenchuk Mykhailo Ostrohradskyi National University, Kremenchuk, Ukraine

Abstract
The article presents a mini-review of key factors significantly affecting the electrical properties of nanofluids. One-step and two-step approaches, together with examples of vacuum sputtering-based techniques, chemical reduction, and mechanical mixing techniques, were explained. The crucial factors enhancing the electric and dielectric responses, such as nanofiller concentration, its type, geometry, uniformity of distribution in the base liquid as well as the base liquid's type, temperature, chemical stability, etc., were analyzed. Special attention was paid to the impact of the parameters on electrical conductivity, permittivity, and dielectric losses. The selected models for nanofluid's conductivity prediction have been presented. The potential and implemented applications of nanofluids in the energy-related industry branches with reference to their electrical properties have been reviewed. Examples of applications in power transformers, solar cell production processes, nanoelectrofuel flow batteries, and other electrotechnologies have been analyzed.

Examples of impacts of mass fraction on the electrical response of nanofluids

Among a wide spectrum of modern nanostructures, liquid nanomaterials deserve special attention due to their physicochemical properties, especially thermal, chemical, and optical ones. Nanofluids (NFs) are considered colloidal suspensions containing nanoparticles (NPs) in a liquid matrix, which is a base fluid (BF). NFs usually contain nanoparticles of pure metals (i.e., Ag, Au, Ni) and metal oxides (i.e., Fe_3O_4, CuO, Al_2O_3), silicon oxide, carbides (SiC, WC, TiC), and carbon nanotubes and graphene of various configurations as nanofillers. In many cases, water, ethylene glycol (EG), oils (transformer, mineral, vegetable), and paraffin are used as the BFs. The example of the Fe_3O_4-H_2O magnetic NFs (Fig. 1b) and the impact of gravity on the sedimentation of nanofiller as well as the differences between mono and hybrid NFs (Fig. 1a) are shown in Fig. 1.

Fig. 2a presents a crucial impact of the nanofiller and temperature on the electrical conductivity of the EG-TiO_2 NF, where A corresponds to the TiO_2 powder with anatase phase.

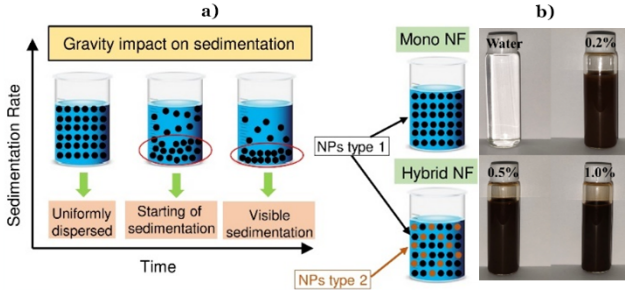

Fig. 15. a) gravity impact on NP sedimentation and mono and hybrid NFs; b) Fe3O4-H2O magnetic nanofluids with Fe_3O_4 ranging from 0.2 wt.% to 1.0 wt.%

An increase in ϕ_v causes a further significant increase in conductivity, showing a maximal enhancement at 45°C of about 1300% (black labels). An increase in temperature from 10°C to 45°C results in an increase in conductivity of about 300%. Fig. 2b and 2c show the drastic impact of the mass fraction on the electric permittivity and dielectric loss factor, respectively. The permittivity increases with a maximum enhancement of about 30%, and the dielectric loss decreases gradually with a maximum drop of 50%.

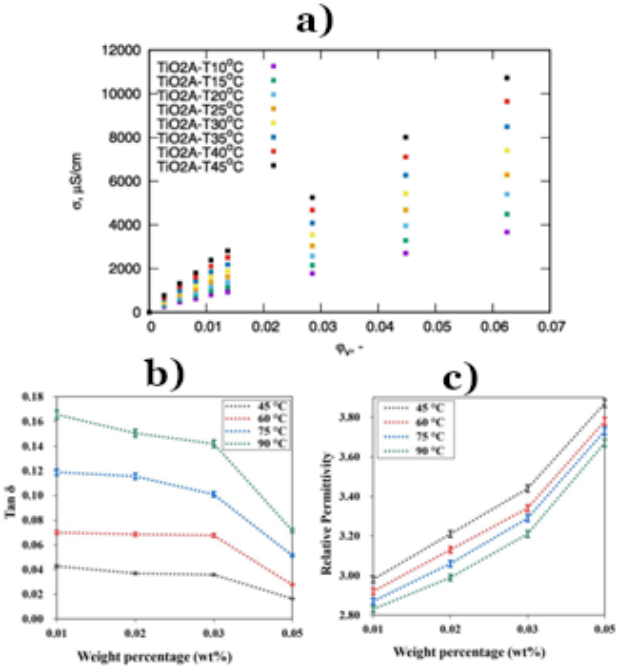

Fig. 16. Impact of volume fraction on the electric properties of NFs: a) conductivity of type A NF, b) relative permittivity and c) dielectric loss of CSO-based Al_2O_3 NFs

Reflective lecture and piano concert Modelling, Simulation and Music

performed by
Krzysztof Kluszczyński

The human mind's ability to create models is the most fascinating feature of the brain. Throughout human history, for many millennia, models have been formulated in linguistic way using words. Since the seventeenth century, thanks to the invention of integral calculus by Gottfried Wilhelm Leibniz (1646-1716), models have been expressed in mathematical terms using differential equations. Nowadays, many scientists are fascinated by artificial intelligence, resulting in models that utilize neural networks, fuzzy sets, expert systems or genetic algorithms.

The most esentiale goal of the lecture and piano concert will be to convince the audience that models can also be described in the language of music and that in many cases such models are better in representing, and illustrating reality than linguistic or mathematical models.

Musical models of various systems and physical phenomena will be presented. These models will focus on highlighting different operating states, behaviours and selected features of the modeled technical objects, as well as the simulated phenomena.

On the example of diferent pieces composed by famous Polish, German and Hungarian artists living in different eras: Fryderyk Chopin, Franz Liszt, Franz Burgmüller, Roman Statkowski and Ignacy Jan Paderewski the music models of selected mechanical systems e.g. a bell, electrical systems having digital or analog nature, well as the models of different types of natural atmospheric phenomena e.g. a storm will be demonstrated on the grand piano.

Visualization and Calibration Free Quantification of Two Dimensional Sound Pressure Distribution with Optical Wave Microphone CT Scanning

Than Nu Nu San[1)], Aung Myint Myat[1)], Si Thu Han[1)], Fumiaki Mitsugi[1)]
[1)]Kumamoto University

The optical wave microphone which uses Fraunhofer diffraction of a laser beam has become an innovative technique in recent years. It shows promise for utilisation in a variety of acoustic domains where the use of conventional microphones is restricted by high electric and/or magnetic fields. The present investigation utilised calibration free quantification and computed tomography (CT) scanning with an optical wave microphone to visualise and measure the two dimensional sound pressure distribution emitted by an ultrasonic oscillator operating at 40 kHz.

Introduction

In some industries, the use of conventional microphones (dynamic and condenser types) is impracticable due to the presence of strong electric, magnetic, and electromagnetic fields. Conventional microphones can cause damage in a strong electromagnetic field, and the sound field may be automatically disrupted when the detector approaches the target. Due to the characteristics of the diaphragm and the multiple reflection of sound between the diaphragm and targets, these microphones are limited in terms of detectable frequency range and measurement precision. Consequently, optical techniques for sound field analysis become indispensable. Because the optical wave microphone (OWM) depends on the far field effect of Fraunhofer diffraction between the probe laser and changes in the refractive index b rought about by acoustic waves. The interoperability of this approach with computed tomography (CT) has been investigated. In this study, an OWM CT scan system without cali bration was used to alter the distance between an ultrasonic oscillator and a laser beam in order to observe and quantify changes in the two dimensional distribution of sound pressure. By means of comparison with the sound pressure distribution measurement s derived from a condenser microphone, the measurement results of the two dimensional sound pressure distribution with the calibration free OWM CT scan were clarified.

Principle of OWM with CT scanning

The experimental configuration of the fiber type optical wave microphone CT scan system is illustrated in Fig. 1. The system incorporates a fiber laser (637 nm, 7 mW, 1.5 mm in diameter), a lens (focal length = 7.93 mm), a fiber (single mode, core diameter: 4.3 μm, length: 5 m), and a detector (Hamamatsu , S5935 01). The optical wave microphone's output waveform is captured using an oscilloscope (Tektronix, TBS2000B Series). The target, an ultrasonic oscillator (40 kHz, Murata, MA40S4S), is driven by a function generator (GWInstek SFG 2004) and is positi oned on two stages that move along the X direction and Θ direction, respectively, both of which are controlled by LabVIEW software. LabVIEW was used to calculate and operate the entire system, which included target movement control, OWM measurement, and data reconstruction.

With projected data from many directions spanning at least 180 degrees, the CT scan system developed for this study was used to reconstruct a cross sectional image of the acoustic field utilizing the projected data. In the reconstructed image, sound pressure was quantified from the amplitude of the signal voltage by employing the equation (1).

$$\Delta p(x) = \frac{V_{AC(x)}}{V_{DC}\frac{k_i d(x)(\mu_0-1)}{\gamma p}\left[e^{-u^2-(u-\Theta)^2}-e^{-u^2+(u+\Theta)^2}\right]\sin\omega_p t} \quad (1)$$

Where, Δp denotes sound pressure (Pa), $d(x)$ represents the inciden t distribution of sound waves, V_{DC} denotes the DC voltag e component of the signal, and $V_{AC}(x)$ denotes the amplitude of the signal voltage. Therefore, t he calibration free optical wave microphone CT scan can facilitate the successful visualization of two dimensional sound pressure distribution and quantify sound pressures derived from this technique are found to be in close agreement with those obtained from the condenser microphone across varying measurement distances.

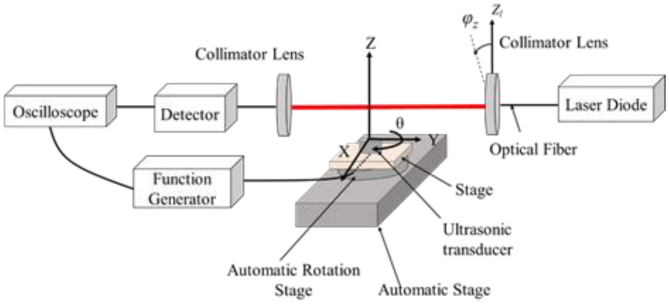

Fig. 17. Experimental configuration of the optical wave microphone computed tomography (CT) scan

References

[1] Evans, D.E., et al., *Fourier optics approach to far forward scattering and related refractive index phenomena in laboratory plasmas*, Plasma Physics, 24(7), p.819, 1982.

[2] Ortiz, P.F.U., *2D and 3D visualization of acoustic waves by optical feedback interferometry*, (Doc toral dissertation, Institut National Polytechnique de Toulouse INPT), 2019..

[3] Mitsugi, F., et al., *Quantification of two dimensional acoustic field generated by a surface barrier discharge with fiber type optical wave microphone computer tomography*, IEEE Transactions on Plasm a Science, 49(11), pp.3589 3596, 2021.

Estimation the direction of arrival sound source using optical wave microphone and raspberry pi camera module

Htet Lin Aung[1)], Yuki Hori1[1)], Fumiaki Mitsugi1[1)]
[1)]Kumamoto University

The use of light that does not affect the sound field allows for the achievement of sound information even in areas where microphone installation is difficult. The sensor part of the optical wave microphone is a laser beam, which enables sound detection in a non-contact state. Photo diodes or other devices that can extract minute changes in light are needed for detection. However, using numerous photodiodes at various positions presents a real-time sound direction estimation challenge. So, a Raspberry Pi camera is installed on the observation plane to capture laser light images. The difference between the laser light images with and without sound is accomplished to clarify where the intensity distribution appears. As a result, the signal intensity distribution in relation to the direction of the sound wave was confirmed, and the signal component due to weak diffracted light was successfully extracted.

Introduction

The direction of arrival sound (DOA) detection has potential applications in video conferencing, noise source tracking, and remote monitoring of abnormal sounds, highlighting its importance in modern technology. The optical wave microphone uses laser light to convert sound into an electrical signal through optical Fourier transformation of weak diffraction light caused by sound-induced phase modulation. The intensity distribution of diffracted light was obtained by taking the difference between the results obtained when ultrasonic waves were applied and when no ultrasonic waves were applied. The intensity distribution of the incoming and outgoing sound waves will show a certain phase and these two types of intensity distributions were always in opposite phases. This indicates that the direction of incident sound waves can be estimated from the intensity distribution even when the direction of incident sound waves is unknown.

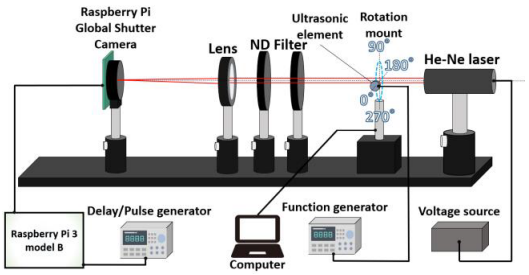

Fig. 18. Experimental setup

Principle of optical wave micropone

When the sound waves at (x0,y0) incident on a laser beam, the sound causes a change in refractive index that will lead to form weak phase modulation of light. This gives weak diffracted light with a Doppler shift of the sound wave's frequency and form a Fourier transform image on the observation surface which was set at the Fraunhofer diffraction region back focal plane (xf , yf) of Fourier Lens. The time-dependent component of intensity Iac is expressed by the following equation,

$$I_{ac} = I_0 \Delta\Phi_0 \left(e^{-(u^2+(u-\theta)^2)} - e^{-(u^2+(u+\theta)^2)} \right) \quad (2)$$

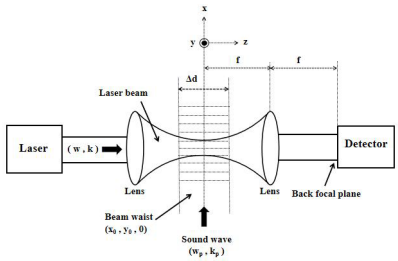

Fig. 19. Basic setup of an optical wave microphone

I_0 is the intensity distribution of the incident laser light and it is described by,

$$I_0 = \frac{2P_0}{\pi w_f^2} e^{-2\left(\frac{\gamma_f}{w_f}\right)^2} \quad (3)$$

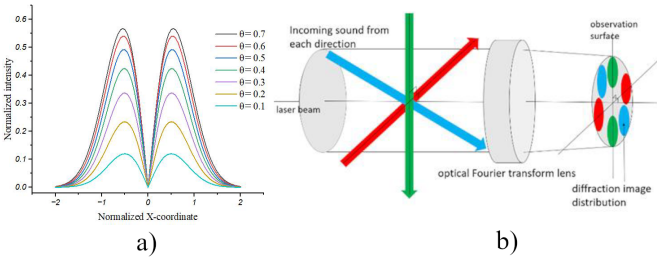

Fig. 20. (a) Intensity Distribution (b) Variation of diffraction image distribution with respect to the direction of sound incidence

References

[1] F. Mitsugi, T. Ikegami, S.I. Aoqui, Y. Tashima, H. Kawasaki, T. Nakamiya, Y. Sonoda, H. Stryczewska, *Application of optical wave microphone to gliding arc discharge*, Przeglad Elektrotechniczny, 88(6), pp.105-107, 2012.

[2] K. Ishikawa, K. Yatabe, Y. Ikeda, Y. Oikawa, T. Onuma, H. Niwa, M. Yoshii, *Optical sensing of sound fields: Noncontact, quantitative, and single-shot imaging of sound using high-speed polarization camera*, In Proceedings of Meetings on Acoustics (Vol. 29, No. 1). AIP Publishing, 2016.

Phase distribution of acoustic pressure visualized by optical wave microphone within the distance of one-cycle wavelength of acoustic wave

Si Thu Han[1)], Fumiaki Mitsugi[1)]
[1)]Kumamoto University

Introduction

The modern technique called "Optical Wave Microphone (OWM)" technique, is based on a Fraunhofer diffraction effect between sound wave and laser beam. The light diffraction technique is very useful to detect the acoustic wave without disturbing the sound field unlike the conventional microphone. OWM can be also applied to realize the visualization of acoustic sound field by computerized tomography (CT) method because the ultra-small modulation by the sound field is integrated along the laser beam path. This method was very useful to perform the high accuracy measurement of slight density change of atmosphere without disturbing electric and sound field. The phase distribution of ultrasonic sound wave is measured by changing the distances between the laser beam and transducer within one wavelength distance of that wave.

Introduction

Predicting sound sources in the electromagnetic field environments is a challenging task because reverberation causes reflection and scattering of sound waves, making it difficult to accurately determine the position of the sound source and the electric field also disturbs the conventional sensors in the strong field region. On the other hand, sound source localization (SSL) is an important technique with widespread applications in different scenarios such as detection of pipeline leakage, electric discharge, laser ablation and auditory navigation for mobile robots. The limitations of conventional microphones such as their detectable frequency range and measurement accuracy, attributable to diaphragm properties and the multi-reflection of sound between the diaphragm and targets. Therefore, the modern measurement technique is developed and it is optical wave microphone (OWM). This measurement system applies the acousto-optic effect, and for the measurement of acoustic pressure, the refractive index, and the environmental conditions such as temperature and atmospheric pressure are taken account. It gives more exact sound information with the changes of the environmental temperature and the refractive index of the environment in which that sound travels. This method can work well even in the electric and magnetic field regions. So, in this research, the computerized tomography (CT) pressure and phase shift distribution, and sound source localization are observed with one ultrasonic oscillator of 40 kHz and it can be estimated to investigate the distance between the sound source and the laser beam.

Experimental setup

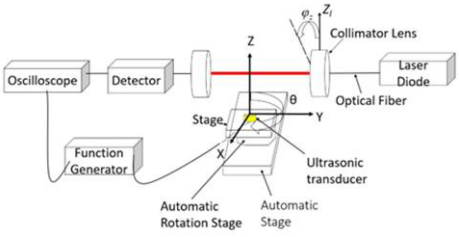

Fig. 21. Experimental setup of Optical Wave Microphone with CT scan

Principal of Optical Wave Microphone

The ultrasonic oscillator is rotated in X-Z axises. By rotating and moving the oscillator like the above way, the results in 8×8 matrix are obtained. In this way, the laser beam is modulated by the sound waves and the voltage signal is obtained. For, by measureing V_{AC}, the sound pressure level is calculated from the following equation:

$$\Delta p(x) = \frac{V_{AC(x)}}{V_{DC}\frac{k_i d(\chi)(\mu_0-1)}{\gamma p}\left[e^{-u^2-(u-\Theta)^2}-e^{-u^2+(u+\Theta)^2}\right]\sin\omega_p t} \quad (4)$$

where Δp= Sound Pressure (Pa), $k_i = 2\pi/\lambda$ = Laser wavenumber, $d(\chi)$= incident width of a sound wave, μ_0 = refractive index, γ= specific heat ratio of air, p = atmospheric pressure, λ= wavelength of laser beam. When the distance between the laser beam and transducer Z is changed, the path difference is Δd and the phase difference is:

$$\Delta\varphi = \frac{\Delta d}{\lambda} \times 360 = \frac{\Delta d}{c} f_u \times 360 \quad (5)$$

where λ= the wavelength of sound wave, c = velocity of sound, and f_u is the frequency of ultrasonic wave. So, according to the above equation, the signal of OWM is shifting by a certain phase in degree with respect to the change in distance Δd . The reconstruction image for the amplitude and phase distribution of complex acoustic pressure can be obtained by inversely projecting the data to X-Z coordinates, in which the filtered back-projection method and Lamp filter function were used as the reconstruction algorithm. The LabVIEW program is developed for the phase shift measurement, and by applying the CT scan, the phase shift distribution is achieved according to the position of the sound source. Therefore, the results of phase shift distribution and sound pressure measurements can estimate the location of the sound source within one-cycle wavelength.

References

[1] Valin, J.; Michaud, F.; Rouat, J.; Letourneau, D., *Robust sound source localization using a microphone array on a mobile robot*, In Proceedings of the 2003 IEEE/RSJ International Conference on Intelligent Robots and Systems (IROS 2003) (Cat. No.03CH37453), Las Vegas, NV, USA, 27–31 October 2003; Volume 2, pp. 1228–1233.

[2] Xu, Q.; Zhang, L.; Liang,W., *Acoustic detection technology for gas pipeline leakage*, Process Saf. Environ. Prot. 2013, 91, 253–261.

[3] Mitsugi, F., Ide, R., Ikegami, T., Nakamiya, T., & Sonoda, Y. (2012), *Optical wave microphone measurement during laser ablation of Si*, Thin solid films, 521, 132-136.

Synchronized Investigation of pressure wave influence on atmospheric pressure plasma jet and plasma-induced liquid flow using optical wave microphone and high-speed camera

Nway Htet Htet Myo, Thuzar Phyo Wai, Fumiaki Mitsugi
Kumamoto University

Plasma-target interaction in atmospheric pressure plasma jets plays a crucial role in biomedical applications, particularly in the transport of reactive oxygen species. In this study, the author has been focused on the impact of pressure wave which was degeneration of the shockwaves, originated from the local heating of the gas around breakdown plasma between electrodes. A novel optical technique, the Optical Wave Microphone (OWM), which was based on Fraunhofer diffraction, was used to detect pressures wave from helium plasma jet. A fibre-type OWM and a high-speed camera were used to investigate the influence of pressure waves on plasma-induced flow and plasma irradiation. The results indicated a strong correlation between pressure wave amplitude and the plasma plume as well as the plasma-induced liquid flow.

Introduction

The schemdic diagram of experimental setup is shown in Figure 1 and it is composed of an atmospheric pressure plasma jet(APPJ) and optical wave microphone. Also, potassium iodide (KI)-starch gel reagent was used to visualize the ROS distribution pattern that are affected by the pressure signal. Plasma plume and induced flow were captured in synchrony using a high-speed camera (Photron FASTCAM SA1.1) with frame speeds of 5,000 fps and resolution of 512 × 384 pixels.

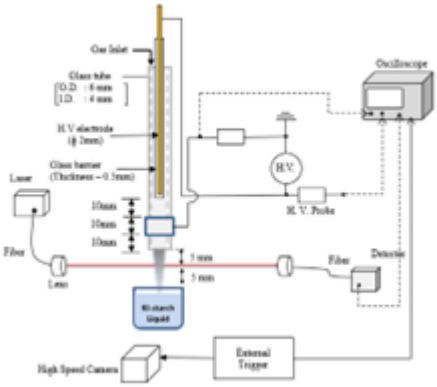

Fig. 22. Schematic diagram of experimental setup

Pressure wave impact on plasm plume and plasma-induced flow

Figure 2. shows the synchronized observation of optical wave microphone and plasma plume images of every 2 ms. To examine the impact of the pressure wave, high-speed camera images were analyzed simutaneously with the optical wave microphone waveform.

As shown in Figure 2, when the amplitude of the pressure waveform was low between 1000-1008 ms, the plasma plume was directed straight at the target. However, with a sharp increase in pressure wave intensity, from 1008-1020 ms, the plume became unstable and curved to the side. From this observation, it was shown that the pressure strongly inluences the instability of the plasma plume. The relationship between the pressure wave impact and plasma-induced liquid flow was also examined. The results indicated that the flow did not originate directly under the center of the plasma jet but rather where the plume curved. From the above results, the influence of the pressure wave should be considered one of the effects that caused the plama-induced flow.

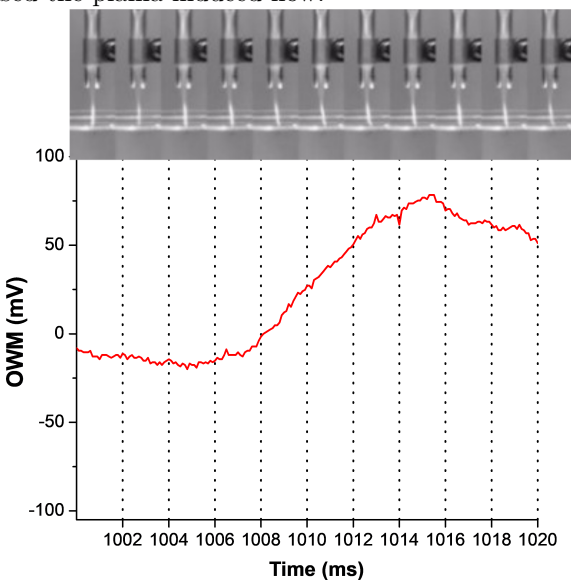

Fig. 23. Synchronized imaging of the plasma plume using the optical wave microphone and high-speed camera. Images are taken at 2 ms intervals

References

[1] F. Mitsugi, T. Nakamiya, Y. Sonoda, and H. Kawasaki, "High-speed camera and fibered optical wave microphone measurements on surface-dielectric-barrier discharges," *IEEE Trans. Plasma Sci.*, vol. 43, no. 8, pp. 2642-2648, Aug. 2015.

[2] F. Mitsugi, S. Kusumegi, T. Nakamiya, Y. Sonoda, and T. Kawasaki, "Detection of pressure wave emitted from plasma jets with fibered optical wave microphone in gas and liquid phases," *IEEE Trans. Plasma Sci.*, vol. 44, no. 12, pp. 3077-3082, Dec. 2016.

[3] F. Mitsugi, T. Nakamiya, Y. Sonoda, and T. Kawasaki, "Time-resolved observation of plasma jets synchronized with fibered optical wave microphone measurement," *IEEE Trans. Plasma Sci.*, vol. 44, no. 11, pp. 2759-2765, Nov. 2016.

Proposal for Security System using Optical Wave Microphone with long-distance laser beam

Seiryu UEDA[1)], Fumiaki MITSUGI [1)], Takashi SAMATSU [2)], Yoshito SONODA[1)]
[1)]Kumamoto University
[1)]Tokai University

Introduction

An Optical Wave Microphone (OWM) using a long-distance laser beam has been proposed as a security system for long-range acoustic monitoring [1, 2]. The OWM detects sound by converting the weak diffracted light, caused by the phase modulation of a laser beam induced by sound waves, into an electrical signal using a photodiode. This system can detect sound directly via the laser beam, offering the advantage of a non-contact method, as there is no need to place objects within the sound field. Additionally, the laser can be easily adjusted with a simple optical setup, allowing for flexible installation. However, for its application as a security system, it is anticipated that a laser beam extending over several tens of meters will be required. Therefore, in this study, an OWM with a laser beam extending over 30 m was configured. Furthermore, by applying low-frequency ultrasound from multiple regions, we confirmed that sound could be detected at any position within the sound field.

Principle of OWM

The theoretical model of the OWM is showed in Fig 1. When sound waves impinge on the laser beam, weak diffracted light is generated. This diffracted light, along with the transmitted light, passes through a lens used for optical Fourier transformation and is then detected by a photodiode. Additionally, the lens on the laser source side is employed to adjust the laser beam diameter.

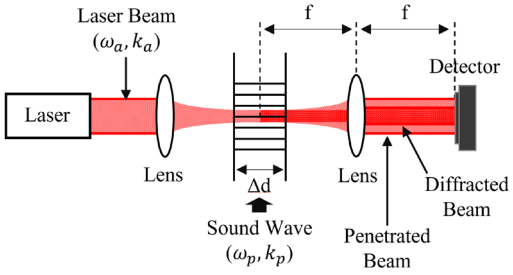

Fig. 24. Theorical model of OWM

Experimental Setup

Fig 2 shows a top view of the experimental setup. A visible light semiconductor laser is used as the laser source. After sound is applied, the laser beam passes through an optical Fourier transformation lens and is then adjusted to the appropriate beam diameter for the detector using lenses f1 and f2. The region between the laser source and the Fourier transformation lens is where sound can be detected, and in this experimental setup, this distance exceeds 30 m. A 25 kHz low-frequency ultrasound element was used as the sound source. The position of the sound source was varied and placed at distances of 0.5, 10, 20, and 30 m from the light source. Although the rayleigh length of the laser is 19.3 m, regions beyond this distance were also examined. The signal observed by the photodiode is amplified and filtered with a high-pass filter by the pre-amplifier (Pre-Amp) before being converted to digital form by the audio interface (Audio I/F) and then captured by the PC as audio signal.

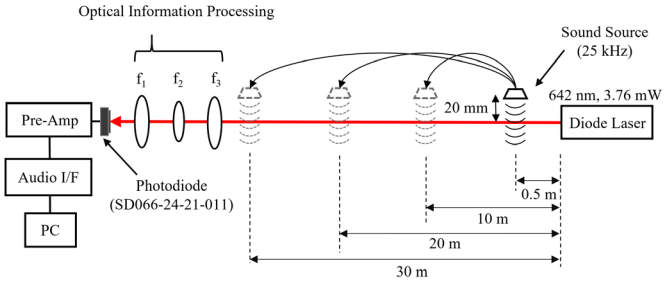

Fig. 25. Experimental Setup (Top View)

Result and Discussion

As a result, sound was successfully detected at all applied positions. When sound was applied from positions of 20 m and 30 m, which exceed the rayleigh length, the laser beam intersecting with the sound waves began to expand, but there was no significant difference in sensitivity. In this research, it was not possible to verify distances beyond 30 m due to excessive expansion of the laser beam diameter. Future research will aim to configure an OWM with a laser beam exceeding 30 m by adjusting the laser diameter using relay lenses. Additionally, in practical security system applications, reflections by mirrors are expected, but they were not included in this setup. Future work will require validation in a setup that more closely resembles an actual security system.

References

[1] Y. Sonoda, M. Akazaki, *Measurement of low-frequency ultrasonic waves by laser light diffraction*, Japan J. Appl. Phys., 1994.

[2] Y. Hayashida, T. Samatsu, Y. Sonoda, *Sound Detection Limit in Optical Wave Microphone System with Long Laser Beam Transmission and Improvement of Signal to Noise Ratio*, ICIC express letters. Part B, 2020.

Wearable Piezoelectric Microphone Using Sol-Gel Composite

Ryota Ono[1)], Tadashi Sakata[2)], Hitomi Maeda[3)], Makiko Kobayashi[1)]
[1)]Kumamoto Univ.
[2)]Kumamoto Prefect. College of Technol.
[3)]Kumamoto Health Sci. Univ.

Introduction

Today's clinical environment have a variety of needs related to sound. Because the wearing of masks reduces the sound pressure level[1] and for medical worker who often wear masks, the wearing of masks interferes with conversational communication, there is a desire to develop tools to assist in conversation while wearing masks. In addition, attempts are being made to record biological sounds. In addition, attempts are being made to record biological sounds. For example, even in today's medical care, where various technologies such as electrocardiograms have been developed for screening for heart disease, listening to heart sounds is an important method for early detection of heart disease, as heart listening is defines as listening to and interpreting heart sounds[2]. The stethoscope used for listening to the heart sound has also expanded the scope of medical practice since 3M Littmann developed an electronic stethoscope in 1999, and in recent years, automated diagnostic techniques using heart sound measurement technology and machine learning technology[3]. Have attracted much attention. However, current electric stethoscopes are hard and large, and there is a need for electronic stethoscopes that are easier to use and allow for long-term monitoring. To meet these needs, a wearable piezoelectric microphone that can be attached directly to the inside of a mask or to the skin was developed.

Sample fabrication

The wearable piezoelectric microphone developed was fabricated using the sol-gel composite method[4]. The sol-gel composite method is a method of fabricating a piezoelectric film by applying a mixture of a sol-gel solution of a metallic compound and ceramic powder to a metal substrate. The microphone developed in this study was mixture of $Pb(Zr,Ti)O_3$(PZT) sol-gel solution and PZT powder, and a sol-gel composite of about 80μm was fabricated on a 50μm stainless substrate. The piezoelectric material fabricated in this way has a porous structure and flexible, so it is not destroyed by large displacement changes (FIG 1). This makes possible a flexible microphone that can be attached inside a mask or on the skin.

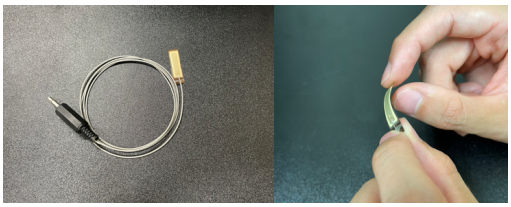

Fig. 26. Piezoelectric microphone using sol-gel composite method

Experiments and results

One adult male and one adult female performed the voice recording test. The voice of "The North Wind and the Sun" was recorded with a developed microphone and a reference throat microphone(NANZU ELECTRIC, E99179), each connected to an IC recorder(Zoom, H5). The developed microphones were attached near the throat and to the mask frame. As a result, the developed microphone showed better speech recognition correctness rate and PESQ value, an objective index of speech quality[5], than the reference throat microphone. Next, biometric sound recording experiments were conducted on nursing practice models that imitated infants and adults. A developed microphone was connected to an IC recorder(Zoom, F3), and the microphone was attached to the chest of the model for recording. As a result, infant heart sounds and adult lung sounds could be recorded. In addition, a swallowing sound recording experiment was conducted on one adult female subject. A developed microphone was connected to an IC recorder, and the microphone was attached to the subject's throat to record swallowing sound as the subject drank water. As a result, the swallowing sound could be recorded.

Conclusion

A wearable piezoelectric microphone was developed using sol-gel composite method. The results suggest the possibility of various applications. Future plans include simulation for structural optimization and construction of a wireless communication system.

References

[1] M. Kitajima, K. Kaetsu, Y. Iino, *How the Patients Hear the Nurses's Voice Who Wear Masks*, Japanese Journal of Nursing Art and Science, 2012.

[2] E. Barbara, *Heart sounds and murmurs: a practical guide*, St. Louis: Mosby, 1997.

[3] N. Mastracci, F. Derakhshan, E. Sykes, D. Khan, *Classification of Heart Sounds Using Machine Learning*, 2023 IEEE International Conference on Digital Health, 2023.

[4] D. Barrow, T.E. Petroff, M. Sayer, *Process for Making Chemically Bonded Sol-Gel Ceramics*, U.S. Patent, US 6,284,682 B1, 1999.

[5] K. Nakaoka, M. Kato, *Evaluation of VoIP Speech Quality using Objective Speech Quality Assessment "PESQ"*, The Institute of Image Information and Television Engineering, 2002.

Effect Of Mixing Ratios Of Different Grain Sizes in Pb(Zr,Ti)O_3/ Pb(Zr,Ti)O_3

Yukino Tokushige, Mako Nakamura, Ryota Ono, Isamu Matsumoto, Kazuhisa Nishimatsu, Hiroyuki Odagawa, Makiko Kobayashi
Kumamoto Univ., Amakusa Ikeda Electric Co., Kumamoto-NCT

Introduction

Speaker warning systems using ultrasonic waves have been developed to prevent accidents on motorways. Conventional manufacturing methods for such speakers are complex and costly, as they use multiple components such as piezoelectric ceramics and metal plates. To address this, the sol-gel composite method[1], which can be applied to large areas and can reduce fabrication costs, was considered. From previous research, it was found that sound pressure can be increased by improving the performance of the piezoelectric film.[2] Pb(Zr,Ti)O_3 (PZT) with a high piezoelectric constant d33 was selected as the material.[3] In this experiment, changes in film thickness, dielectric constant, ultrasonic response and frequency response of PZT-L/PZT(L/PZT) prepared by mixing PZT powder HIZIRCO L with PZT sol-gel solution in mixing ratios of 100:0, 75:25 and 50:50 with particle sizes of 1.2 µm and 0.6 µm were investigated.

Sample fabrication

First, HIZIRCO L and PZT sol-gel solutions mixed in three different mixing ratios were each mixed for 24 hours by a ball mill machine. The mixed sol-gel composite solution was sprayed onto a titanium substrate 3 mm thick, 30 mm long and 30 mm wide using an automatic sprayer. Subsequently, drying was carried out for 5 min in the spray device, followed by 10 min in a 150 °C baking furnace and 5 min in a 650 °C baking furnace. The process from spray application to firing was repeated five times. Polling was then carried out using positive corona discharge for 5 min. The DC supply voltage used for poling was approximately 47 kV. The humidity during poling was kept below 20Finally, an upper electrode with a diameter of 6 mm was produced by screen printing. Silver paste was used as the electrode material.

Experimental method

Film thickness, relative permittivity ε_r, sensitivity of ultrasonic response and frequency response were used as evaluation indices. Sensitivity was calculated using equation (1).

$$Sensitivity = -(20\log(V_1/V_2) + P/RGain) \qquad (6)$$

The reference amplitude V_1 was set to 0.1 V and V_2 to V_{p-p} of the first reflected wave from the bottom of the substrate.

Results

Table 1 shows the experimental results for each mixing ratio. Averages are the means of three samples in each condition. The 100:0 ratio has the highest average permittivity, but the 75:25 mixture shows a more uniform film thickness, with the highest centre frequency indicating the lowest film thickness. However, the sensitivity is lowest due to impedance mismatch caused by the larger electrode size.

Conclusion

This study used PZT powder HIZIRCO L with particle sizes of 1.2 μm and 0.6 μm to create L/PZT mixtures in ratios of 100:0, 75:25, and 50:50. The 75:25 mix ratio showed the highest central frequency (fC) and stable dielectric constant, indicating low porosity, but had low sensitivity, likely due to impedance mismatch. Future research will focus on optimizing electrode size and increasing experimental cycles.

Tab. 27. Experimental results per mixing ratio (1.2 :0.6)

Evaluation index		100:0	75:25	50:50
Film thickness[µm]	Average	29	26	25
	Decentralisation	2.2	2.6	2.3
ε_r	Average	300	280	250
	Decentralisation	530	90	240
Sensitivity[dB]	Average	6.0	5.9	9.3
	Decentralisation	0.11	0.48	1.3
f_C[MHz]	Average	20	25	22
	Decentralisation	2.5	0.0024	4
BW[MHz]	Average	18	22	20
	Decentralisation	2.8	2.4	6.2

$$\Delta p(x) = \frac{V_{AC(x)}}{V_{DC}\frac{k_i d(\chi)(\mu_0-1)}{\gamma p}\left[e^{-u^2-(u-\Theta)^2}-e^{-u^2+(u+\Theta)^2}\right]\sin\omega_p t} \qquad (7)$$

References

[1] M. Kobayashi, C.-K. Jen, J.-F. Moisan, N. Mrad, S.B. Nguyen, *Integrated ultrasonic transducers made by the sol-gel spray technique for structural health monitoring*, Smart Mater. Struct., 2007.

[2] S. Kim, H. Lee, *Piezoelectric Ceramics with High d33 Constants and Their Application to Film Speakers*, Materials, 2021.

[3] M. Sakuragi, K. Kimoto, M. Matsumoto, M. Kobayashi, *Effect of particle size of piezoelectric powder phase on sol-gel composites*, Proceedings of Symposium on Ultrasonic Electronics, 2014.

Nitrogen Spray Corona Discharge Method for Poling under High Humidity

Mako Nakamura[1)], Ryota Ono[1)], Kei Nakatsuma[1)], and Makiko Kobayashi[1)]
[1)]Kumamoto UniversityKumamoto University

Introduction

Ultrasonic waves are widely used in non-destructive testing (NDT) in industrial fields. However, conventional transducers are unsuitable for high-temperature environments due to the need for backing and couplant materials. To address this, we are developing sol-gel composite ultrasonic transducers that can be used in high-temperature environments [1]. These films have many pores that substitute for backing materials and can be directly attached to measurement objects without couplant.

We are also studying on-site fabrication for direct attachment to large and immovable pipes in power plants, which requires on-site polarization. Corona discharge polarization has been challenging in high-humidity environments (80

Sample fabrication

As the sol-gel composite, PZT(Pb(Zr,Ti)O3)) ceramic powder and PZT sol-gel solution were mixed for 24 hours and sprayed onto 30mm×30mm×3mm titanium substrates. The piezoelectric films were dried at room temperature and 150degC for 5 minutes each. And then, they were fired at 650degC for 5 minutes. This process was repeated until the film thickness reached 50μm. After the fabrication of the films, the PZT/PZT films were poled with negative corona discharge. Polarization was conducted under the following three conditions to verify the feasibility of the proposed method using direct nitrogen spraying. The first was the conventional method, in which the box was filled with nitrogen and the humidity was kept around 20%. The second was the nitrogen directly sprayed method in a low-humidity environment (around 20% humidity). The third was the nitrogen directly sprayed method under high humidity (around 90% humidity). The distance from the tip of the electrode needle to the surface of the PZT/PZT piezoelectric film was fixed at approximately 3cm, and the DC power supply voltage was approximately 40 kV. After poling, Ag paste was attached to the surfaces of the films.

Experimental methods

The performance evaluation of the films polarized under each condition was investigated regarding piezoelectric constant (d33), ultrasonic reflected wave, and sensitivity. The ultrasonic reflected wave was obtained to connect the pulser/receiver, oscilloscope, and fabricated samples. The sensitivity was calculated using the following equation.

$$Sensitivity = -20\log\left(\frac{V_1}{V_2} + Gain\right) \tag{8}$$

The reference amplitude V_1 was set to 0.1V, and V_2 was set to V_{P-P} of the first reflected wave from the bottom of the substrate.

Results

The d_{33} of the films by Nitrogen spraying under 20% humidity were large dispersion, however, some values of them were as good as that by Nitrogen filling in a fixed space. The d_{33} of the films by Nitrogen spraying around 90% humidity was lower than that of the conventional method. However, poling under high humidity was revealed to be possible by this proposed method though negative corona discharge was not available under high humidity in conventional studies [2]. About the averages of each sensitivity, the tendency was consistent with that of d_{33}.

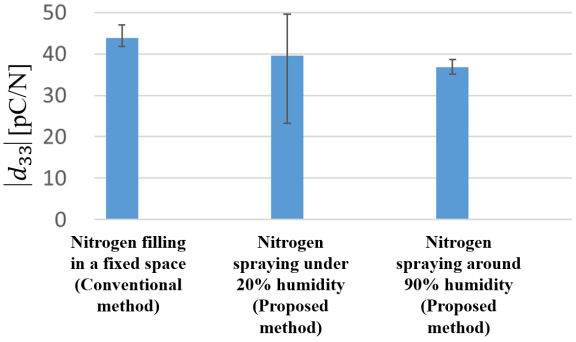

Fig. 28. The d33 results of 9 samples: The average of the conventional method was 4.4pC/N, that of Nitrogen spraying under 20% humidity was 4.0pC/N, and that by Nitrogen spraying around 90% humidity was 3.7pC/N

Conclusion

In this study, we proposed the nitrogen directly spraying method during corona discharge for on-site polarization. It was found that the piezoelectricity by the proposed method varied and was affected slightly by humidity. However, polarization at 80% or higher, which was impossible with the conventional method, was successfully achieved. Future experiments will be conducted with more samples to accurately determine d_{33} and sensitivity variations.

AS

$$\Delta p(x) = \frac{V_{AC(x)}}{V_{DC}\frac{k_i d(x)(\mu_0-1)}{\gamma p}\left[e^{-u^2-(u-\Theta)^2}-e^{-u^2+(u+\Theta)^2}\right]\sin\omega_p t} \tag{9}$$

References

[1] M. Kobayashi, C.-K. Jen, J. F. Bussiere, and K.-T. Wu, *High-Temperature Integrated and Flexible Ultrasonic Transducers for Nondestructive Testing*, NDT&E International, 2009.

[2] M. Hidaka, K. Nakatsuma, and M. Kobayashi, *Ambient Condition Effect of Porous Piezoelectric Film Poling by DC Corona Discharge*, Journal of the Institute of Electrostatics Japan, 2022.

Research of dependences of engine oil viscosity on electrical parameters for quality control in a cyber-physical measurement system

Maryna MIKHALIEVA[1)], Volodymyr HERA[1)], Krzysztof PRZYSTUPA[2),3)],Yuryi SHABATURA[1)], Lubomyra ODOSII[1)], Artūras KILIKEVIČIUS[1)]
[1)]Hetman Petro Sahaidachnyi National Army Academy: Lviv, Ukraine
[2)]Lublin University of Technology, Poland
[3)]Vilnius Gadiminas Technical University, Lithuania

The main power plant of modern transportation systems remains the internal combustion engine. These engines are complex units designed for efficient, reliable, and long-lasting operation, involving numerous diverse subsystems that may be developed as electromechanical complexes in the future. One of the most important subsystems is the engine lubrication system.

Therefore, continuous monitoring of the oil condition is essential to determine its suitability for use and to diagnose equipment wear. To ensure the longevity and reliable starting of the engine, it is necessary to use oil that meets the operational properties of its design (brand). It is essential to investigate the oil's viscosity at operating and ambient temperatures. Standard methods for controlling the composition and properties (viscosity) require routine laboratory work (titration, using densitometric and viscometric methods, etc.).

Research on the electrical properties of liquids in electromagnetic fields of different frequencies allows for obtaining information about their composition and properties in non-laboratory conditions within a short time frame.

Currently, the development of advanced methods for the operational control of engine oil, which will later be used in controlled electromechanical lubrication systems, is relevant. The method is based on measuring changes in the oil's dielectric permittivity caused by contamination, degradation, and wear of mechanisms. This method will allow determining changes in oil properties caused by water content, fuel contamination, oxidation, and the presence of metallic impurities.

The purpose of this research is to develop an electrical method for the quantitative and qualitative analysis of oil composition for engines. In this context, model liquids of known composition and properties were studied for the dependency of the electrical parameter (capacitance) on the frequency of the electromagnetic field. Based on the experimentally obtained patterns, a method for the operational control of the composition and properties of engine oil (according to the known brand) is proposed.

Based on theoretical and practical research, a method for the operational control of the composition of engine oil is proposed, based on the dependency of electrical parameters on the signal frequency. This method allows for the quantitative and qualitative assessment of controlled components (or standard viscosity parameter) in non-laboratory conditions in a short time (up to 2 seconds) and ensures uninterrupted operation of the equipment during its use.

Comparison Study of Critical Current Angular Dependence in YBCO Tapes

Krzysztof Habelok[1)], Paweł Lasek[1)], Kamil Gruszczyk[2)], Mariusz Stępień[1)]
[1)]Department of Power Electronics, Electrical Drives and Robotics, Silesian University of Technology,
[2)]A student at the Electrical Department of the Silesian University of Technology

Introduction

The selection of an appropriate high-temperature superconducting (HTS) tape is crucial for the design of superconducting devices. This process requires consideration of not only the critical current value Ic, specified for self-field measurements but also the comprehensive dependence of this current value on the external magnetic field and the tape's orientation [1]. Given the anisotropic properties of second-generation high-temperature superconducting materials and the implementation of various forms of artificial pinning to mitigate these effects, precise angular characteristics must be determined through laboratory measurements.

A comparative analysis of the angular dependence of critical currents $I_c(B,\theta)$ in 2G HTS tapes produced by SuperPower has been presented and discussed in this study. To facilitate this comparison, studies were conducted on three HTS tapes placed in a magnetic field with a low value of less than 500 mT . This analysis is relevant for devices such as superconducting power cables and superconducting transformers, which typically operate in magnetic fields of such magnitudes. The studies focused on three samples of tapes with different artificial pinning parameters, which directly affected the angular dependence of the critical current. The specific samples analyzed were SCS4050, SCS4050-AP, and SCS4050-AP-i. For the characterization of the current-angular dependence, a custom research setup was used. This test bench used NdFe14 permanent magnets in a Halbach array configuration to generate a homogeneous magnetic field on the surface of the HTS tape samples

Test Bench based on Halbach Array

The developed test setup represents a novel approach to the characterization of HTS tapes. Unlike traditional setups that utilize electromagnets [2], this system employs permanent magnets to generate a homogeneous magnetic field within the working area where the HTS sample is placed. The inclusion of a worm gear allows for the adjustment of the orientation of the homogeneous magnetic field relative to the tape surface.

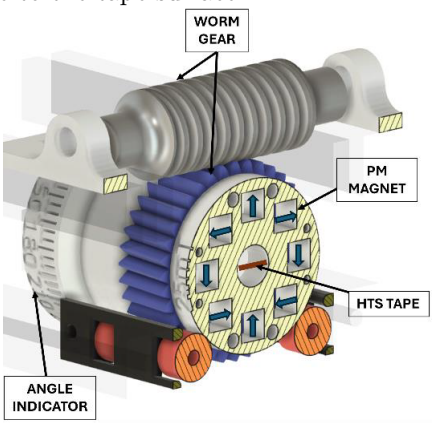

Fig. 29. Cross-Section of the Test Setup Model

The concept of utilizing 3D printing technology for constructing the setup was driven by the potential to ensure rapid prototyping and to verify the functionality of the setup. Polylactic Acid (PLA) filament was used as the primary material. The variation in the magnetic field strength was achieved through interchangeable discs with magnets arranged in Halbach arrays. These discs enabled the generation of magnetic fields of 75 mT and 225 mT, respectively.

Results

The presented results indicate the relative critical current values as a function of the magnetic field and the angle between the magnetic field lines and the tape. Based on these results, a comprehensive characterization of the selected HTS tapes was performed. The data analysis facilitated a deeper understanding of the tapes' performance under varying magnetic field orientations.

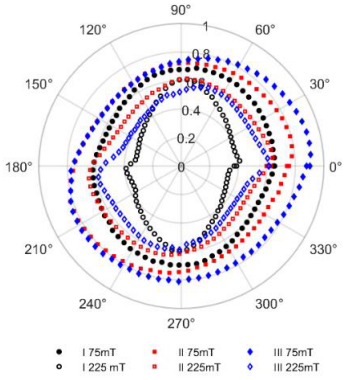

Fig. 30. Comparison of Relative Critical Current Values for B=75 mT and B=225 mT for SCS4050, SCS4050-AP, and SCS4050-AP-i Tapes

References

[1] Hajdasz S., et al., *Critical Current Degradation in HTS Tapes for Superconducting Fault Current Limiter under Repeated Overcurrent.*, Applied Sciences 13.7 (2023): 4323.

[2] Kubiczek, K., et al, *Characterization of high-temperature superconducting tapes.*, IEEE Transactions on Instrumentation and Measurement 69.6 (2019): 2959-2965. .

Cooperation of the plasma reactor with a converter power supply equipped with a five-limb matching transformer of special design

Grzegorz Komarzyniec
Lublin University of Technology, Department of Electrical Engineering and Superconducting Technologies
Nadbystrzycka 38A, 20-618 Lublin, Poland, e-mail: g.komarzyniec@pollub.pl

Introduction

Three-phase gliding arc discharge plasma reactors are devices in which it is difficult to maintain stable plasma parameters. Plasma parameters are strongly influenced by the design of the power system. This paper examines the interaction of a plasma reactor with an AC/DC/AC converter equipped with different transformer solutions to adapt the output parameters to the requirements of the plasma reactor. A new design of matching transformer using a five-limb core and integrating both the functions related to sustaining the discharge in the reactor, with appropriate power supply parameters, and the functions related to the initiation of the discharge ignition are proposed. The research indicates that the design of the transformers has a significant impact on the parameters of the generated plasma, the performance characteristics of the plasma reactor and the stability of the discharge burning in the reactor.

Gliding arc plasma reactors

The problem of supplying power to gliding arc discharge plasma reactors is to ensure optimum plasma generation conditions, while ensuring good interaction with the power grid and limiting the disturbances generated by the plasma reactor. The main problem is the instability of the free arc plasma burning in a three-electrode three-phase system FIG 1. The plasma parameters of such an arc can change rapidly and stochastically making them difficult to analyse in terms of physical and chemical parameters. Furthermore, even small changes in the power supply, physical or chemical parameters of the process gases lead to changes in the burning conditions of the arc, which in turn induce self-regulating reactions in the plasma that alter the arc structure and its characteristics.

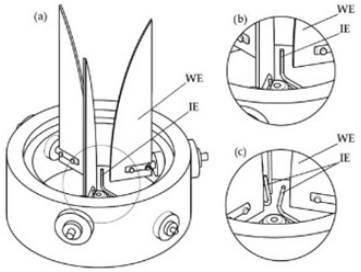

Fig. 31. Three-phase plasma reactor with gliding arc discharge. (a) Overview drawing, (b) one-ignition electrode system and (c) two-ignition electrode system. WE—working electrodes; IE—ignition electrodes

Power supply system

Apart from the design of the plasma reactor and the parameters of the plasma-generating gases, it is the power supply system that plays a decisive role in shaping the plasma parameters. These parameters can be influenced by selecting the type, value and frequency of voltage and the value of the arc current. The use of transistor converters in the power supply enables these parameters to be adjusted smoothly. A transformer that matches the parameters of the power supply to the requirements of the plasma reactor has a major influence on the operation of the plasma reactor.

The simplest solution is to use single-phase matching transformers. The disadvantage of the solution is the need for an additional ignition system to initiate the discharge in the rector. Another solution has been proposed in the form of a three-phase five-limb matching transformer, in a special design, integrating the ignition and discharge sustaining functions in a single device.

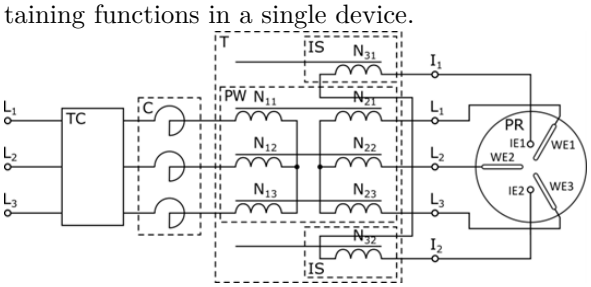

Fig. 32. Converter power supply with five-limb transformer

Operating characteristics

The plasma reactor performance characteristics FIG 3 obtained do not clearly indicate an improvement in the performance of the generated plasma. These characteristics are clearly different from those obtained by using single-phase matching transformers.

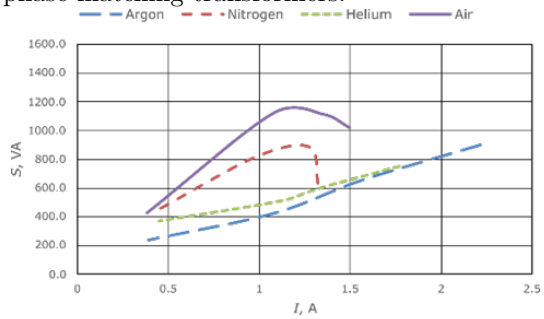

Fig. 33. Arc power characteristics for gas volume flow of 2.1 m^3/h

By changing the design of matching transformers, i.e. the type and material of the core, the shape of the windings, the way in which the windings are connected, the plasma generated parameters and the stability of the electric arc can be influenced. In the case of the five-column transformer, however, a significant improvement in the operating conditions of the converter power supply was achieved. This was mainly achieved by reducing the harmonic content of the arc voltage and current and reducing the overvoltage associated with the initiation of the discharge ignition in the reactor.

Study on Recovery Time of a Conduction–Cooled Resistive Superconducting Fault Current Limiter

Janusz Kozak
Lublin University of Technology

Introduction

This paper presents the influence of superconducting tape insulation on the recovery time of superconducting fault current limiters. The analysis is based on experimental results of short-circuit tests. The reduction of the thermal and dynamic effects of the passage of a fault current can be achieved by limiting the short-circuit time and the value of the surge current. An ideal Fault Current Limiter is required to have almost zero impedance at operating currents and significant impedance at fault conditions. A Superconducting Fault Current Limiter (SFCL) meets these requirements under certain conditions. The recovery time – a very important parameter – shows the ability of the limiter to return to the superconducting state to be ready to limit the subsequent short circuit. The experimental results show that the recovery time can be significantly reduced with the application of thin-film insulation and an appropriate design of the conduction cooling of the HTS tape.

The Concept of the Fast Recovery SFCL

A limitation of both the short-circuit time and the value of the maximum initial fault current reduces the thermal and dynamic effects of the passage of a fault current. The use of devices that limit the value of a fault current can reduce the required short-circuit capacity of the entire system. However, the chosen means of fault current limitation must meet power quality standards. An ideal fault current limiter would have substantial impedance in fault conditions and zero impedance at operating currents. These requirements are met by a superconducting fault current limiter (SFCL). An increase in current caused by the occurrence of a fault current causes the super-conducting material to go from the superconducting state to the resistive state. This increases the impedance of the short-circuit loop, allowing the fault current value to decrease [1]. A significant body of literature exists on the study and improvement of the performance of different types of short-circuit current limiters. Numerous papers have addressed the topic of inductive-type fault current limiters [2–6]. To enhance their performance and reduce their size, a novel approach to saturated-core fault current limiters has been proposed [7–9]. Resistive fault current limiters are also employed for the rapid limitation of short-circuit currents in HVDC transmission systems [10]. To meet the demand for reclosing, fast recovery is essential [11]. The concept of the fast recovery SFCL is to involve the use of the anodised aluminium alloy to accelerate the heat transfer from the HTS tape to the cold mass. The aluminium alloy block, which ensures appropriate heat capacity and electrical resistance through a thin layer achieved in the anodising process, can shorten the recovery time. The idea behind the proposed solution is to reduce the thermal resistance between the superconducting tape and the cold mass. This is so that, after a short circuit, the temperature of the superconducting tape reaches its pre-short-circuit value as quickly as possible. There are many insulating materials that can provide good insulating properties, but not all are suitable for cryogenic temperatures. On the one hand, the insulation thickness of superconducting tape has a positive effect on the breakdown voltage; on the other hand, it increases the thermal resistance. Using a single layer of insulation and reducing the thickness improve the thermal conductivity conditions. Constructing a superconducting fault current limiter using very thin single-layer insulation can be technically very difficult. The superconducting tape may move slightly during cooling due to the different expansion of the materials used in the construction of the SFCL. Also, the HTS tape may move during a short circuit as a result of dynamic forces and a rapid temperature rise. Small displacements of the superconducting tape can cause degradation of the insulation and result in electrical breakdown. The concept presented here uses durable but thin insulation to provide good thermal conductivity between the HTS tape and the aluminium blocks in order to ensure adequate heat capacity. It also uses a second insulation to provide the required breakdown voltage between the anodised sectioned aluminium blocks and the cold mass. The aluminium anodising process ensures a durable insulating film thickness in the order of micrometers. The thickness of the obtained anode layer on aluminium depends on the anodising time. A suitable insulation layer can, therefore, be produced easily and accurately. Three sets of square insulated aluminium profiles were prepared for measurement purposes. The first set was insulated with double polyamide tape, the second set was insulated with single polyamide tape, and the third set was anodised to a coating thickness of 30 μm. The aluminium blocks insulated in this way were placed on both sides of the HTS tape and pressed with a force of approximately 500 N.

Measurement Setup

Sample blocks were made of 6060 aluminium alloy, anodised in the sulphuric acid process Type II to a thickness of 30 μm. Anodising is a conversion coating that transforms aluminium on the surface of components into aluminium oxide. The overall thickness of the coating formed is 67 percent penetration in the substrate and 33 percent growth over the original dimension of the part. For comparison, identical non-anodised blocks were prepared with polyimide tape insulator were 50 and 100 μm in thickness. The laboratory setup shown in Figure 1 consists of a sample holder, a power supply and a computer with software. The sample holder is equipped with current terminals and voltage terminals. The voltage clamps are located on the

interior and allow the measurement of the voltage of the HTS tape over a distance of 0.2 m.

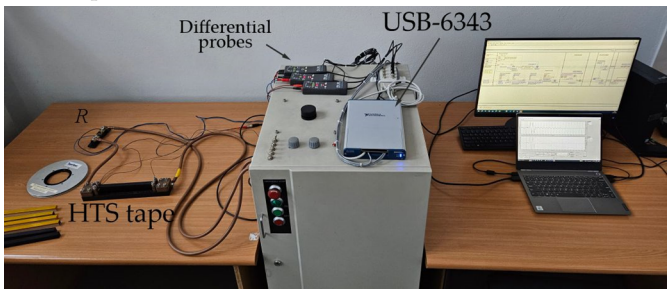

Fig. 34. Laboratory test bench for recovery time

Measurement Results

The 2G SF4050 superconducting tape from SuperPower was utilised in the measurements. This superconducting tape is 4 mm in width and 50 μm in thickness. The tests were performed for a temperature range of 300–430 K. This range partly overlaps with the operating range of the SFCL and is sufficient to compare the effect of superconductor insulation on the cooling rate. Figure 2 shows a comparison of the temperature of the HTS tape during a short-circuit test for three insulation thicknesses at an electric field strength of 125 V/m for the HTS tape. A short circuit lasts from 0 ms to 40 ms and at the beginning of the short circuit, the characteristics coincide because the current is limited equally for the polyimide insulation and the anodised layer. During a short circuit, the temperature of the HTS tape rises to 430 K when polyimide insulation is used in both 50 μm and 100 μm thicknesses. In contrast, if anodised aluminium is used, the maximum temperature is lower and reaches approximately 410 K.

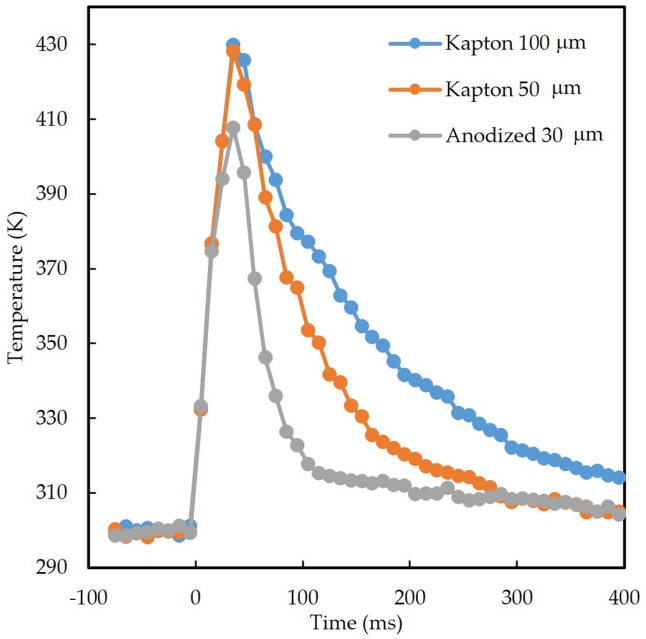

Fig. 35. A comparison of the temperature of HTS tape during a short-circuit test at an electric field strength of 125 V/m for HTS tape

Discussion

The anodised aluminium provides the fastest cooling of the HTS tape following the termination of a short circuit. A comparison of the temperature drop rate by 100 K, from 410 K to 310 K, for all cases reveals that for an insulation thickness of 100 μm, the time required is approximately 400 ms, for an insulation thickness of 50 μm, it is 240 ms, while for an insulation thickness of 30 μm, it is only 170 ms. Furthermore, the initial 50 K drop takes only 25 ms for the aluminium with a 30 μm anodised layer, while for the insulation of 50 μm and 100 μm, it takes 45 ms and 90 ms, respectively. When dissipating heat from the superconducting tape through the insulation to a component with a much lower temperature, good contact is also important. Even when employing a single-layer insulation, two contact surfaces are present. In contrast, anodised aluminium affords only a single contact surface. The interface thermal resistance plays a key role in heat conduction between two materials. This paper describes the research carried out to improve an important parameter of a superconducting fault current limiter. Tests were carried out to reduce the recovery time of the superconducting fault current limiter to its rated operation. The return of a superconducting tape to the superconducting state after a short circuit is switched off depends on the type and thickness of the used insulation. In order to achieve this, insulation made of polyimide tape and a thin layer of anodised aluminium were compared.

Conclusions

The use of the insulation proposed in this paper, i.e., a thin layer of anodised aluminium, allowed the recovery time of the superconducting fault current limiter to be greatly reduced without adversely affecting the rate of temperature rise and the limiter's performance during the limitation of short-circuit current. The thickness of the anodic layer produced on the aluminium surface can be appropriately selected over a wide range, which is of great significance in the design of an SFCL with a very short recovery time. Based on these tests, a contact-cooled limiter will be built and subjected to short-circuit testing in an accredited short-circuit laboratory, as with previous designs.

References

[1] Kozak, J., *Forces and Stresses in the Windings of a Superconducting Fault Current Limiter*, Energies 2022, 15, 6519.

[2] Naeckel, O.; Noe, M., *Design and Test of an Air Coil Superconducting Fault Current Limiter Demonstrator*, IEEE Trans. Appl. Supercond. 2013, 24, 5601605.

[3] Kvitkovic, J.; Pamidi, S.V.; Graber, L.; Chiocchio, T.; Steurer, M.; Usoskin, A., *AC loss and magnetic shielding measurements on 2G HTS inductive fault current limiter prototype modules*, IEEE Trans. Appl. Supercond. 2014, 24, 5600604.

[4] Heydari, H.; Sharifi, R., *Three-Dimensional Pareto-Optimal Design of Inductive Superconducting Fault Current Limiters*, IEEE Trans. Appl. Supercond. 2010, 20, 2301–2311.

[5] Wang, C.; Hong, W.; Lu, J.; Li, B.; Xin, Y.; Li, W.; Yang, T.; Zhang, Y., *Experiment Studies of a DC Inductive Superconducting Fault Current Limiter with Energy Dissipation Capability*, IEEE Trans. Appl. Supercond. 2024, 34, 5600505.

[6] Chen, Y.; Wang, Z.; Shen, B.; Wang, B.; Sheng, J., *Optimization of Inductive Superconducting Fault Current Limiter for Distribution Networks*, IEEE Trans. Appl. Supercond. 2021, 31, 5603705.

[7] Yuan, J.; Ye, C.; Zhou, H.; Liu, J.; Zheng, Y.; Dong, W.; Ni, Z.; Wei, L., *A Compact Saturated Core Fault Current Limiter Magnetically Integrated with Decoupling Windings*, IEEE Trans. Power Deliv. 2023, 38, 2711–2723.

[8] Lei, H.; Gui, J.; Johnson, B., *Impact of Saturated Iron Core Superconducting Fault Current Limiters on Traveling-Wave-Based Protection*, IEEE Trans. Appl. Supercond. 2023, 33, 5601308.

[9] Zhang, Z.; Yuan, J.; Hong, Y.; Chen, H.; Zou, C.; Zhou, H., *Hybrid Multifunctional Saturated-Core Fault Current Limiter*, IEEE Trans. Power Deliv. 2022, 37, 4690–4699.

[10] Prakash Reddy, S.R.; Kar. S.; Rajashekara, K., *Resistive SFCL Integrated Ultrafast DC Hybrid Circuit Breaker for Subsea HVDC Transmission Systems*, IEEE Trans. Ind. Appl. 2022, 58, 5977–5986.

[11] Li, L.; Song, M.; Zhang, Q.; Xiang, B.; Yuan, Z.; Tang, Z.; Liu, Z.; Geng, Y.; Wang, J., *Effects of Lamination Thickness on Recovery Characteristics of a Variable Resistance SFCL*, IEEE Trans. Appl. Supercond. 2024, 34, 5600405.

Exploring the Interaction of Ferromagnetic Nanoparticles with RF Electromagnetic Fields for Medical Purposes

Katarzyna Wojtera, Łukasz Szymański
Institute of Mechatronics and Information Systems, Lodz University of Technology

Introduction

Carbon nanotubes (CNTs) have significant medical applications due to their biocompatibility, derived from being made of carbon. After proper functionalization, they can safely interact with the human body. CNTs can cross biological barriers, making them effective drug delivery systems, transporting therapeutic agents directly to diseased tissues. Initially used for cancer therapy and viral infections, their potential in immunotherapy and gene therapy has also been demonstrated [1].

Cancer remains a major health threat, with 17.0 million new cases and 9.5 million deaths worldwide in 2018. By 2040, these figures are expected to rise to 27.5 million new cases and 16.3 million deaths annually [2]. The primary challenge in cancer treatment is early detection, as late diagnoses often limit treatment options and increase the risk of metastasis. Cancer can affect any organ or system.

A promising application of CNTs is their use in selectively destroying cancer cells. CNTs filled with ferromagnetic materials can be directed to diseased cells, where they are externally heated via thermal ablation, causing targeted cell death through increased temperature [3-4]. This method spares healthy tissues and is effective because proteins coagulate at temperatures above 42°C, leading to cell death [5-6].

This study hypothesizes that ferromagnetic carbon nanotubes filled with iron can be used to hyperthermally destroy cancer cells in a radiofrequency electromagnetic field. The paper details the synthesis of iron-filled multi-walled carbon nanotubes (Fe-MWCNTs) and investigates their magnetic properties. Fe-MWCNTs were created using catalytic chemical vapor deposition (CCVD). The nanoparticles were functionalized for biomedical applications, and their magnetic properties were analyzed to assess heat generation efficiency when exposed to an external electromagnetic field. The samples' responses were measured over 45 minutes of exposure, showing a temperature increase proportional to concentration. Laboratory results were compared with simulations conducted using COMSOL software. This study aimed to explore the use of carbon nanomaterials in medicine, focusing on their properties, functionalization for thermal ablation therapy, and the behavior of ferromagnetic nanocontainers in electromagnetic fields. This work continues the research detailed in "Examination of the Effect of RF Field on Fe-MWCNTs and Their Application in Medicine" [7].

Methodology

To evaluate the heating capabilities of Fe-MWCNTs, the temperature increase of magnetic liquids was measured after exposure to electromagnetic fields at five different frequencies (110, 165, 330, 428, 650 kHz and 1 MHz). The study aimed to compare the outcomes across various concentrations and suspensions. Detailed descriptions of the experiment and the setup can be found in the referenced papers [7-13]. The laboratory experiment results were then compared with simulations of the heating phenomenon conducted using COMSOL software.

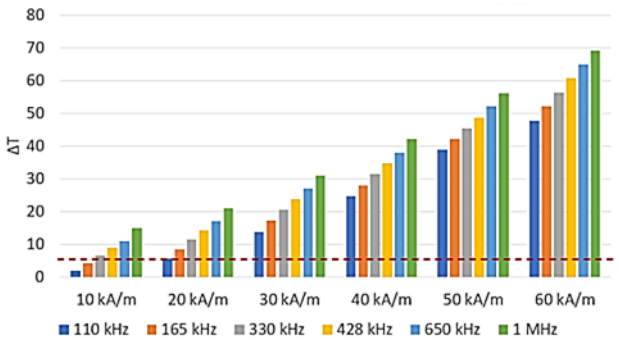

Fig. 36. Bar graph of all measurements [own elaboration]

Conclusions

The results of this experiment provide valuable insights that serve as a solid foundation for further research. One objective is to develop an effective dispersion method to continue studying the heating properties of the suspension at specific concentrations and to initiate cell line testing. During this phase, it will be essential to estimate the quantity of nanocarriers required for effective cell destruction and to determine the precise field parameters for the proposed method. Successfully completing this phase is critical, paving the way for in vitro studies. This will involve determining the amount and concentration of nanoparticles in a biocompatible solution and defining the exposure parameters to focus on the cellular response to the heating medium.

References

[1] Chen et al., *The Advances of Carbon Nanotubes in Cancer Diagnostics and Therapeutics*, Journal of Nanomaterials, 2017.

[2] American Cancer Society, *Global Cancer Facts & Figures*, Cancer, vol. 18, no. 700, pp. 1-4, 2007.

[3] Chen, D.; Wang, C.; Nie, X.; Li, S.; Li, R.; Guan, M.; Liu, Z.; Chen, C.; Wang, C.; Shu, C.; et al., *Photoacoustic Imaging Guided Near-Infrared Photothermal Therapy Using Highly Water-Dispersible Single-Walled Carbon Nanohorns as Theranostic Agents*, Adv. Funct. Mater. 2014, 24, 6621–6628.

[4] Zhang, M.; Wang, W.; Wu, F.; Yuan, P.; Chi, C.; Zhou, N., *Magnetic and Fluorescent Carbon Nanotubes for Dual Modal Imaging and Photothermal and Chemo-Therapy of Cancer Cells in Living Mice*, Carbon 2017, 123, 70–83.

[5] Samali, A.; Holmberg, C.I.; Sistonen, L.; Orrenius, S., *Thermotolerance and Cell Death are Distinct Cellular Responses to Stress: Dependence on Heat Shock Proteins*, FEBS Lett. 1999, 461, 306–310.

[6] Roti, J.L.R., *Cellular Responses to Hyperthermia (40–46°C): Cell Killing and Molecular Events*, Int. J. Hyperth. 2008, 24, 3–15.

[7] Wojtera, K.; Smółka, K.; Szymanski, L.; Wiak, S., *Examination of the Effect of RF Field on Fe-MWCNTs and Their Application in Medicine*, Electronics. 2022, 11, 10.3390/electronics11132099.

[8] Raniszewski, G.; Kolacinski, Z.; Szymanski, L., *Ferromagnetic Nanoparticles Synthesis in Local Thermodynamic Equilibrium Conditions*, IEEE-NANO 2015 - 15th Int. Conf. Nanotechnol., pp. 323–326, 2015.

[9] Wojtera, K.; Walczak, M.; Pietrzak, L.; Fraczyk, J.; Szymanski, L.; Sobczyk-Guzenda, A., *Synthesis of Functionalized Carbon Nanotubes for Fluorescent Biosensors*, Nanotechnology Reviews, vol. 9, no. 1, pp. 1237–1244, Jan. 2020, doi: 10.1515/ntrev-2020-0096.

[10] Raniszewski, G.; Miaskowski, A.; Wiak, S., *The Application of Carbon Nanotubes in Magnetic Fluid Hyperthermia*, J. Nanomater., vol. 2015, 2015.

[11] Szymanski, L.; Kolacinski, Z.; Wiak, S.; Raniszewski, G.; Pietrzak, L., *Synthesis of Carbon Nanotubes in Thermal Plasma Reactor at Atmospheric Pressure*, Nanomaterials, vol. 7, no. 2, p. 45, Feb. 2017, doi: 10.3390/nano7020045.

[12] Jeszka, J.K.; Pietrzak, L., *Polylactide/Multiwalled Carbon Nanotube Composites – Synthesis and Electrical Properties*, Polimery, 55(7-8), 2010, 524–528.

[13] Szymanski, L.; Kolacinski, Z.; Raniszewski, G.; Gryska, E., *CNTs Synthesis on Steel Strip in Microwave Plasma Reactor for Medical Application*, IEEE-NANO 2015 - 15th Int. Conf. Nanotechnol., pp. 1062–1065, 2015.

Modern training courses increasing awareness of environmental protection

Michał Jeleń[1)], Marcin Zygmanowski[1)], Mariusz Stępień[1)], Anton Rassõlkin2[2)]
[1)]Silesian University of Technology, Gliwice, Poland
[2)]Tallinn University of Technology, Tallinn, Estonia

Introduction

Environmental protection in different areas of activity (energy saving, water saving, circular economy, reduction of transport related pollutions) is a very hot topic in modern global community. It relates also to education at all levels, including higher education. Especially in areas related to electrical engineering, electronics, mechatronics and automation strong attention is paid for developing of systems with reduced influence on the natural environment. Important target group which can require proper education in this matter is composed of people who are already working, but changing their activity from heavy industry to high tech industry. Such trends are observed over the world including some parts in Europe where heavy industry is successively replaced by modern industry of high technology like robotics, automation, artificial intelligence, etc. [1].

As a response on described above problems and expectations new international initiative were undertaken within Strategic Partnership Erasmus+ program. The initiative is a project to develop platform for retraining courses for workers willing to re-educate from heavy industry (mostly fossil fuel mining industry) to modern industry based on environmental friendly technologies like high efficiency power conversion, modern electrical drives and motors, automation and robotics, control of industrial processes and condition monitoring and diagnosis of machines. The paper is devoted to describe most important project goals and results and discuss influence of training process on better understanding of environmental protection.

REMAKER project structure

Described in the paper platform and educational activities are part of an educational project REMAKER entitled: "Retraining of Fossil Fuel Mining Area Workforce for Modern Industry" [2]. The project has been implemented by international team composed of four universities from Estonia, Poland, Germany and Czech Republic. The idea was to offer educational platform for self-education for workers of heavy industry located mostly in Estonia (oil shale industry) and Poland (mining industry). The project was implemented within Erasmus+ Strategic Partnership (KA2) frame for higher education sector. Two types of activities were undertaken. The first one was mentioned educational platform and the second one was a set of study visit at factories and enterprises of modern industry in Germany and Czech Republic. The aim of the project was to promote activities focused on high-efficiency, low-cost technological solutions that minimize energy and media consumption and are therefore friendly to the natural environment.

Retraining course content

The training platform developed as result of the project contains five educational modules: i) electrical drives, ii) automation, iii) power electronics, iv) robotics and v) condition monitoring of industrial systems. Each module contains 6 to 8 lectures (lessons). Each lesson was composed of video with a lecture, training materials (slides) and final quiz to check achieving of expected knowledge. Each module was considered as a separate training topic, so after completing all lessons of the module trainee received a certificate confirming completion of the training. So the platform is an universal, intuitive tool for self-training with open access for everybody interested with increasing their knowledge in areas of the course described above.

The interface of the platform (part) is presented in Fig. 1.

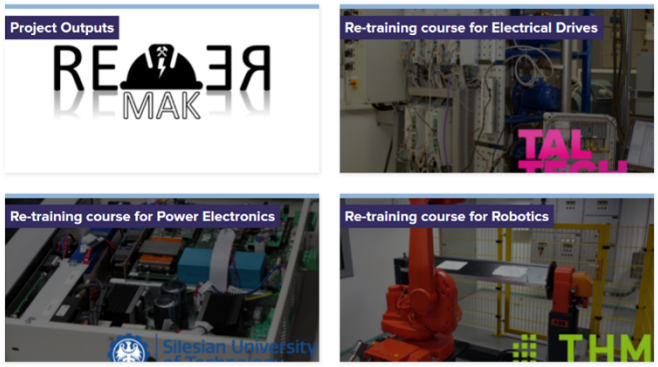

Fig. 37. Interface of REMAKER platform (part)

Project training activities

The second group of activities (apart developing of educational platform) was organization of study visits, dedicated mostly for staff elaborating content of training platform, in companies offering high quality industrial processes. Participants visited e.g. Bosh Thermoelectric and ABB in Germany and Skoda Electric in Czech Republic. Visits were focused on expectations from newly employed staff and training systems in companies. More detailed description of study visits with details related to environmental aspects and also more detailed description of training content will be included in the final paper. Discussion about benefits from self-training and potential target group of students will be discussed.

References

[1] C. Hennick, *Retraining American workers for green energy jobs*, U.S. Green Building Council, www.usgbc.org, 2017.
[2] REMAKER project webpage, *taltech.ee/en/remaker*, 2024.

The new model of conduction-cooled current leads for superconducting fault current limiters

Michał Majka
Department of Electrical Equipment and High Voltage Techniques,
Faculty of Electrical Engineering and Computer Science, Lublin University of Technology, Lublin

Introduction

Current leads are part of superconducting electrical equipment. Current leads are part of a cryostat connecting external devices operating at room temperature to devices operating at cryogenic temperatures. The warm end of the current lead connected to the current source is at room temperature (T_H = 293 K), the cold end of the current lead connected to the superconducting device operates at cryogenic temperatures TL. Current leads can be made of both non-superconducting and superconducting material, both HTS and LTS (Fig. 1). The paper presents the problem of cooling current leads, which are the main elements of superconducting devices, and the aim of the paper is to present a method for calculating contact-cooled copper current feedthroughs.

In superconducting devices, the power losses generated in the current leads have a large portion of the thermal energy that the cooling system is designed to dissipate so as to maintain the temperature of the superconducting device at a specified level. When the cooling power of the cryocooler is too low, the heat flux entering the cryostat through the current leads and the Joule heat generated in the current leads by the current supplying the electrical device can prevent the superconducting device from cooling to the required operating temperature. Due to the need to minimise resistance, current leads should have as large a cross-section as possible. On the other hand, a large heat flux flows through the large cross-section to the inside of the cryostat by thermal conduction.

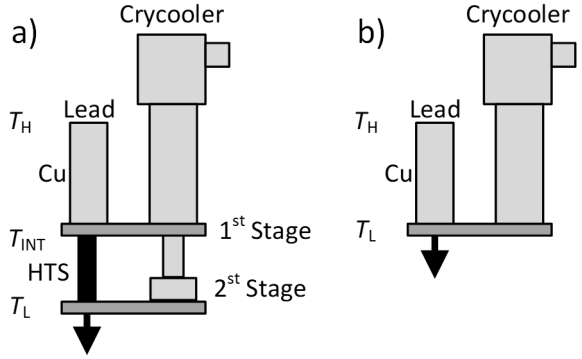

Fig. 38. Conduction-cooled current leads: a) hybrid copper-HTS leads (cooled by a 2 stage cryocooler), b) copper leads (cooled by a 1 stage cryocooler)

Reducing the cross-sectional area of the current leads reduces the heat input from the outside, but at the same time increases the Joule losses in the current leads, through which a large current flows. Copper current leads may have a graduated cross-section, because as the temperature of the pass decreases, the resistivity of copper decreases and the cross-section can be reduced without causing an increase in Joule losses but reducing the heat flow along the current leads. Current leads adapted for contact cooling operate in a vacuum, and heat is removed from them by thermal conduction [1-2]. Power losses that occur in current leads amount to about 30–50% of the total power losses in the cryostat. Reducing power losses in current leads is crucial for reducing cooling costs and increasing the stability of operation and minimizing the operating costs of superconducting devices. Several methods have been developed so far to optimize the cooling of current feedthroughs cooled by gas vapors and using contact cooling [3-10]. In this paper, the mathematical model of conduction-cooled current leads for superconducting fault current limiters will be presented.

References

[1] Kozak S., *Modelowanie elektrycznych urządzeń nadprzewodnikowych*, Prace Instytutu Elektrotechniki, zeszyt 221, Warszawa, 2005.

[2] Janowski T., Stryczewska H. D., Wac-Włodarczyk A. (red.), *Technologie nadprzewodnikowe i plazmowe w energetyce*, Lublin, 2009.

[3] Buyanov Y. L., Fradkov A. B., Shebalin I. Y., *A review of current leads for cryogenic devices*, Cryogenics, vol. 15, no. 4, pp. 193-200, Apr. 1975.

[4] Buyanov Y. L., Shebalin I. Y., *Current leads to a cryostat working under short-term load conditions*, Cryogenics, 15(10):611–3, 1975.

[5] Chang H.-M., Kim M. J., *Optimization of conduction-cooled current leads with unsteady operating current*, Cryogenics, vol. 49, no. 5, pp. 210–216, May 2009.

[6] Chang H. M., Byun J. J., Jin H. B., *Effect of convection heat transfer on the design of vapor-cooled current leads*, Cryogenics, 46(5):324–32, 2006.

[7] Chang H. M., Choi Y. S., Van Sciver S. W., Miller J. R., *Optimization of current leads cooled by natural convection of vapor*, Advances in Cryogenic Engineering, 49:944–51, 2004.

[8] Chang H. M., Kim Y. S., Kim H. M., Lee H., Ko T. K., *Current-lead design for cryocooled HTS fault current limiters*, IEEE Transactions on Applied Superconductivity, 17(2), 2244–7, 2007.

[9] Chang H.-M., Lee S. I., *Current Leads for Conduction-Cooled Magnets at 20–30 K*, IEEE Transactions on Applied Superconductivity, Volume: 23, Issue 3, Page(s) 4801004 – 4801004, 2013.

[10] Chang H.-M., Van Sciver S. W., *Thermodynamic optimization of conduction-cooled HTS current leads*, Cryogenics, vol. 38, no. 7, pp. 729-736, 1998.

Application of machine learning methods to the analysis of brain neural networks: perspectives and potential benefits

Katarzyna Mróz
Faculty of Mathematics and Information Technology
Lublin University of Technology, 20-618 Lublin, Poland

Introduction

Presentation will focus on the perspectives and potential benefits arising from my doctoral research, which aims to apply machine learning methods to the analysis of brain neural networks using electroencephalography (EEG) data. The EEG studies will collect data on participants brain activity, which will then be analyzed to identify key biological features associated with anxiety disorders. In the next stage, various machine learning algorithms will be applied to develop a classifier capable of effectively distinguishing individuals with diagnosed anxiety disorders from healthy individuals. The study will involve a group of 80-100 participants, divided into a control group (healthy individuals) and an experimental group (individuals suffering from anxiety). Participants will perform cognitive load tasks, and their responses will be recorded using EEG. The EEG data will then be analyzed using graph theory and statistical analysis to compare EEG responses between individuals with high and low levels of anxiety. After the experiment, participants will be asked to assess their level of anxiety and subjective experiences during the task. The potential benefits of these methods will be presented, including the possibility of developing new diagnostic tools and their integration into clinical practice. The presentation will focus on the theoretical challenges and advantages associated with the use of machine learning, such as improving the accuracy of anxiety disorder diagnosis, personalizing therapy, and better understanding the neurobiological mechanisms underlying mental disorders. Through the application of graph theory and statistical analyses, these methods can support innovative approaches to mental health monitoring, which in the future may bring significant benefits to both patients and healthcare professionals.

References

[1] Cudo A., Zabielska E., Bałaj B., *Wprowadzenie w zagadnienie interfejsów mózg-komputer*, Wydawnictwa KUL, 2011.

[2] Jackson M.M., Mappus R., *Applications for Brain-Computer Interfaces*, Brain-Computer Interfaces, Chapter 6, 2010.

[3] Jonak K., *Widespread Reductions of Spontaneous Neurophysiological Activity in Leber's Disease—An Application of EEG Source Current Density Reconstruction*, Brain Sci., 2020.

[4] Krukow P., Jonak K., *Relationships between resting-state EEG functional networks organization and individual differences in mind wandering*, Scientific Reports, 2022.

Radiated Emission of PLC Controllers Used in Drive Systems

Ryszard Goleman[1] Mariusz Holuk[2], Kamil Bańka[2]
[1]Lublin University of Technology, Department of Electrical Engineering end Superconducting Technologies, Nadbystrzycka 38A, 20-618 Lublin, Poland, e-mail: r.goleman@pollub.pl
[2]The University College of Applied Sciences in Chelm
The Institute of Technical Sciences and Aviation, Pocztowa 54, 22-100 Chelm

Introduction

The paper presents the results of electromagnetic emission measurements of radiated disturbances for the following basic components of the SINAMICS S120 system, namely:

- Sinamics Control Unit CU320-2 PIN, which is responsible for drive control and coordination, communication and signal processing;
- Sinamics S120 Smart Line Module, which is responsible for supplying and managing the drive's electrical power, enabling precise motion control in industrial applications;
- Sinamics S120 Single Motor Module drive system module, which enables precise motor motion control, providing high performance and flexibility in industrial applications. They are part of drive systems at the Laboratory of Electrical Machines and Drives of the University College of Applied Sciences in Chelm. The test results were related to the EMC Directive and the permissible limits in harmonized standards. The measurements showed that the tested components meet the requirements related to EMC issues in terms of radiated emissions, with their qualification to category C3.

Test stand and results

Electromagnetic compatibility requirements for drive systems are set out in EN IEC 61800-3 and apply to drive systems used in residential, commercial and industrial environments [1, 3]. With regard to interference emissions from drive systems, the standard distinguishes four categories (C1, C2, C3 and C4) [1].

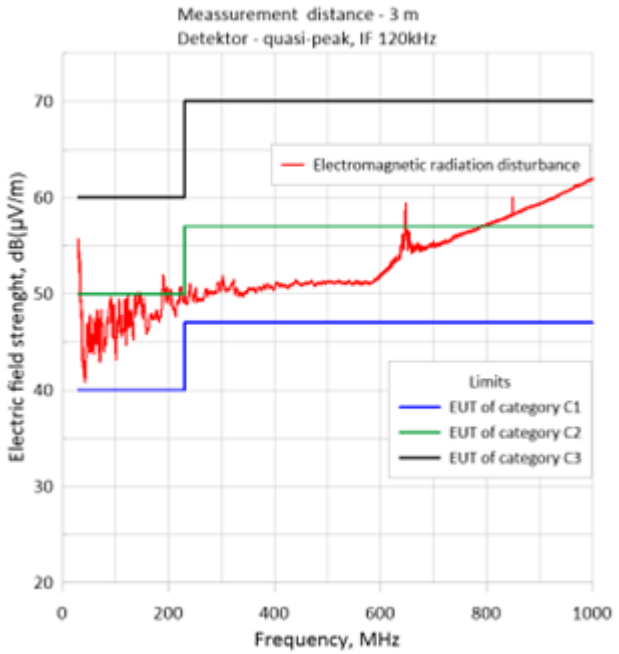

Fig. 39. Result of measurement of radiated emissions from components of the Sinamics S120 drive system, when the motor is loaded with a torque of 7Nm, at a distance of 3 m

For example, category C3 equipment is characterised by a rated input voltage of less than 1,000 V, is intended for use in industrial locations and is not intended for use in residential, commercial or industrial locations. The test bench consists of a GTEM 1000 chamber from TESEQ with a septum height of 1m, a TDEMI 1G spectrum analyser from Gauss Instruments and software to automatically control the analyser and collect data from individual measurement series [2, 4]. Selected results of radiation emission measurements of Sinamics S120 drive system components are shown in Figure 1. Radiated emission studies were performed at 230 V over the full frequency range from 30 MHz to 1 GHz, using a quasi-peak detector and a bandwidth of 120 kHz. In the first phase of the study, background measurements were made with the controller switched off. Then, with the device connected to the power supply (running the controller without the motor connected), at no load and under the conditions of operating the drive system with a synchronous machine, with different values of the motor load torque. Radiated emissions from the modules are low and do not exceed acceptable limits in industrial areas. However, they exceed the limits in residential, commercial or light industrial areas. The tests carried out confirm that the Siemens products tested are of high quality and meet acceptable EMC requirements in category C3.

References

[1] *EN IEC 61800-3, Adjustable speed electrical power drive systems - Part 3: EMC requirements and specific test methods for PDS and machine tools*, 2023.

[2] *PN-EN IEC 61000-4-20:2022-11. Electromagnetic compatibility (EMC). Part 4-20: Test and measurement methods. Test for emissions and immunity in transverse electromagnetic waveguides (TEM)*, 2022.

[3] *Directive 2014/30/EU of the European Parliament and of the Council of 26 February 2014 on the harmonisation of the laws of the Member States relating to electromagnetic compatibility*, Official Journal of the European Union, L 96/79J.

[4] Goleman R., Mazurek P., Holuk M., *3D printers – are they electromagnetically compatible?*, Przegląd Elektrotechniczny, R. 98 NR 12/2022, pp. 246-249.

Characteristics of a compact induction motor model with 50Hz/150Hz frequency converter and 3/2 number of phases

Ryszard Goleman
Lublin University of Technology,
Department of Electrical Engineering end Superconducting Technologies, Nabystrzycka 38A, 20-618 Lublin, Poland, e-mail: r.goleman@pollub.pl

Introduction

Electric machines are the most popular devices used in everyday life and the number of their types is increasing with the development of science, engineering and technology [1]. This paper presents the structure of a compact model of an induction motor supplied from a three-phase mains and associated with a magnetic converter. In the converter, a frequency change from 50Hz to 150Hz is implemented while changing the number of phases from three to two. This allows the speed of the motor to be increased three times that of a direct 50Hz mains supply. In the model presented here, the connection arrangement of the frequency converter windings with the two-phase motor winding was modified. In relation to the known connection arrangement [2, 3], two artificial neutral points were created by connecting capacitors in a two-star arrangement. The two-phase motor windings were inserted between the neutral points of the converter windings connected in a zigzag and the neutral points of the capacitor system. The presented modification of the motor model makes it possible to reduce the contribution of the third harmonic to the power source currents, to limit the reactive component of the source current and to obtain a voltage increase on the two-phase winding, which ensures a smooth motor start-up.

Motor model characterisation

The basic element of the motor model is a magnetic circuit made up of elements operating on the non-linear part of the magnetisation characteristic, which allows the magnetic flux to be deformed. In the magnetic circuit, four groups of columns can be identified, each group forming three columns, creating a system that generates the third harmonic of the magnetic flux.

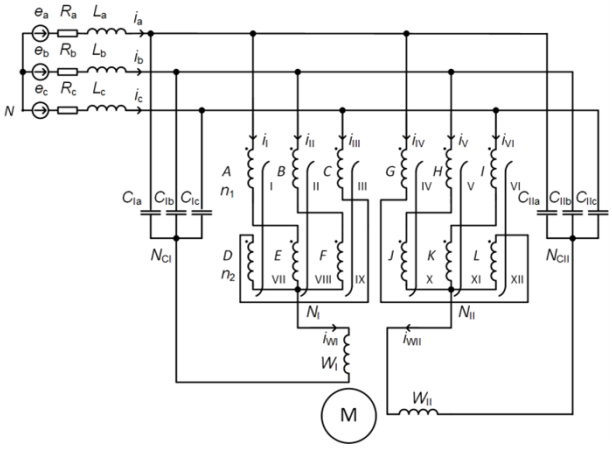

Fig. 40. Circuit diagram of a three-phase hybrid induction motor, A, B, C, D, E, F and G, H, I, J, K, L - windings of the first and second frequency converter, respectively, I, II, ... XII - magnetic circuits of frequency converter, W_I, W_{II} - coils of two-phase winding, C_{Ia}, C_{Ib}, C_{Ic} and C_{IIa}, C_{IIb}, C_{IIc} - capacitors forming star connected circuit

The windings located on the columns of the non-linear part of the magnetic circuit are supplied from the three-phase mains and form a system of two frequency converters. The windings of the frequency converters are connected in a zigzag pattern (Fig. 1). The coils of the two-phase winding are connected between the neutral points of the frequency converter windings and the capacitor system. The voltages between these points are shifted in phase by 90°.

An example of a motor model characteristic showing the variation of electromagnetic torque as a function of speed is given in Figure 2.

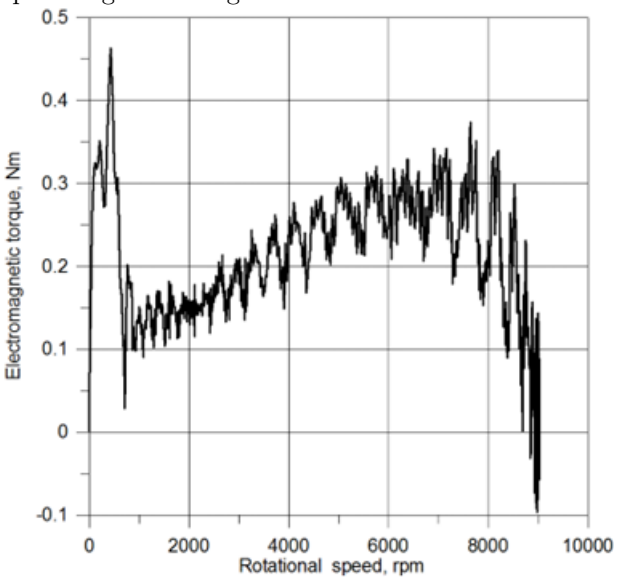

Fig. 41. Mechanical characteristic of the motor model at no-load

References

[1] Gieras J. F., *Advancements in electric machines*, Springer, 2008.

[2] Goleman R., *Performance and characteristics of a hybrid induction motor with magnetic frequency changer*, Przegląd Elektrotechniczny, 2020, vol. 96, nr 12, pp. 170-173.

[3] Goleman R., *Three phase induction motor integrated with a magnetic frequency changer*, Journal of Magnetism and Magnetic Materials, 254-255, 2003, pp. 229-301.

Analysis of the properties of HTS 2G SCS and SF windings during failure states of superconducting transformers

Łukasz Woźniak, Paweł Surdacki
Lublin University of Technology,

Abstract

The article presents a numerical model of a superconducting transformer with HTS 2G SCS and SF windings, based on PSpice software for the analysis of electrical circuits, which allows for the determination of equivalent parameters and properties of such a transformer in the steady state and in emergency states. This model uses user-defined ABM (Analogue Behavioural Modelling) computational blocks, the level two Jiles-Atherton magnetic hysteresis model and Rhyner's power law describing the E-J relationship of the HTS superconducting tape. This model was experimentally verified by measurements of a real 10 kVA HTS transformer. On this basis, an extensive numerical model of a superconducting transformer with a more complicated winding structure and a higher power of 21 MVA was developed. For such a transformer, power losses were analysed and the time courses of resistance, current and temperature of superconducting windings made of HTS 2G tapes of the SCS type with a copper stabiliser and SF without a stabiliser were examined during emergency states, such as connecting the transformer to the network and operational short circuit. A discussion was carried out on the effectiveness of using both types of HTS tapes to limit the current in emergency situations posing a risk of loss of superconductivity and destruction of superconducting windings.

The article presents a numerical model of a two-winding HTS superconducting transformer with a power of 21 MVA and a voltage of 70/10.5 kV. For the construction of the transformer windings, it was proposed to use superconducting tape of the SCS 12050 type (with a copper stabiliser layer) and SF 12050 (without a stabiliser). The circuit model of superconducting tapes developed in the PSpice software environment includes a description of the magnetic circuit using the second-level Jiles-Atherton magnetic hysteresis model and Rhyner's power law. A properly designed and modelled superconducting transformer with appropriate electrical and thermal properties can reduce currents during a fault. It can therefore successfully fulfil its purpose.

The resistance of the transformer windings is responsible for attenuating the transformer's connection current to the network and the short-circuit current. In the superconducting state, this resistance is zero. It increases rapidly when the winding goes into a resistive state, which can happen when the turn-on or short-circuit current exceeds the critical value for the superconductor. During the wave of this current, the winding can exit and return to the superconducting state many times. This translates into changes in other operating parameters, including e.g. the decay time of the switching current of superconducting transformers, compared to conventional transformers. The behavior of superconducting windings in emergency situations is determined by the parameters of the superconducting material from which they are made.

Due to the fact that limiting short-circuit currents in a superconducting transformer is based on the transition of HTS tapes to the resistive state, the short-circuit reactance of such a transformer can be designed at a very low level. This is facilitated by the favourable insulating properties of liquid nitrogen, significantly better than those of transformer oil. This allows for reducing the width of the air gap between the primary and secondary windings and thus reducing the dissipation flux, which in turn significantly reduces the variability of the voltage supplied to consumers.

It is possible to build a superconducting power transformer cooled with liquid nitrogen based on currently available superconducting materials and technologies for making structural elements. Taking into account the losses occurring in the cryogenic cooling system, a high-power superconducting transformer based on the second-generation HTS superconducting tape will have higher efficiency than its conventional counterpart, and will also be lighter, smaller, easier to transport and safe in operation. The use of supercon-ducting transformers leads to minimisation of load losses in the transformer windings and, as a result, to an increase in its energy efficiency.

In subsequent works, the authors plan to analyse the model's sensitivity to changes in input data, together with the estimation of measurement errors, and to compare the modelling results using the circuit method and the finite element method.

Phase distribution of ultrasonic field visualized by optical wave microphone CT scan

Si Thu Han[1)] Than Nu Nu San[1)], Fumiaki Mitsugi[1)], Toshiyuki Nakamiya[2)], Yoshito Sonoda[2)]
[1)]Kumamoto University,
[1)]Tokai University

The novel method, which we call the "Optical Wave Microphone (OWM)" technique, is based on a Fraunhofer diffraction effect between sound wave and laser beam. The light diffraction technique is very useful to detect the acoustic wave without disturbing the sound field. OWM also can be used to realize the visualization of acoustic sound field by computerized tomography (CT) method because the ultra-small modulation by the sound field is integrated along the laser beam path. This method was very useful to perform the high accuracy measurement of slight density change of atmosphere without disturbing electric and sound field.

Introduction

In the strong electromagnetic field, it can cause damage to the conventional microphones and when the detector is near to the target, the sound field is also disturbed by itself. However, OWM is a probe beam technique to measure the sound pressure level without the effect of an electromagnetic field, and the relationship between beam width and detectable frequency of photoacoustic waves is taken into account. In this study, the ultrasonic oscillators with two frequencies: 40 kHz, 110kHz and 200kHz are utilized as a sound source. The signal given by the photodetector, that detected the diffracted laser from the optical wave microphone, gives the phase shift value. By changing the distance between the ultrasonic oscillators and laser beam, there are some phase shift differences depending on these distances.

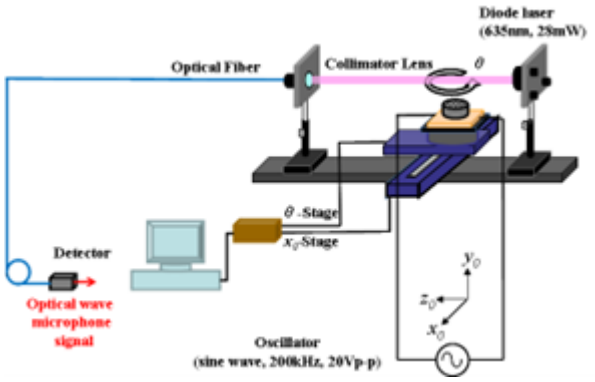

Fig. 42. OWM setup coupled with CT method to detect the ultrasound wave distribution

Principle of OWM coupled with CT

CT method can reconstruct a cross-sectional image of the sound field using projected data from many directions of at least 180 degrees. In Fig.2 , two-dimensional sound field $S(x_0, z_0)$ along the propagation direction of the y_0 is the subject area of our present research. The projected data $D(r, \psi)$ which is the detected signal can be written as the next equation.

$$D(r, \psi) = \int_L S(x_0, z = 0)\, ds \tag{10}$$

where $r - s$ coordinates are rotated by ψ from the $x_0 - z_0$ coordinates as shown in Fig.2. The reconstruction image can be obtained by inversely projecting the data to $x_0 - z_0$ coordinates, in which the filtered back-projection method and Lamp filter function were used as the reconstruction algorithm. The LabVIEW program is developed for the phase shift measurement, and by applying the CT scan, the phase shift distribution is achieved according to the position of the sound source. Therefore, the results of phase shift distribution and sound pressure measurements can estimate the location of the sound source.

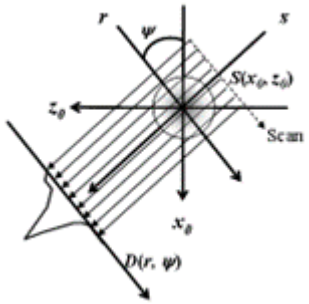

Fig. 43. OWM setup coupled with CT method to detect the ultrasound wave distribution

References

[1] T. Nakamiya et al., *Visualization of Electric Discharge Sound Fields in Atmospheric Pressure Plasma using Fraunhofer Diffraction*, Proceedings of PIERS 2013, Vol. 1, pp. 364-367, 2013.

[2] T. Nakamiya et al., *A Tomographic Visualization of Electric Discharge Sound Fields in Atmospheric Pressure Plasma using Laser Diffraction*, The European Physical Journal - Applied Physics, Vol. 61, 24310, pp. 1-8, 2013.

Analysis of electricity consumption in road lighting installations

Joanna Kozieł
Lublin University of Technology, Faculty of Electrical Engineering and Computer Science

Introduction

The article presents an analysis of the consumption of electricity in road lighting. Currently, the biggest trend is the modernization of road lighting based on LED technology. This brings many financial and ecological benefits, but also carries concerns about disruptions related to the disruption of the power grid. The study includes a lighting project and indicates guidelines that should be taken into account when designing lighting. The topic of proper lighting of pedestrian crossings was also raised.

Overview of existing road lighting solutions

The aim of the article is to review existing road lighting solutions, present the results of computer simulation of various road situations, analysis of lens selection, height of posts and their arrangement, and other parameters influencing the distribution of the photometric solid. The results of a research survey conducted among users of motor vehicles traveling on Polish roads are included.

Fig. 1. A road illuminated by means of luminaires with a sodium source is presented.

Fig. 44. A road illuminated by means of luminaires with a sodium source

Fig. 2 presents the implementation of lighting on composite poles with birch graphics illuminated by an internal additional light source. Pabianice, Lewityn MOSIR.

Fig. 45. Implementation of lighting on composite poles with birch graphics illuminated by an internal additional light source. Pabianice, Lewityn MOSIR

Measuring planes at a pedestrian crossing

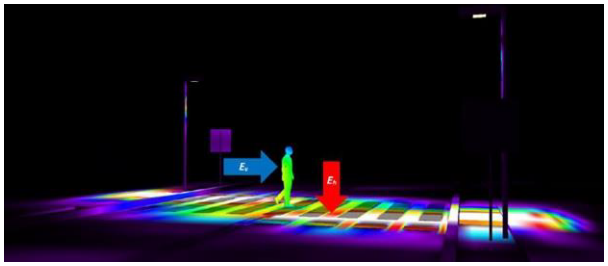

Fig. 46. Visualization of measurement planes at a pedestrian crossing

Illuminance parameters are also used to assess the lighting condition at pedestrian crossings. Thanks to the availability of measurement tools (lux meters), using intensity parameters allows determining values on planes considered representative of the pedestrian crossing area.

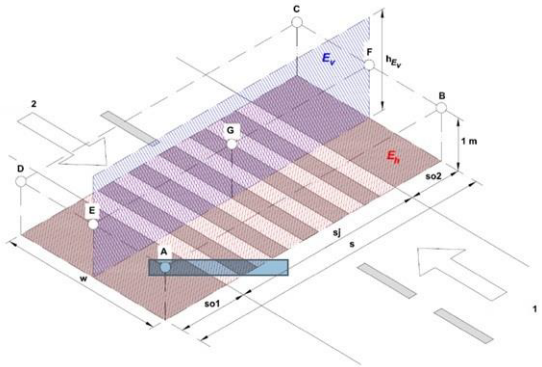

Fig. 47. Measurement planes at a pedestrian crossing

Two planes can be distinguished at a pedestrian crossing:

- vertical E_v - related to the illuminance on the pedestrian's silhouette,
- horizontal E_h - related to the illuminance of the roadway (lanes) and waiting areas.

The number of vertical planes passing through the axis of the pedestrian crossing depends on the directions of vehicle movement. The following parameters can be determined for each direction of vehicle movement:

- minimum vertical illuminance E_{vmin},
- maximum vertical illuminance E_{vmax},
- average vertical illuminance $E_{vśr}$,
- uniformity of illuminance in the vertical plane $E_{vmin}/E_{vśr}$,

- parameter E_{vmin}/E_{vmax} defining the greatest difference in illuminance values in the vertical plane.

For the horizontal plane, related to the lighting of the roadway on which the crossing is located and the waiting zones, the following values can be determined:

- minimum horizontal illuminance E_{hmin},
- maximum horizontal illuminance E_{hmax},
- average horizontal illuminance $E_{hśr}$,
- uniformity of illuminance in the horizontal plane $E_{hmin}/E_{hśr}$,
- parameter E_{hmin}/E_{hmax} defining the greatest difference in illuminance values in the horizontal plane.

Based on the illuminance values, it is not possible to conclude about the possibility of noticing a pedestrian by a driver of a motor vehicle approaching the crossing. The illuminance parameters do not answer the question of what contrast is created between the luminance of the pedestrian's silhouette and the luminance of the surroundings in which the pedestrian is perceived. However, the use of illuminance criteria allows for the verification of the assumed design values and control of the lighting status of existing lighting installations.

Results of the survey conducted among drivers of motor vehicles

Due to the small number of studies in the field of road lighting, road users, and the impact of lighting on safety while driving, a survey was conducted among drivers of motor vehicles. 100 people took part in the survey: 77% of women and 23% of men, all with a driving license, aged 18 to 80.

Among the respondents were 48% of people who had a driving license for 3 to 10 years, and another significant group were people with a driving license for 10 to 20 years—30%. The respondents are everyday road users in 67%. They travel by motor vehicle up to 4 hours, which means commuting to work, shopping, short trips outside the place of residence—this is how 97% of respondents spend their time in the vehicle. This is a group of young drivers up to 40 years of age who are not exposed to presbyopia and reliably perceive visual stimuli of the surrounding reality. Among the respondents, 75% of people declared the importance of caring for the environment. This favors the choice of LED technology, which reduces CO_2, mercury production, and other harmful substances for the environment. Therefore, in connection with such a group of survey participants, reliable conclusions can be drawn and based on analysis.

Only 45% of road users prefer a light color of around 4000K, and 18% of respondents said the color of light is indifferent. In question 6, which covered the problem of switching off lighting in built-up areas, 74% of respondents expressed the opinion that they do not see the need for such a procedure. It is known that this is due to the search for savings, but the safety of drivers and pedestrians should be the priority.

Almost all respondents believe that road lighting has a significant impact on pedestrian safety, and 78% answered that pedestrian crossings are poorly marked or inadequately lit. Therefore, it is encouraged to build lighting for pedestrian crossings and the area around the crossing, entrusting the project to experienced engineers from professional companies. It is worth entrusting lighting investments to people who have received education in this matter—54% and 48% respectively stated that they have often observed the effect of glare on roads or pedestrian crossings. Such situations, in which a driver or pedestrian is exposed to the risk of losing their health or life due to reprehensible lighting, are unacceptable. Talks are underway with the government on introducing legal regulations regarding the profession of a lighting designer. The skills of a person designing lighting are burdened with a great responsibility, of which many people are not aware. According to the Association of Rural Communes of the Republic of Poland and the Polish Association of the Lighting Industry, "good, energy-efficient lighting of our communes (cities) and counties is in our national interest and serves to improve the perception of Poland in the international arena". Respondents have a similar opinion, as many as 95% agreed with the statement that good, correct lighting can be a city's showcase. Such information should encourage city, commune, and road managers to modernize lighting not only to be more energy-efficient and environmentally friendly.

Conclusions

Designing road lighting is a skill burdened with responsibility for the health and life of road users. In Poland, there are no mandatory legal acts that would impose on lighting designers any parameters that they should follow when selecting lighting devices and creating a project. Anyone who watches a few instructional videos on the Internet can become a lighting designer. On the other hand, based on the author's experience, office employees who are responsible for creating technical specifications for public procurement related to road lighting or pedestrian crossing lighting do not have the technical knowledge and are not able to independently create requirements for a given lighting investment, let alone control its correctness. Many public entities are obliged to trust contractors or independent inspectors to accept measurements after the investment task is carried out.

On the other hand, we should ask ourselves whether lighting modernization is becoming a necessity. Looking at the economic aspect, road safety, user comfort - it certainly is. It is necessary to remember about appropriate compensation of reactive power, so that the monthly payment for electricity is actually lower. Rising electricity prices affect everyone, both commercial and private customers, as well as local governments.

The survey analysis is a clear appeal to lighting managers not to turn off road lighting at night and to look at it from the perspective of maintaining the safety and comfort of travelers.

References

[1] Żagan Wojciech, *„Oprawy oświetleniowe”*, OWPW, Warszawa 2012.

[2] Polska Norma PN-EN 13201:2007, *„Oświetlenie dróg”*, PKN, Warszawa 2007 r.

[3] Polska Norma PN-EN 13201:2016, *„Oświetlenie dróg”*, PKN, Warszawa 2016 r.

[4] Żagan Wojciech, *„Podstawy techniki świetlnej”*, OWPW, Warszawa 2014.

[5] *Wytyczne organizacji bezpiecznego ruchu pieszych, Wytyczne prawidłowego oświetlenia przejść dla pieszych, Część I – raport z przeprowadzonych studiów i analiz*, Gdańsk, Warszawa - grudzień 2017.

[6] CEN/TR 13201-1:2016-02, *Oświetlenie dróg – Część 1: Wytyczne dotyczące wyboru klas oświetlenia.*

[7] PN-EN 13201-2:2016-03, *Część 2: Wymagania eksploatacyjne.*

[8] PN-EN 13201-5:2016, *Oświetlenie dróg – Część 5: Wskaźniki efektywności energetycznej.*

Determination of the typical course values of aircraft parameters for the new measurement system in the case of aircraft takeoff and landing

Joanna Michałowska[1)], Paweł Tomiło[2)]
[1)]Lublin University of Technology, Department of Electrical Engineering and Superconductivity Technologies,
[2)]Lublin University of Technology, Faculty of Management

Introduction

Monitoring flight parameters is a very important research aspect, especially during training flights. Current pilot training standards lead to a continuous effort to improve the level of safety. For many years, various types of recording devices have been installed in aircraft to analyse aviation incidents. The European Aviation Safety Agency (EASA) recommends the need to conduct research into monitoring flight parameters. Such actions lead to improved safety as well as increased quality of training. In addition, there are also reports that the influence of high-frequency sounds may impair cognitive abilities. Large-scale electronic avionics systems are considered to be the source of rapidly changing fields. These fields are also propagated from external sources. Putting low-cost prototype measurement systems on aircraft allows for data monitoring as a common way to improve safety. rtificial intelligence and neural networks have great potential to perform detailed analyses concerning the recognition of aspects of flight parameters, such as: acceleration, Euler angles and the electric component of the electromagnetic field (E_{RMS})

Method and materials

For two measurement systems were placed in the PZL 110 Koliber 150 aircraft - an interial measurement system with 9 degrees of freedom and an electromagnetic field. Indications from both systems were collected for the moment the aircraft took off and landed. Measurements were made under varying weather conditions with temperatures ranging from 18 to 24 °C and wind velocities ranging from 5 to 29 Knots.

The data were used to train the developed a generative artificial neural network model, on the basis of the results of which typical time courses of acceleration values, Euler angles and electromagnetic field values were indicated for time series covering the moment of aircraft takeoff and landing. The presented solution can serve as a system for detecting irregularities in timeseries of 3-axis acceleration and Euler Angles and occurrences of electromagnetic field outliers in the takeoff and landing procedure.

First, in order to create a larger dataset that will allow the generalized signal characteristics to be determined later in the analysis, a generative artificial neural network model based on the variational autoencoder (VAE) architecture was developed.

Aby przeanalizować występowanie wartości odstających w zgeneralizowanym szeregu czasowym dla danej wartości, zastosowano metodę podobną do Piecewise Aggregate Approximation (PAA). Podobnie jak w metodzie PAA, redukcję wymiarowości przeprowadzono, dzieląc oryginalny szereg czasowy $X = (x_1, \ldots, x_M)$ na ramki o równej wielkości $X' = (x'_1, \ldots, x'_M)$. Wymiar został zredukowany z n do M przy użyciu równania (1).

$$\overline{X}_i = \frac{M}{n} \sum_{j=\frac{n}{M}(i-1)+1}^{\frac{n}{M}\cdot i} x_j \quad (1) \qquad (11)$$

For each frame created, the median was determined, as well as two intervals from the first quartile (Q1) to the third quartile (Q3) and from the same interval will increase by 1.5 the inter-quartile range (IQR). The second interval is assumed to be the interval of acceptable values, which means that values outside this interval are counted as outliers. Figure 1 shows an example of determining the occurrence of outliers for an E_{RMS} time series.

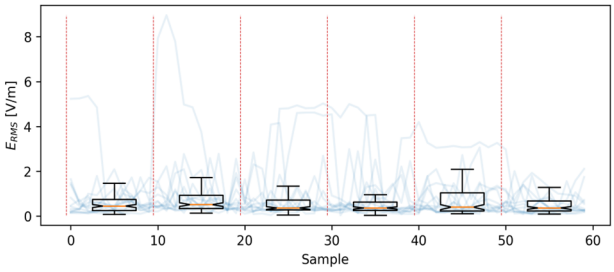

Fig. 48. Example of determining the occurrence of outliers for the E_{RMS}, V/m time series

Table 5: Summary of values obtained for the ERMS, V/m time series

Frame	Q1-1.5IQR	Q1	Q3	Q3+1.5IQR
1	0.081	0.24850	0.381546	1.466
2	0.135	0.33850	0.432120	1.723
3	0.044	0.27775	0.302223	1.341
4	0.039	0.25525	0.312880	0.960
5	0.100	0.22925	0.290102	2.093
6	0.084	0.23100	0.303155	1.283

References

[1] Pytka J., Budzyński P., Tomiło P., Michałowska J., Błażejcza D., Gnapowski E., Pytka J., Gierczak K., *Measurement of aircraft ground roll distance during takeoff and landing on a grass runway*, Measurement, 2022.

[2] Michałowska J., Tomiło P., *Measurement System of an Electromagnetic Field for Aircrafts with the Use of Machine Learning Model*, Metrology and Measurement System, 2024.

[3] Zhang C., Chen Y., Yin A., Qin Z., Zhang X., Zhang K., Jiang Z. L., *An Improvement of PAA on Trend-Based Approximation for Time Series*, Springer, 2018.

[4] Kingma D. P., Welling M., *An Introduction to Variational Autoencoders*, Now Foundations and Trends, 2019.

Overview of cold plasma and high temperature superconductors application in medicine

Joanna Kozieł Henryka Danuta Stryczewska
Lublin University of Technology, Department of Electrical Engineering and Superconducting Technologies

Introduction

Many modern electromagnetic technologies are used in medicine for the diagnosis, healing and rehabilitation of diseases. The development of new methods is related to the progress in the area of basic, applied and developmental sciences. It requires interdisciplinary research, ranging from medical, biological, chemical, physical, engineering and technical sciences to social and economic sciences. The presentation overviews selected applications of cold plasma and high temperature superconductivity phenomena that are already used in medicine, and indicates those applications that have the greatest potential for their implementation in medical practice.

Plasma and Superconductivity Phenomena for Medical Applications

The development of superconducting and plasma technologies dates back to the beginning of the 20th century, when the phenomena on which they are based were discovered and named. The main factor underlying both phenomena is temperature. Plasma and superconductivity occupy opposing ranges on the thermodynamic temperature scale (Figure 1). The phenomenon of superconductivity is a combination of the magnetic and electrical properties of a material (metals and alloys) manifested by the disappearance of electrical resistance, accompanied by the forces of magnetic ordering.

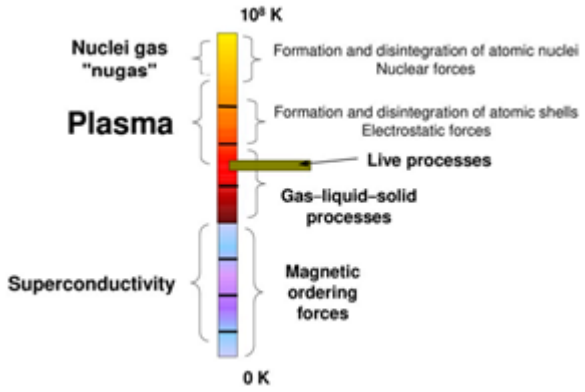

Fig. 49. Thermodynamic scale of temperatures with marked phenomena of plasma and superconductivity

A much larger part of the thermodynamic scale presented in Figure 1 is occupied by plasma, an ionized gas with electrically conductive properties, whose particles such as electrons, ions and neutrals have energies between 0.05 eV and 104 eV. A distinction is made between low-temperature plasma and high-temperature plasma. For medical purposes, low-temperature plasma produced at atmospheric pressure, commonly referred to as cold plasma, is used.

Medical applications of cold plasma

The effects of cold plasma on living organisms include the action of high-energy electrons that gain energy in an electrical discharge field, ionised atoms and molecules, the action of free radicals including oxygen, nitrogen (RONS), UV radiation, hydrogen peroxide and ozone. Cold plasma medical application includes:

- Sterilisation of human and animal tissues, blood and surface wounds;
- Sterilisation of medical instruments and surgical materials, especially those made of materials not resistant to high temperatures;
- Treatment and healing in dentistry, dermatology, cancer, skin wounds, diabetic foot, ulcers, erythematous, oozing lesions;
- Covering implants, contact lenses, prostheses with biocompatible surfaces;
- Tissue engineering - production of bioactive agents and drugs, immobilisation of biological molecules, modification of cell surfaces to control their behaviour, improvement of blood adhesion;
- Medical diagnostics - manufacture of polymer-based sensors and amorphous thin films for medical analysis and biochemical analysis.

Medical applications of high temperature superconductors
The generation of a consistently strong and homogeneous magnetic field over a large area is one of the most important applications of superconductivity in medicine, which include:

- Magnets with high magnetic inductions for applications:
  - in radiotherapy (cyclotrons),
  - isotope production,
  - therapeutic beam delivery of protons and ions,
  - magnetic resonance imaging (MRI).

  MRI is currently the largest commercial application of superconductivity. Superconducting magnets in MRI make it possible to obtain high-quality diagnostic information as well as to discover the function of biological systems and study biochemical processes.
- SQUIDs (Superconducting Quantum Interference Device) using the Josephson junction as ultrasensitive transducers of electromagnetic signals. With these devices, significant advances are being made in biological imaging and biochemical analysis.

Effects of the operation of a cogeneration system on the example of an installation in a sugar factory

Krzysztof Nalewaj[1] Ryszard Goleman[2], Krzysztof Mięczak[3], Sławomir Bajda[3]
[1]The University College of Applied Sciences in Chelm, The Institute of Technical Sciences and Aviation, Pocztowa 54, 22-100 Chelm, Poland,
[1]Lublin University of Technology, Department of Electrical Engineering end Superconducting Technologies, Nadbystrzycka 38A, 20-618 Lublin, Poland,
[3]National Food Company S.A. in Toruń, Branch "Sugar Factory Werbkowice" in Werbkowice, Werbkowice, ul. Przemysłowa 2, Poland

Introduction

Until 2018, pulp drying in the Werbkowice Sugar Factory drying building was carried out in the two drying lines installed, for which the heat source was the PS 10 drying oven with a thermal power of 11.6MW powered by hard coal. The concept of cogeneration in the conditions of the Werbkowice Sugar Factory involved the use of waste heat generated in the sugar production process instead of the existing heating system, where the primary fuel was hard coal. The recovered thermal energy of the barometric circuit - 5.10MWh, the energy of the condensate circuit - 8.15MWh and the energy of steam - 5.45 MWh was supplemented with thermal energy from the cogeneration system - 1.70 MWh. This enabled a total of 20.40 MWh of thermal energy to be generated, which was mainly used for the drying of the pulp.

Combined heat and power (CHP) system as part of the energy system of a sugar factory

The cogeneration system installed at Cukrownia Werbkowice is one of the heat sources used for pulp drying. A cogeneration system is a system in which the energy contained in the fuel (natural gas) is converted into electrical and thermal energy. The basic structure of CHP systems includes: gas engine, generator and heat exchangers. By using waste heat and heat from cogeneration, about 8 tonnes of dry pulp with a moisture content of 8% can be obtained from (24-26) tonnes of wet pulp with a dry matter content of about 30

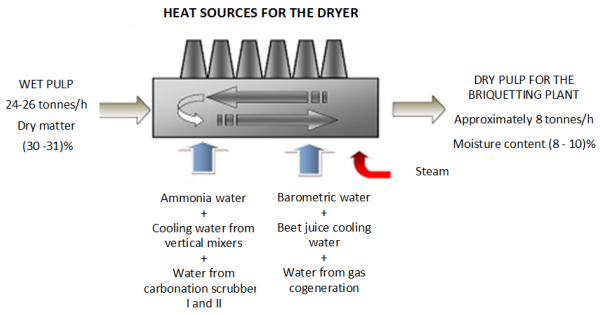

Fig. 50. Block diagram of waste heat and CHP heat use for pulp drying

The installed cogeneration system (Fig.2), powered by natural gas, had the following technical parameters:

- rated electric power - 1,56MW,
- maximum thermal power - 1.56MW,
- working voltage - 400V,
- total efficiency of the system - 90.5
- gas consumption - 240m3/MW.

Fig. 51. View of a cogeneration system with an electrical output of 1.5MW and a thermal output of 1.7MW

The thermal energy produced by the CHP system was used during the campaign to dry the pulp, but also for social purposes, heating the packing house and silos. The electrical energy from the CHP system not only made up the energy deficit, but also significantly reduced the energy consumption from the grid. In conclusion, it can be said that the use of a CHP system increases the energy security of the plant, as its system can successfully operate off-grid, i.e. it makes the company independent of electricity suppliers. The use of the cogeneration system secures the Sugar Plants with their own electric energy, not only for the campaign period but also for a significant part of the overhaul period. In addition, the system has a high overall efficiency of over 90%. In turn, the reduction in the use of hard coal as fuel significantly reduces emissions of CO_2, dust and SO_2

References

[1] Pytka J., Budzyński P., Tomiło P., Michałowska J., Błażejcza D., Gnapowski E., Pytka J., Gierczak K., *Measurement of aircraft ground roll distance during takeoff and landing on a grass runway*, Measurement, 2022.

[2] Michałowska J., Tomiło P., *Measurement System of an Electromagnetic Field for Aircrafts with the Use of Machine Learning Model*, Metrology and Measurement System, 2024.

[3] Zhang C., Chen Y., Yin A., Qin Z., Zhang X., Zhang K., Jiang Z. L., *An Improvement of PAA on Trend-Based Approximation for Time Series*, Springer, 2018.

[4] Kingma D. P., Welling M., *An Introduction to Variational Autoencoders*, Now Foundations and Trends, 2019.

The influence of the type of plasma reactor power supply on the possibility of regulating the discharge power in process gases

Michał Aftyka, Grzegorz Karol Komarzyniec
Lublin University of Technology, Department of Electrical Engineering end Superconducting Technologies,
Nadbystrzycka 38A, 20-618 Lublin, Poland

Introduction

So far, many different in terms of design and operating principles of arc plasma reactors and dedicated power supply systems have been developed. None of the power supply designs are universal enough to be used to power any type of plasma reactor, used in any plasma process. Many of the power supplies in use were developed with incorrect assumptions made at the design stage. This is mainly related to the problems caused by powering a receiver that is difficult to describe and analyze, such as an electric discharge. This article attempts to present the impact of the power supply design on the ability to regulate the discharge power in various gases. The tests were performed for four different power supply designs. This work will allow for the elimination of errors made at the design stage of a power supply for powering a plasma reactor.

In the article

The problem of powering plasma reactors with electricity comes down to providing the plasma parameters required for the process involved, while ensuring good cooperation with the power grid and limiting the interference generated by the plasma reactor. Figure 1 shows a three-phase plasma reactor with sliding arc discharge.

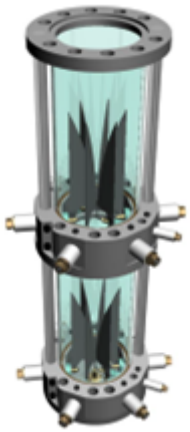

Fig. 52. Plasma reactor

Three-phase sliding arc discharge plasma reactors are devices in which it is difficult to maintain stable plasma parameters, both in electrical and physicochemical terms. The main cause of plasma instability is its source, which is the free electric arc. Such an arc is an unstable discharge that generates many electromagnetic disturbances, voltage dips and surges, surges, noise and harmonic distortion. Such an arc, due to its heterogeneous structure, both with respect to cross-section and along the axis, is difficult to analyze in terms of physical and chemical parameters. In a free arc, even small changes in power parameters, physical or chemical parameters of process gases lead to changes in arc burning conditions, which in turn induces self-regulating reactions in the plasma that change the structure of the arc and its characteristics.

The article deals with the cooperation of a plasma reactor with four types of power supply systems for electricity. The tested power supplies differ in design mainly due to the construction of transformers. One of the power supplies is a transistor transformer equipped with a matching transformer. The construction of power supplies significantly affects the characteristics of the operation of the plasma reactor and its cooperation with the power supply system. The type of plasma gas used has a great influence on the characteristics of the reactor operation and its cooperation with the power supply system for electricity.

Regulation of plasma parameters comes down to regulation of electrical power supply parameters, regulation of physical parameters of process gases and modification of their chemical composition. Regulation of plasma parameters using electrical parameters is a complex, multithreaded and not fully understood problem. Shape of plasma parameters is possible by choosing the voltage between DC and AC, choosing the power supply voltage frequency, choosing the voltage and current values, choosing the voltage shape, controlling the harmonic contents in voltage and current. It should be remembered that the power supply design itself affects the discharge parameters. In the case of transformer power supplies, the type of core material may be affected, and in three-phase circuits, the connection method may be affected.

References

[1] George A., Shen B., Craven M., Wang Y., Kang D., Wu C., Tu X., *A Review of Non-Thermal Plasma Technology: A novel solution for CO_2 conversion and utilization*, „Renewable and Sustainable Energy Reviews", Volume 135, January 2021, p. 109–702.

[2] Domonkos M., Tichá P., Trejbal J., Demo P., *Applications of Cold Atmospheric Pressure Plasma Technology in Medicine, Agriculture and Food Industry, Heat string model of bi-dimensional dc Glidarc*, „Appl. Sci.", 2021.

[3] Felea C. I., Astanei D., *Electrical characterization of the double crossing Glidarc reactor with cylindrical symmetry*, International Conference on Optimization of Electrical and Electronic Equipment (OPTIM) & 2017 Intl Aegean Conference on Electrical Machines and Power Electronics, 2017, May ACEMP, pp. 1039–1044.

System for decision monitoring technical objects

Radosław Gad[1)]
[1)]Lublin University of Technology

Abstract

The paper is devoted to the presentation of the information system for decision monitoring of objects. There is described the problem of diagnostic monitoring automotive vehicles. Developed method of relational diagnostic monitoring is based on certain models of cognitive maps. Computer system of decision monitoring is presented. There is also presented realization of the work of System for Decision Monitoring Technical Objects State (SMDSOT) on the example of diagnosing ignition system in automotive vehicles.

The Impact of Renewable Energy Sources on the Reliability Parameters of Power Grids

Alicja Zielonka[1)], Paweł Węgierek[1)], Damian Kostyła[1)]
[1)]Department of Electrical Devices and High Voltage Technology, Faculty of Electrical Engineering and Computer Science Lublin University of Technology

Introduction

The increasing share of renewable energy sources (RES), such as wind and solar power, is a key element of the ongoing energy transition in both Poland and Europe. RES play a significant role in reducing CO_2 emissions and increasing the proportion of clean energy in the energy mix, which is crucial for lowering the carbon footprint and achieving climate goals. However, the dynamic integration of renewable energy sources into existing power infrastructure poses a number of challenges related to maintaining the reliability of energy supply.

Reliability Indicators in Power Systems

The SAIDI (System Average Interruption Duration Index) and SAIFI (System Average Interruption Frequency Index) indicators are widely used in assessing the reliability of power systems. In Poland, the values of these indicators are higher than in Western European countries such as Germany or Denmark [1]. For instance, in 2022, the SAIDI in Poland reached 123 minutes, compared to only 20 minutes in Germany. These differences result from varying levels of development in energy infrastructure and the degree of implementation of modern grid management technologies [2].

The Variability of RES and Its Impact on Grid Stability

Due to their variability, RES introduce significant unpredictability into power systems. The generation of electricity from wind or solar energy depends on weather conditions, which can lead to sudden fluctuations in energy supply [3]. In systems not adequately prepared for such changes, this can result in a higher frequency of outages and network overloads. In Poland—where the distribution and transmission infrastructure is still undergoing modernization—these issues are especially noticeable in regions with intensive renewable energy production [4], [5].

Technological Solutions for Enhancing Grid Reliability

Improving the reliability of power grids requires substantial investment in advanced technological solutions, such as smart grid management systems that enable faster responses to fluctuations in energy production, as well as energy storage technologies [4]. Energy storage is essential for balancing periods of RES overproduction with times when demand exceeds current generation. In Germany and Denmark, the implementation of such solutions has already yielded positive results, as evidenced by their low SAIDI and SAIFI values [6].

The Need for Infrastructure Modernization in Poland

To meet the challenges posed by the growing share of RES, Poland must accelerate the modernization of its power networks. The expansion and upgrading of transmission infrastructure, along with investments in energy storage facilities, can significantly enhance the stability of energy supply, which is vital in light of increasing energy demands and decarbonization requirements [7].

Future Outlook and Strategic Recommendations

Forecasts for the coming years indicate that Poland must continue to invest in the development of technologies and infrastructure to meet the demands of modern energy systems [4]. The implementation of these investments is necessary to ensure the stability of the power system amid the growing share of renewable energy sources, and to minimize the risk of failures and grid overloads. The deployment of smart monitoring systems, automation, and energy storage are among the key actions that can improve grid reliability indicators in Poland [4], [7].

References

[1] Energy Regulatory Office (URE) - Raport roczny o niezawodności dostaw energii elektrycznej, 2022.
[2] German Federal Network Agency - Electricity Supply Quality and Reliability Report, 2022.
[3] International Renewable Energy Agency (IRENA) - Integracja odnawialnych źródeł energii z sieciami elektroenergetycznymi, 2022.
[4] Ministerstwo Klimatu i Środowiska - Polityka Energetyczna Polski do 2040 roku.
[5] International Energy Agency (IEA) - World Energy Outlook: Renewable Energy Integration, 2023.
[6] European Network of Transmission System Operators for Electricity (ENTSO-E) – Annual Report on Electricity System Adequacy, 2023.
[7] Council of European Energy Regulators (CEER) - 2023 Benchmarking Report on Quality of Electricity Supply.

Pressure Monitoring in Medium-Voltage Vacuum Interrupters

Damian Kostyła[1)], Paweł Węgierek[1)], Alicja Zielonka[1)]
[1)]Department of Electrical Devices and High Voltage Technology, Faculty of Electrical Engineering and Computer Science Lublin University of Technology

Introduction

Outdated energy infrastructure disrupts the continuity of electricity supply, hindering economic innovation. Interruptions in energy supply lead to higher SAIDI and SAIFI reliability indices. Quality and reliability requirements have sparked interest in enclosed energy devices. Vacuum technology has played a crucial role in insulating electrical switchgear and extinguishing electric arcs for over four decades. However, the lack of real-time pressure monitoring systems for vacuum devices, especially enclosed disconnectors, limits their use as isolation switches. Potential insulation failure poses a risk to maintenance teams and can lead to unplanned outages, further degrading the quality of energy supply. This paper presents an innovative pressure monitoring system for vacuum interrupters, utilizing fiber Bragg gratings as a measurement sensor, enabling pressure measurement in the range of 20 Pa-5×10^5 Pa.

Research Stands, Materials, and Methods

Pressure measurement in vacuum devices is one of the key elements determining their usability and ensuring appropriate isolation gaps during operation. The research team designed, constructed, and successfully tested a fiber optic sensor for measuring pressure in vacuum switching and distribution equipment, combining the advantages of fiber optic measurement and metal deformation. Figure 1 presents the experimental setup for evaluating the developed solution.

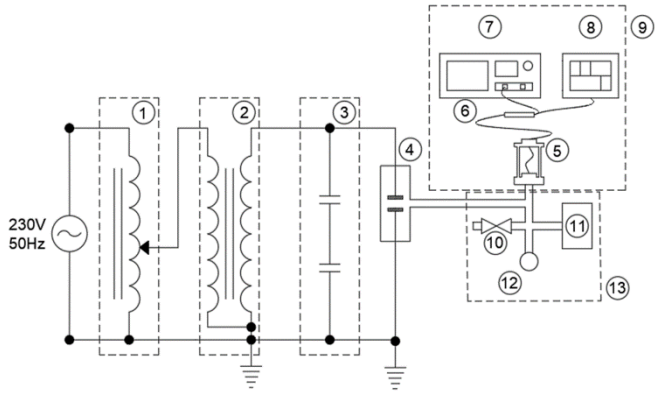

Fig. 1. Diagram of a measuring station equipped with vacuum chamber intended for empirical tests of vacuum sensors: 1 – control panel, 2 –transformer, 3 – capacitive divider, 4 – removable vacuum chamber, 5 – tested measuring head, 6 – measuring circulation system, 7 – optical spectrum analyzer, 8 –light source with superluminescent diode, 9 – fiber optic measuring system, 10 – dosing valve, 11 – pump set, 12 – vacuum meter, 13 – vacuum system.

Using a custom-designed experimental setup, the measurement capabilities of the developed sensor were tested (Figure 2). By performing measurements with an optical spectrum analyzer and a vacuum gauge, the optical power for specific pressure values was determined, which allowed for the determination of the pressure in the vacuum device using the developed sensor design.

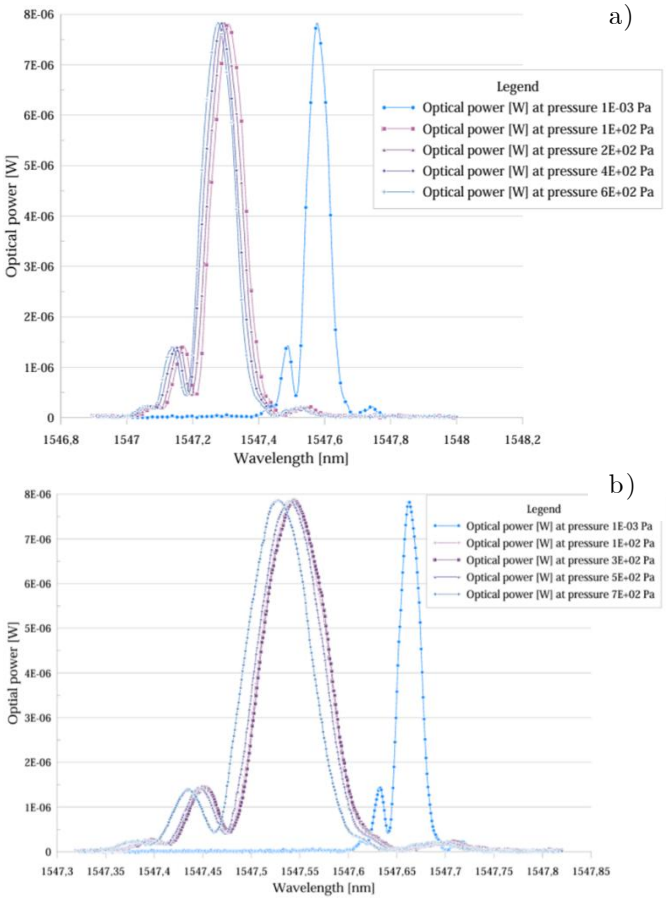

Fig. 2. Pressure-load-induced response of the measuring head examined with an optical spectrum analyzer: (a) measuring head with a stainless steel membrane; (b) measuring head with an INCOTEL 718 membrane.

Summary

The upcoming research efforts are focused on the miniaturization of the sensor system and the selection of diaphragm material that allows operation over a wider pressure range. An important aspect of the planned work is also to increase the measurement sensitivity of the proposed system.

Innovative Cheneau brace as an optimised alternative to static orthosis improving idiopathic scoliosis therapy using self-learning and decision-making system

Patrycja Tymińska-Wójcik[1)], Katarzyna Zaborowska-Sapeta[2)], Tomasz Giżewski[3)]
[1)] Department of Electrical Devices and High Voltage Technology, Faculty of Electrical Engineering and Computer Science, Lublin University of Technology, Poland
[2)] Department of Rehabilitation and Orthopaedics, University of Warmia and Mazury in Olsztyn, Poland
[3)] Department of Electrical Engineering and Superconductivity Technologies, Faculty of Electrical Engineering and Computer Science, Lublin University of Technology, Poland

Introduction

This study analyses the dynamics of forces in an intelligent Cheneau brace prototype, an advanced solution for treating idiopathic scoliosis. Traditionally, the static Cheneau brace is the primary method used to correct spinal deformities by exerting multi-point pressure on the patient's torso. This research, part of a doctoral dissertation, focuses on data collected during clinical trials with a small patient group. The goal is to systematize these findings and develop guidelines for implementation in a decision-making system.

Materials and Methods

The intelligent Cheneau brace is a portable system based on an STM32 microcontroller, designed to collect real-time data on force values from sensors mounted within the orthosis. This setup aims to identify the optimal pressure levels to enhance the effectiveness of scoliosis treatment. A device with a measurement frequency of one per second was developed, utilizing custom-made thin-film graphene sensors. These sensors are strategically placed in the same areas on all patients to ensure consistent data comparison. This approach helps identify where the highest pressure values occur and whether these high-force areas are consistent across different patients. The essence of the research is to determine the force distribution in specific areas across various patients, assess which sensors are most active during the day, and evaluate if these patterns are consistent among different individuals. Data collection occurs every second, with results averaged into optimal time samples for analysis. The study also explores how different times of day affect the pressure exerted by the brace on the torso and how various activities (e.g., sleeping, standing, sitting) influence these forces. Force patterns within the brace are determined by a self-learning algorithm, which is calibrated based on input from the physician. This system accounts for individual factors such as the type of scoliosis, degree of bone maturity, patient age, gender, spinal mobility, and pelvic rotation. The algorithm's output, which determines the degree of correction, is derived from the sensor readings within the brace.

Results and Discussion

The collected data were analysed, focusing on the interaction between individual sensors in the spine and thorax areas. As the study involved a larger patient group, it was possible to compare force values across different individuals and activities throughout the day. This comparison, coupled with X-ray images taken during the treatment cycle, allowed for an assessment of how wearing the brace impacts the correction of spinal curvature. The study reveals that the analysis of a person's skeletal system and the forces generated by the brace can optimize posture correction methods. Effective management of scoliosis therapy with orthopaedic braces requires a complex system that monitors, analyzes, and automatically adjusts the forces applied by the orthosis. Developing a self-learning algorithm to control these forces involves several key steps: data collection, analysis, adaptation to the individual patient's needs, and continuous improvement based on therapy results. The rehabilitation brace operates as follows (Fig. 1.): pressure data are collected from sensors attached inside the orthosis and sent to a microcontroller. The data are then transmitted to a control device, where the required pressure forces needed to correct the spine's position are calculated. This information is used to adjust the pressure in pneumatic cushions within the brace. The pressure in these cushions is dynamically regulated based on feedback from the sensors, ensuring that the forces are optimal for postural correction.

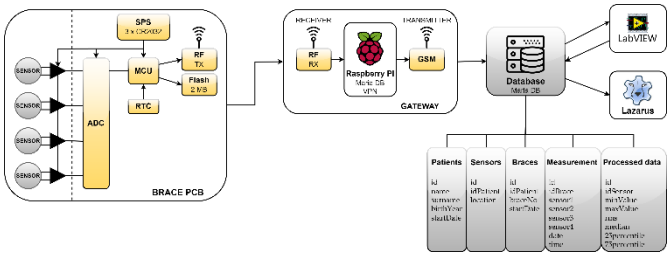

Fig. 1. Schematic of the measurement system in an intelligent Cheneau brace

To design effective brace control algorithms, regular tests were conducted on multiple patients over an extended period. The control algorithm considers several important parameters, including the patient's age, degree of curvature (Cobb angle), fat volume, duration of orthosis wear, daily activity levels, and current sensor

readings. The algorithm is regularly updated based on the doctor's feedback during periodic patient evaluations. The doctor assesses whether the current control plan is improving posture, ensuring patient comfort, and avoiding excessive correction that could cause pain. This iterative process refines the control algorithm for each patient, ultimately leading to a decision system that adjusts brace forces to provide the most effective postural correction, surpassing that of a static orthosis

Conclusion

The primary task of the Cheneau-type orthopaedic brace is to collect data on the pressure forces exerted by the rigid orthosis on the body. This data is used to determine the optimal pressure settings for the pneumatic cushions, controlled by a distributed decision-making system. Periodic X-ray images taken during the treatment process show significant improvements in spinal curvature, confirming the initial assumptions. The regular and precise use of the orthosis, with patients wearing the brace for up to 23 hours a day, achieves the desired therapeutic outcomes. X-ray images quantitatively show the reduction in Cobb angle throughout the treatment, correlating with measured forces and confirming the effectiveness of the therapy. This data is instrumental in developing a decision-making system incorporating neural and genetic algorithms to optimize scoliosis treatment outcomes.

References

[1] Ali A., Fontanari V., Schmölz W., Agrawal S. K., *Active*
Soft Brace for Scoliotic Spine: A Finite Element Study to
Evaluate in-Brace Correction, Robotics, 2022.

[2] Chalmers E., Pedrycz W., Lou E., *Predicting the outcome*
of brace treatment for scoliosis using conditional fuzzy clustering, Joint IFSA World Congress and NAFIPS Annual Meeting (IFSA/NAFIPS), 2013.

[3] Dehzangi O., Iftikhar O., Bache B. A., Wensman J., Li Y., *Force and activity monitoring system for scoliosis patients wearing back braces*, IEEE International Conference on Consumer Electronics (ICCE), 2018.

[4] Zhang Q., Chon T., Zhang Y., Baker J. S., Gu Y., *Finite element analysis of the lumbar spine in adolescent idiopathic scoliosis subjected to different loads*, Computers in Biology and Medicine, 2021.

[5] Tymińska P., Zaborowska-Sapeta K., Janczak D., Giżewski T., *TLSO with Graphene Sensors—An Application to Measurements of Corrective Forces in the Prototype of Intelligent Brace*, Sensors, 2022.